

Estimating Heterogeneous Treatment Effects for Spatio-Temporal Causal Inference: How Economic Assistance Moderates the Effects of Airstrikes on Insurgent Violence

Lingxiao Zhou* Kosuke Imai† Jason Lyall‡ Georgia Papadogeorgou§

December 20, 2024

Abstract

Scholars from diverse fields now increasingly rely on high-frequency spatio-temporal data. Yet, causal inference with these data remains challenging due to the twin threats of spatial spillover and temporal carryover effects. We develop methods to estimate heterogeneous treatment effects by allowing for arbitrary spatial and temporal causal dependencies. We focus on common settings where the treatment and outcomes are time-varying spatial point patterns and where moderators are either spatial or spatio-temporal in nature. We define causal estimands based on stochastic interventions where researchers specify counterfactual distributions of treatment events. We propose the Hájek-type estimator of the conditional average treatment effect (CATE) as a function of spatio-temporal moderator variables, and establish its asymptotic normality as the number of time periods increases. We then introduce a statistical test of no heterogeneous treatment effects. Through simulations, we evaluate the finite-sample performance of the proposed CATE estimator and its inferential properties. Our motivating application examines the heterogeneous effects of US airstrikes on insurgent violence in Iraq. Drawing on declassified spatio-temporal data, we examine how prior aid distributions moderate airstrike effects. Contrary to expectations from counterinsurgency theories, we find that prior aid distribution, along with greater amounts of aid per capita, is associated with increased insurgent attacks following airstrikes.

Keywords: point process, stochastic intervention, unstructured interference, spatial-temporal data, causal inference

*Department of Statistics, University of Florida

†Department of Government and Department of Statistics, Harvard University

‡Department of Government, Dartmouth College

§Department of Statistics, University of Florida

1 Introduction

Estimation of causal effects based on spatio-temporal data is becoming increasingly important in many disciplines, including public health, ecology, environment, and social sciences (e.g., [Meierrieks and Gries, 2013](#); [Brunello et al., 2016](#); [Bind, 2019](#); [Wang et al., 2022](#); [Christiansen et al., 2022](#)). Recent examples include the effects of air pollution on child cognitive development ([Wodtke et al., 2022](#)), the use of cellphone records to track population mobility during war ([Christia et al., 2022](#)), and the automated collection of millions of attacks during ongoing wars with precise date and geographic coordinates ([ACLED, 2020](#)).

Yet valid causal inference with spatio-temporal data remains a challenge due to the potential existence of spatial spillover and temporal carryover effects. Since much of the existing literature has not directly dealt with spatio-temporal data, there is an urgent need to develop causal inference methods for such settings without imposing strong assumptions on the structure of spillover and carryover effects.

We develop a statistical methodology for estimating heterogeneous treatment effects based on spatio-temporal data. The proposed methodology extends the approach proposed by [Papadogeorgou et al. \(2022\)](#) to the estimation of conditional average treatment effects (CATE). We consider settings where treatment and outcome variables are time-varying spatial point patterns and where moderators are either spatial or spatio-temporal variables.

Our motivating application comes from the Iraq War (2003–2011), where the United States (US) used both economic aid and airstrikes to reduce insurgent violence as principal components of the “hearts and minds” counterinsurgency campaign ([coi, 2007](#)). We focus on the period of the so-called “Surge” (2007–2008), when US policy makers, alarmed by escalating violence, deployed additional forces, aid, and airstrikes in a concerted effort to crush Sunni and Shia insurgents operating in Baghdad, the neighboring Sunni Triangle,

and other areas. Drawing on newly declassified geolocated data, we examine how prior aid programs and spending, meant to win over locals, moderated the effects of US airstrikes on insurgent violence.

Existing studies of aid and airstrikes have reached mixed conclusions about their effectiveness in reducing insurgent violence (e.g., [Kocher et al., 2011](#); [Crost et al., 2014](#); [Johnston and Sarbahi, 2016](#); [Dell and Querubin, 2018](#); [Lyall, 2019a,b](#); [Rigterink, 2021](#); [Zürcher et al., 2022](#)). This disagreement stems in part from the relative absence of high-frequency geolocated data for aid, airstrikes, and insurgent violence in a given conflict setting. This has forced scholars to aggregate their data along coarse temporal windows (e.g., years) or administrative boundaries (e.g., provinces). Moreover, many scholars have studied aid or airstrikes in isolation, ignoring possible moderating effects. Indeed, we are unaware of any study that explicitly tests how aid moderates airstrike effects in wartime. Finally, these studies have adopted research designs that cannot capture carryover and spillover effects. Our analysis offers an important test of the widespread, but often untested, claim that aid and violence (here, in the form of airstrikes) work in tandem to reduce insurgent attacks.

We begin by defining the CATE in spatio-temporal settings under a stochastic intervention. We propose a two-step estimation procedure. We first estimate the treatment effect for each time period and in each small geographical area or “pixel” based on inverse probability weighting (IPW). In the second step, we regress the time- and pixel-specific estimates on prespecified functions of the moderators to characterize the effect heterogeneity. As shown in our simulation studies, the proposed estimator which uses stabilized weights (Hájek), tends to exhibit much smaller variance than the standard IPW estimator.

Leveraging martingale theory, we establish that the proposed CATE estimator is consistent and asymptotically normal, provided that the propensity score is correctly estimated.

Although our asymptotic variance is not identifiable, we derive its upper bound and propose its consistent estimator. Our simulation studies indicate that the empirical coverage of the resulting confidence intervals, based on the proposed variance bound, closely approximates the nominal level, even in complex data-generating scenarios.

These asymptotic results for the proposed Hájek estimator are new in the spatio-temporal causal inference literature. In fact, previous work has not established the asymptotic normality of a similar Hájek estimator for the average treatment effect (ATE) (Papadogeorgou et al., 2022). Furthermore, we introduce an asymptotically valid statistical test of no heterogeneous treatment effect. Rejecting the null hypothesis of this test implies the existence of heterogeneous treatment effects.

Lastly, we also show that the asymptotic variance of the proposed estimator with stabilized weights is smaller with the estimated propensity score than when the true propensity score is known. Although a similar result has been derived for the IPW estimator in the i.i.d. setting (Hirano et al., 2003), we are the first to extend this result to the Hájek estimator and to the spatio-temporal setting.

Our empirical analysis considers a stochastic intervention that increases the average daily airstrikes from 1 to 6 over a varying number of consecutive days while keeping their spatial distributions unchanged. We estimate the effect of this change in airstrike intensity on insurgent attacks as a function of US economic aid provided in each district in the previous month. We find that districts receiving aid in the previous month tend to experience increased insurgent attacks following intensified airstrikes. These effects become greater as the amount of aid per capita increases, although this pattern is found when the per capita aid amount is relatively small. Our findings challenge the prevailing expectations that economic aid and airstrikes work together to reduce short-term insurgent attacks.

Related Literature. The literature on spatio-temporal causal inference remains sparse due to the challenges of confounding and interference across space and time (Wang, 2021). One exception is Christiansen et al. (2022), which proposes a latent spatial model to adjust confounders that vary across time or space, but not both. The model assumes a specific graphical model among different locations, specifying how treatment, outcome, and latent confounders are causally related. In contrast, we extend the spatio-temporal causal inference framework of Papadogeorgou et al. (2022), which avoids structured interference assumptions and allows for arbitrary spatial spillover and temporal carryover effects.

To our knowledge, Zhang and Ning (2023) is the only study that provides a method for estimating heterogeneous treatment effects with spatio-temporal data. Their approach leverages a spatially interrupted time-series design to assess the causal effect of a fixed intervention implemented during a specific time period. The authors examine the heterogeneity of the treatment effect across a finite number of spatial units with varying attributes. In contrast, we consider a different setting, in which the treatment and outcome follow spatial point processes and the moderator is either spatial or spatio-temporal variables.

Existing work on spatial causal inference relies on design-based inference with randomized experiments (e.g., Wang et al., 2020) or imposes structures on the patterns of spatial spillover effects (e.g., Bardaka et al., 2018; Kolak and Anselin, 2020; Zigler et al., 2013; Papadogeorgou et al., 2019; Barkley et al., 2020; Tchetgen Tchetgen et al., 2021; Giffin et al., 2023). Instead, our methodology can be applied to both experimental and observational studies without making any assumptions about the structure of spillover effects. This is possible because we view spatio-temporal data as a time series of spatial data.

Our work also contributes to a broader causal inference literature on the estimation of CATE by considering spatio-temporal settings where the data exhibit complex dependent

structures over space and time. Much of the existing literature on CATE has focused on i.i.d. settings without considering interference (e.g., [Imai and Ratkovic, 2013](#); [Abrevaya et al., 2015](#); [Athey et al., 2019](#); [Hahn et al., 2020](#); [Kennedy, 2020](#); [Fan et al., 2022](#); [Yang et al., 2023](#)). Similarly, existing approaches to CATE estimation for spatial data typically lack a temporal dimension and rely on structural assumptions about spillover effects such as clustered network interference (e.g., [Credit and Lehnert, 2023](#); [Bargagli-Stoffi et al., 2020](#)). Unlike these methods, we do not impose any structural assumptions about spatial spillover or temporal carryover effects.

The remainder of this paper is organized as follows. Section 2 provides an overview of our data and substantive questions of interest. In Section 3, after introducing our causal setting and estimand, we present our assumptions, propose the new CATE estimator, and derive the theoretical results. In Section 4, we evaluate the empirical performance of the proposed estimator through simulation studies. Section 5 presents the empirical findings of our analysis, showing how the effects of airstrikes differ as a function of prior economic assistance. Finally, we conclude with a discussion of future research directions in Section 6.

2 Airstrikes, Insurgent Attacks, and Aid Spending

We analyze newly declassified high-frequency data recording the date and precise location of US airstrikes and insurgent attacks against Coalition forces during the Iraq War. We combine these data with wartime district-level aid spending (in US dollars) by the US military and US Agency for International Development (USAID). We focus on the 2007–08 time period, which encompasses both the Surge (January 2007 – July 2008) itself and the subsequent drawdown of American forces ([United States Army, 2019](#)).

The information about insurgent attacks is based on the declassified Significant Act (SIGACT) data collected by Coalition forces in Iraq and stored in their Combined In-

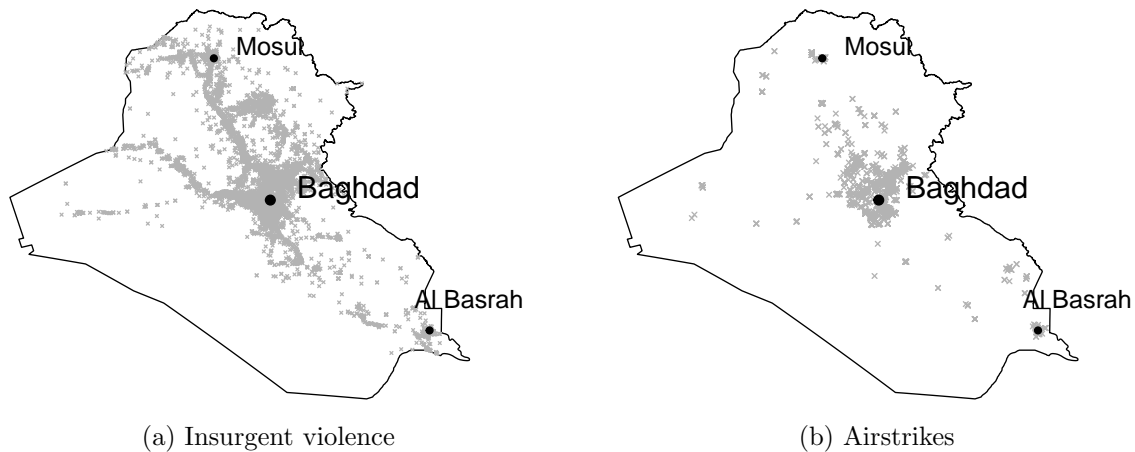


Figure 1: Distribution of US Airstrikes and Insurgent Attacks. Panels (a) and (b) illustrate the spatial distribution of all insurgent attacks (small arms fire and roadside improvised explosive devices) and all airstrikes from February 23, 2007 to July 5, 2008, respectively.

formation Data Network Exchange (CIDNE). During this period, some 68,573 insurgent attacks against US forces were recorded across 57 different types of events, including Small Arms Fire (SAF), Improvised Explosive Device (IED), and Indirect Fire. Each incident report includes the time, date, and nature of an attack, along with precise military grid reference system (MGRS) coordinates that permit spatio-temporal analysis at a very fine-grained level. Figure 1a plots the spatial distribution of all insurgent attacks.

We use newly declassified data on airstrikes obtained from the US Air Force’s Combined Air Operations Center (CAOC) as our treatment variable. A total of 2,446 airstrikes were recorded during our study period. As with CIDNE data, each event records the date, MGRS coordinates, weapons type and number, and aircraft type(s) involved in the airstrike. Figure 1b plots the spatial distribution of these airstrikes. Given its strategic importance, Baghdad, along with neighboring regions such as the Sunni Triangle (a densely populated region encompassing Baghdad, Ramadi, and Tikrit, and villages within this area), received the brunt of all airstrikes during this time period.

The goal of our analysis is to examine how the effects of airstrikes on insurgent violence

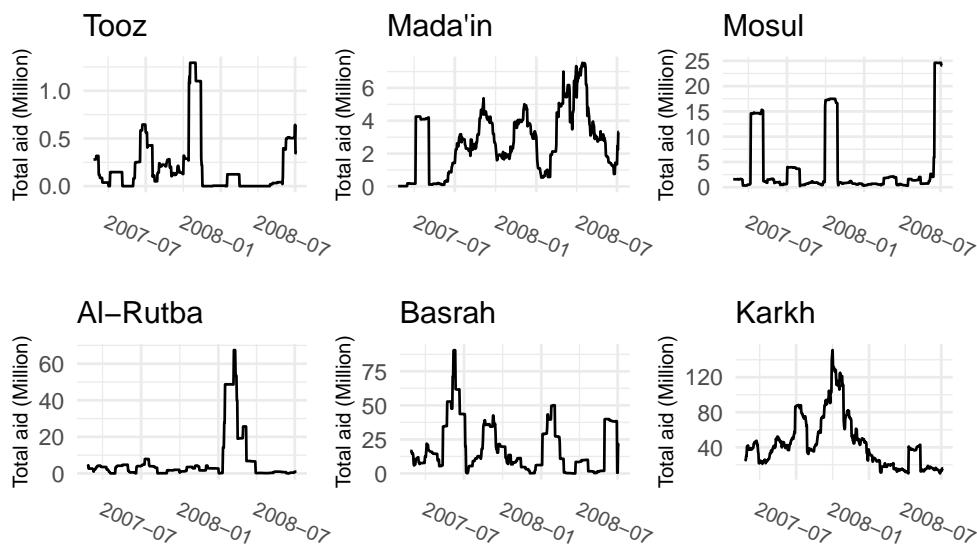


Figure 2: Total aid amount (in million US dollars) over the previous month for six selected districts across Iraq, spanning from February 23, 2007, to July 5, 2008. Aid spending shows significant variation across districts and over time throughout the study period.

depend on the prior provision of aid. We draw on a dataset of aid spending (in US dollars) as recorded by the US military and USAID. Some 23,204 aid projects totaling \$4.97 billion were delivered during this period. Two programs, the Commander’s Emergency Response Program (CERP) and its USAID equivalent, Economic Support Funds (ESF), dominate these aid expenditures, representing about 50% (n=11,714) and nearly 45% (n=10,370) of all completed projects, respectively.

CERP was explicitly designed to sway “hearts and minds” through the provision of immediate, short-term, humanitarian and reconstruction funds (Berman et al., 2011). These projects were typically small scale in nature (mean expenditure: \$97,654) and were often, though not always, earmarked for violent villages and neighborhoods. ESF were smaller (mean: \$15,429) but were similarly aimed at reconstruction efforts, with an eye toward shaping Iraqi perceptions and lowering violence (Special Inspector General for Iraqi Reconstruction, 2013). As Figure 2 illustrates, aid spending during the previous month varied widely across districts and over time during the study period due to shifting priorities,

budgetary cycles, and patterns of insurgent violence.

3 The Proposed Methodology

In this section, we describe the proposed methodology for estimating the CATE based on spatio-temporal data. We begin by defining the causal estimands and then introduce the new CATE estimator. Finally, we derive the asymptotic properties of the proposed estimator and discuss testing the null hypothesis of no heterogeneity.

3.1 Setup

We adopt the methodological framework developed by [Papadogeorgou et al. \(2022\)](#) for causal inference with spatio-temporal treatment and outcome processes. Suppose that we observe the data over T discrete time periods, $t \in \mathcal{T} = \{1, 2, \dots, T\}$. Let Ω denote the entire space under consideration that contains a potentially infinite number of possible treatment and outcome locations. We use $W_t(s) \in \{1, 0\}$ to indicate whether or not location $s \in \Omega$ receives the treatment at time t , whereas $W_t = W_t(\Omega) \in \mathcal{W}$ denotes the treatment point pattern at time t with \mathcal{W} representing the set of all possible point patterns. For simplicity, this set is assumed to be identical across time periods. In addition, we assume that the number of treated locations at each time period is finite. We use $\overline{\mathbf{W}}_t = (W_1, W_2, \dots, W_t)$ to denote the collection of treatment history up to time t , and $\overline{\mathbf{w}}_t = (w_1, w_2, \dots, w_t)$ for its realization.

Let $Y_t(\overline{\mathbf{w}}_t)$ represent the potential outcome for the space Ω at time $t \in \mathcal{T}$ for any given treatment sequence $\overline{\mathbf{w}}_t \in \mathcal{W}^t = \mathcal{W} \times \dots \times \mathcal{W}$. We do not restrict the form of $Y_t(\overline{\mathbf{w}}_t)$ and allow for arbitrary interference in terms of both spatial spillover and temporal carry-over effects. We only observe the outcome point pattern at time t corresponding to the observed treatment sequence, and thus the observed outcome point pattern is given by $Y_t = Y_t(\overline{\mathbf{W}}_t)$.

We use $\bar{\mathbf{Y}}_t = \{Y_1, Y_2, \dots, Y_t\}$ to represent the collection of observed outcomes up to and including time period t . Lastly, we let $\bar{\mathcal{Y}}_T = \{Y_t(\bar{\mathbf{w}}_t) : \bar{\mathbf{w}}_t \in \mathcal{W}^t, t \in \mathcal{T}\}$ to denote the collection of potential outcomes for all treatment sequences and all time periods.

Furthermore, we use \mathbf{X}_t to denote the set of possibly time-varying confounders that are realized prior to W_t but after W_{t-1} , where $\bar{\mathbf{X}}_t = (\mathbf{X}_1, \mathbf{X}_2, \dots, \mathbf{X}_t)$ denotes the collection of observed covariates over the time periods $1, 2, \dots, t$. We use $\bar{\mathcal{X}}_T = \{\mathbf{X}_t(\bar{\mathbf{w}}_{t-1}) : \bar{\mathbf{w}}_{t-1} \in \mathcal{W}^{t-1}, t \in \mathcal{T}\}$ to denote the set of potential values for the covariates under all treatment sequences and all time periods. Then, the observed covariates are given by $\mathbf{X}_t = \mathbf{X}_t(\bar{\mathbf{W}}_{t-1})$.

Finally, we use $\bar{H}_t = \{\bar{\mathbf{W}}_t, \bar{\mathbf{Y}}_t, \bar{\mathbf{X}}_{t+1}\}$ to present the observed history preceding the treatment at time $t + 1$. Since our statistical inference is based on a single time series, the randomness comes only from the treatment assignment W_t given the complete history that includes all factual and counterfactual values \bar{H}_{t-1}^* , where $\bar{H}_t^* = \{\bar{\mathbf{W}}_t, \bar{\mathcal{Y}}_T, \bar{\mathcal{X}}_T\}$. That is, we consider the potential values of confounders and outcomes as fixed quantities.

3.2 Causal estimands

We continue to adopt the framework of [Papadogeorgou et al. \(2022\)](#), and consider estimands under a stochastic intervention F_h that defines a counterfactual distribution over the treatment point pattern. We assume that this stochastic intervention is fixed and does not depend on \mathbf{X}_t and Y_t , both of which can be affected by the treatment. For concreteness, we consider the Poisson process, which is specified by its intensity function $h : \Omega \rightarrow [0, \infty)$, though our methodology can accommodate alternative stochastic intervention distributions.

Unlike [Papadogeorgou et al. \(2022\)](#), however, our goal is to investigate treatment effect heterogeneity under stochastic interventions on the treatment. Specifically, we study how the causal effects of a change in the stochastic intervention vary across regions based on their characteristics, which may be spatial or spatio-temporal variables. These characteristics

are potential moderators for the treatment effect under study.

Formally, we partition the space Ω into a total of p regions or “pixels” in set $\mathcal{S} = \{S_1, S_2, \dots, S_p\}$, where $\Omega = \bigcup_{i=1}^p S_i$ with $S_i \cap S_{i'} = \emptyset$ for $i \neq i'$. For each pixel, we represent the moderator of interest using either its original value (if constant within the pixel) or a summary statistic of its values within the pixel (e.g., mean). Thus, we use $\mathbf{R}_{it} \in \mathcal{R}$ to denote the value of the potential moderator for pixel S_i at time t where \mathcal{R} is the support of the variable. In our empirical analysis, a pixel is a small geographical area, and the moderator of interest is the amount of prior aid provided during the previous month within the district to which the pixel belongs.

Intervention over a single time period. The discretization of space for the potential moderator enables us to analyze effect heterogeneity at the pixel level without any restrictions on the structure of spatial spillover or temporal carryover effects. Specifically, we define the expected number of outcome events within pixel S_i at time t under stochastic intervention F_h as:

$$N_{it}(F_h) = \int_{\mathcal{W}} N_{S_i}(Y_t(\overline{\mathbf{W}}_{t-1}, w_t)) dF_h(w_t)$$

where $N_{S_i}(Y_t(\overline{\mathbf{W}}_{t-1}, w_t))$ is the number of outcome events that fall within pixel S_i at time t based on the treatment path $(\overline{\mathbf{W}}_{t-1}, w_t)$. Then, the treatment effect of $F_{h'}$ versus $F_{h''}$ for time period t and pixel S_i is defined as the contrast in the expected number of outcome events between the two stochastic intervention regimes:

$$\tau_{it}(F_{h'}, F_{h''}) = N_{it}(F_{h''}) - N_{it}(F_{h'}).$$

We are interested in estimating how this pixel-level treatment effect varies as a function of the moderator \mathbf{R}_{it} . Thus, we define the conditional average treatment effect (CATE) at

time t when the moderator takes a specific value $\mathbf{r} \in \mathcal{R}$ as:

$$\tau_t(\mathbf{r}; F_{h'}, F_{h''}) = \frac{1}{\sum_{i=1}^p I(\mathbf{R}_{it} = \mathbf{r})} \sum_{i=1}^p \tau_{it}(F_{h'}, F_{h''}) I(\mathbf{R}_{it} = \mathbf{r}) \quad (1)$$

where I represents the indicator function. For notational simplicity, we instead write the CATE as $\tau_{t,h',h''}(\mathbf{r})$. For example, in our empirical analysis, if we use the receipt of aid in the previous month as the dichotomous moderator, then $\tau_{t,h',h''}(1)$ represents the average effect on the expected number of insurgent attacks for a district that received aid, when changing the distribution of airstrikes from $F_{h'}$ to $F_{h''}$.

We characterize the CATE by projecting the pixel-level treatment effect $\tau_{t,h',h''}(\mathbf{r})$ onto a space of \mathbf{R}_{it} using an interpretable model $\tau_{t,h',h''}^{\text{Proj.}}(\mathbf{r}; \boldsymbol{\beta}_t)$, which is indexed by a low-dimensional vector $\boldsymbol{\beta}_t$. For example, one may choose a linear model with \mathbf{R}_{it} as predictors and $\boldsymbol{\beta}_t$ as their coefficients (see [Kennedy et al., 2019](#); [van der Laan et al., 2011](#); [Ding et al., 2019](#), for similar estimands based on projections). Formally, we focus on the projection estimand defined as:

$$\tau_{t,h',h''}^{\text{Proj.}}(\mathbf{r}; \boldsymbol{\beta}_t^*) \quad \text{where} \quad \boldsymbol{\beta}_t^* = \arg \min_{\boldsymbol{\beta}_t} \sum_{i=1}^p \left[\tau_{t,h',h''}(\mathbf{R}_{it}) - \tau_{t,h',h''}^{\text{Proj.}}(\mathbf{R}_{it}; \boldsymbol{\beta}_t) \right]^2.$$

This quantity represents the best approximation to the true CATE curve that can be achieved with the selected parametric model $\tau_{t,h',h''}^{\text{Proj.}}(\mathbf{r}; \boldsymbol{\beta}_t)$.

Finally, we average the time-specific projected CATEs over all time periods to define the following overall projected CATE:

$$\tau_{h',h''}^{\text{Proj.}}(\mathbf{r}; \boldsymbol{\beta}_1^*, \dots, \boldsymbol{\beta}_T^*) = \frac{1}{T} \sum_{t=1}^T \tau_{t,h',h''}^{\text{Proj.}}(\mathbf{r}; \boldsymbol{\beta}_t^*).$$

When the moderator takes a finite number of values, the true $\tau_{t,\mathbf{h}',\mathbf{h}''}(\mathbf{r})$ defined in Equation (1) can be represented exactly based on a saturated parametric model, and the projection estimand coincides with the true CATE. For a continuous moderator, projecting the estimand onto an interpretable, lower-dimensional space allows us to better understand how the CATE varies with the moderator.

Intervention over multiple time periods. We generalize our estimand to the settings with stochastic interventions defined over multiple consecutive time periods. Consider a stochastic intervention over M time periods, denoted by $F_{\mathbf{h}} = F_{h_1} \times F_{h_2} \times \dots \times F_{h_M}$, where the treatment is assigned according to F_{h_t} at time t , $F_{h_{t-1}}$ at time $t - 1$, and so on until time $t - M + 1$ when the intervention distribution is given by F_{h_M} . Formally, we define the expected number of outcome events in pixel S_i at time t under this multi-period stochastic intervention as follows:

$$N_{it}(F_{\mathbf{h}}) = \int_{\mathcal{W}^M} N_{S_i}(Y_t(\overline{\mathbf{W}}_{t-M}, w_{t-M+1}, \dots, w_t)) dF_{\mathbf{h}}(w_{t-M+1}, \dots, w_t)$$

We define the pixel-specific effect and the CATE between the two stochastic interventions, $F_{\mathbf{h}'}$ and $F_{\mathbf{h}''}$, for time t as

$$\begin{aligned} \tau_{it}(F_{\mathbf{h}'}, F_{\mathbf{h}''}) &= N_{it}(F_{\mathbf{h}''}) - N_{it}(F_{\mathbf{h}'}), \\ \tau_{t,\mathbf{h}',\mathbf{h}''}(\mathbf{r}) &= \frac{1}{\sum_{i=1}^p I(\mathbf{R}_{i,t-M+1} = \mathbf{r})} \sum_{i=1}^p \tau_{it}(F_{\mathbf{h}'}, F_{\mathbf{h}''}) I(\mathbf{R}_{i,t-M+1} = \mathbf{r}), \end{aligned}$$

respectively, where \mathbf{R}_{t-M+1} represents the moderator that immediately precedes the intervention time periods and hence is a variable that occurs before the hypothetical intervention. Since the moderator cannot be affected by the treatment, the use of the pre-intervention value \mathbf{R}_{t-M+1} avoids any post-treatment bias.

Finally, the projection estimand for this multi-period case is defined as

$$\tau_{t,h',h''}^{\text{Proj.}}(\mathbf{R}_{i,t-M+1}; \boldsymbol{\beta}_t^*) \quad \text{where} \quad \boldsymbol{\beta}_t^* = \arg \min_{\boldsymbol{\beta}_t} \sum_{i=1}^p \left(\tau_{t,h',h''}(\mathbf{R}_{i,t-M+1}) - \tau_{t,h',h''}^{\text{Proj.}}(\mathbf{R}_{i,t-M+1}; \boldsymbol{\beta}_t) \right)^2.$$

Averaging this quantity over time, we have the overall CATE defined as

$$\tau_{h',h''}^{\text{Proj.}}(\mathbf{r}; \boldsymbol{\beta}_M^*, \dots, \boldsymbol{\beta}_T^*) = \frac{1}{T - M + 1} \sum_{t=M}^T \tau_{t,h',h''}^{\text{Proj.}}(\mathbf{r}; \boldsymbol{\beta}_t^*).$$

Working model. When the moderator is continuous or takes a large number of distinct values, the working model $\tau_{t,h',h''}^{\text{Proj.}}(\mathbf{r}; \boldsymbol{\beta}_t)$ can be viewed as an approximation to the true CATE curve. Since the working model does not have to be correctly specified, different model specifications can be chosen under different goals. Here, for simplicity and interpretability, we consider the following model for each time period:

$$\tau_{t,h',h''}^{\text{Proj.}}(\mathbf{r}; \boldsymbol{\beta}_t) = \sum_{l=1}^L \beta_{t,l} z_l(\mathbf{r}) = \mathbf{z}(\mathbf{r})^\top \boldsymbol{\beta}_t, \quad (2)$$

where $\mathbf{z}(\mathbf{r}) = (z_1(\mathbf{r}), \dots, z_L(\mathbf{r}))^\top$ are the known functions that can be selected based on one's domain knowledge or, in the absence of such knowledge, simply the basis functions of splines.

Although we focus on a working model in this paper that is linear in the pre-specified $z_l(\mathbf{r})$ functions, future work could consider semi-parametric models, such as series estimators discussed in [Kennedy \(2020\)](#). While these semi-parametric models are effective with independent and identically distributed data, extending them to spatio-temporal data is beyond the scope of this paper. In addition, determining the optimal number of bases in a series expansion is typically achieved through cross-validation, which is challenging

in the spatio-temporal setting due to dependence across space and time. We leave these extensions to future work.

3.3 Assumptions

We require two assumptions about the treatment assignment mechanism that are similar to those in the classical causal inference literature. For notational simplicity, we focus on the scenario where the intervention distribution is identical and independent over M time periods, $F_{\mathbf{h}} = F_h \times \cdots \times F_h$, though it is straightforward to extend our theory to the cases where the intervention distribution is different and/or dependent across these time periods.

Assumption 1 (Unconfoundedness). $f(W_t | \overline{\mathbf{W}}_{t-1}, \overline{\mathcal{Y}}_T, \overline{\mathcal{X}}_T) = f(W_t | \overline{H}_{t-1})$

Assumption 2 (Bounded relative overlap). *There exists $\delta_W > 0$ such that $e_t(w) > \delta_W f_h(w)$ for all $w \in \mathcal{W}$ such that $f_h(w) > 0$, where $e_t(w) = f(W_t = w | \overline{H}_{t-1})$*

Assumption 1 states that conditional on the observed history of treatments, confounders, and outcomes, the treatment assignment at time t is independent of all unobserved potential outcomes and confounders, past or future. Assumption 1 is more restrictive than the standard sequential ignorability assumption made in the longitudinal causal inference literature (e.g., [Robins et al., 2000](#)) because the independence is assumed for all potential outcomes and potential confounders across all time periods, i.e., $\overline{\mathcal{Y}}_T$ and $\overline{\mathcal{X}}_T$. Assumption 2 states that the ratio of the propensity score to the counterfactual intervention density is bounded away from zero, which ensures that all treatment patterns that are feasible under the stochastic intervention are observable under the treatment assignment mechanism.

3.4 Two-step estimation procedure

We develop a two-step estimation procedure by building on existing methods that estimate the CATE with i.i.d. data (e.g., [Kennedy, 2020](#); [Fan et al., 2022](#); [Yang et al., 2023](#)).

Specifically, we first construct a pseudo-outcome based on the estimated propensity score, and then regress contrasts of pseudo-outcomes on the moderators of interest. This two-step procedure maintains a simple CATE analysis regardless of the complexity of propensity score estimation.

We construct a pseudo-outcome by weighting the observed number of events in each pixel at each time period using the estimated propensity score and the density of the stochastic intervention. Specifically, the (IPW) pseudo-outcome in pixel S_i at time t is given by

$$\tilde{Y}_{it}^I(F_{\mathbf{h}}; \hat{\boldsymbol{\gamma}}) = \rho_{t\mathbf{h}}(\hat{\boldsymbol{\gamma}}) N_{S_i}(Y_t), \quad (3)$$

for any $i = 1, 2, \dots, p$ and $t = M, M + 1, \dots, T$, and for weight that is equal to

$$\rho_{t\mathbf{h}}(\hat{\boldsymbol{\gamma}}) = \rho_{t\mathbf{h}}(\mathbf{W}_{j-M+1:j}; \hat{\boldsymbol{\gamma}}) = \prod_{j=t-M+1}^t \frac{f_{\mathbf{h}}(W_j)}{e_j(W_j; \hat{\boldsymbol{\gamma}})},$$

where $f_{\mathbf{h}}$ is the density corresponding to the stochastic intervention $F_{\mathbf{h}}$, $e_t(W_t; \boldsymbol{\gamma})$ is a parametric propensity score model with a K -dimensional vector of parameters $\boldsymbol{\gamma} \in \mathbb{R}^K$, and $\hat{\boldsymbol{\gamma}}$ is an estimate of $\boldsymbol{\gamma}$.

In practice, the above IPW-based pseudo outcome can produce large weights for some time periods when the estimated propensity score is much smaller than the intervention density. Therefore, we consider the following ‘‘Hájek’’ pseudo-outcome based on the stabilized weights,

$$\tilde{Y}_{it}^H(F_{\mathbf{h}}; \hat{\boldsymbol{\gamma}}) = \frac{\rho_{t\mathbf{h}}(\hat{\boldsymbol{\gamma}})}{\frac{1}{T-M+1} \sum_{t=M}^T \rho_{t\mathbf{h}}(\hat{\boldsymbol{\gamma}})} N_{S_i}(Y_t). \quad (4)$$

Given these pseudo-outcomes, we can compare two intervention distributions, $F_{\mathbf{h}'}$ and

$F_{\mathbf{h}'}$, at each pixel using

$$\tilde{\tau}_{it}^H(F_{\mathbf{h}'}, F_{\mathbf{h}''}; \hat{\gamma}) = \tilde{Y}_{it}^H(F_{\mathbf{h}''}; \hat{\gamma}) - \tilde{Y}_{it}^H(F_{\mathbf{h}'}; \hat{\gamma}).$$

Below, for notational simplicity, we use $\tilde{\tau}_{it}^H(\hat{\gamma})$ as a shorthand for $\tilde{\tau}_{it}^H(F_{\mathbf{h}'}, F_{\mathbf{h}''}; \hat{\gamma})$, and use $\tilde{\boldsymbol{\tau}}_t^H(\hat{\gamma}) = (\tilde{\tau}_{1t}^H(\hat{\gamma}), \dots, \tilde{\tau}_{pt}^H(\hat{\gamma}))^\top$ to denote the vector of pseudo-outcome contrasts for the p pixels. Analogous quantities can also be defined using the IPW pseudo-outcomes.

We regress the pseudo-outcome contrast at time t , $\tilde{\tau}_t^H(\hat{\gamma})$, on the moderator as shown in Equation (2). This gives the following Hájek estimator of $\boldsymbol{\beta}_t$,

$$\hat{\boldsymbol{\beta}}_t^H = \arg \min_{\boldsymbol{\beta}_t} (\tilde{\boldsymbol{\tau}}_t^H(\hat{\gamma}) - \mathbf{Z}_t \boldsymbol{\beta}_t)^\top (\tilde{\boldsymbol{\tau}}_t^H(\hat{\gamma}) - \mathbf{Z}_t \boldsymbol{\beta}_t),$$

where $\mathbf{Z}_t = [\mathbf{z}(\mathbf{R}_{1,t-M+1}) \dots \mathbf{z}(\mathbf{R}_{p,t-M+1})]^\top$. The estimates $\hat{\boldsymbol{\beta}}_t^H$ are obtained by fitting a separate regression model for each time period rather than a pooled regression. This is because, using a separate regression, the resulting estimating equations have a conditional mean of zero for each individual time period, and therefore form a martingale difference sequence with respect to the history filtration. This allows us to derive the asymptotic properties of the estimator in Section 3.5 using the martingale central limit theorem.

Finally, we obtain the projected CATE estimator by averaging across time periods,

$$\hat{\tau}_{\mathbf{h}', \mathbf{h}''}(\mathbf{r}) = \tau_{\mathbf{h}', \mathbf{h}''}^{\text{Proj.}}(\mathbf{r}; \hat{\boldsymbol{\beta}}_M^H, \dots, \hat{\boldsymbol{\beta}}_T^H) = \mathbf{z}(\mathbf{r})^\top \left(\frac{1}{T-M+1} \sum_{t=M}^T \hat{\boldsymbol{\beta}}_t^H \right). \quad (5)$$

3.5 Asymptotic properties

We now derive the asymptotic properties of the proposed CATE estimators. All proofs are presented in the appendix. In particular, we show that the Hájek estimator is consistent and

asymptotically normal. Unfortunately, the asymptotic variance is unidentifiable because we only observe a single time series. Nevertheless, we derive a variance upper bound and propose a consistent estimator of this bound.

In the spatio-temporal causal inference literature, these results are new. In particular, [Papadogeorgou et al. \(2022\)](#) derive the asymptotic properties of the IPW estimator and yet only suggest that future work should study the asymptotic behavior of the Hájek estimator. We also show that when the propensity score is estimated, the asymptotic variance of the Hájek estimator is no greater than when the true propensity score is known. This generalizes the well-known result of [Hirano et al. \(2003\)](#) in the i.i.d. setting to the spatio-temporal setting with stabilized weights.

We formally state the asymptotic normality of the Hájek estimator based on the estimated propensity score. Besides the two assumptions in [Section 3.3](#), we need to assume some standard regularity conditions, which are formally stated in the appendix.

Theorem 1 (Asymptotic Normality of the Hájek Estimator Using the Estimated Propensity Score). *Suppose that Assumptions 1 and 2 hold, along with the regularity conditions specified in Assumptions A.1, A.2, A.4 and A.5. Let $\hat{\gamma}$ be the estimate of the propensity score parameters obtained by solving the estimating equation specified in Assumption A.2. Then as $T \rightarrow \infty$, we have that*

$$\frac{1}{\sqrt{T - M + 1}} \sum_{t=M}^T (\hat{\beta}_t^H - \beta_t^*) \xrightarrow{d} N(\mathbf{0}, \mathbf{J} \mathbf{V}^H \mathbf{J}^\top),$$

where $\mathbf{V}^H = \tilde{\mathbf{V}}^H - \mathbf{U}^\top \mathbf{V}_{ps}^{-1} \mathbf{U}$ for matrices \mathbf{J} , $\tilde{\mathbf{V}}^H$ defined in [Theorem A.4](#), \mathbf{V}_{ps} defined in [Assumption A.2](#), and \mathbf{U} in [Assumption A.5](#).

In [Theorem A.4](#) shown in [Appendix C](#), we establish that the estimator based on the true propensity score is asymptotically normal with variance $\mathbf{J} \tilde{\mathbf{V}}^H \mathbf{J}^\top$. Then, the difference between the asymptotic variance based true and estimated propensity score is $\mathbf{J} \mathbf{U}^\top \mathbf{V}_{ps}^{-1} \mathbf{U} \mathbf{J}^\top$. This quantity is large when the estimating equation based on the true propensity score is strongly correlated with the score function of the propensity score model. By showing

that this difference is a positive semidefinite matrix, we establish that the use of estimated propensity score yields asymptotic efficiency.

Theorem 2 (Asymptotic Efficiency under the Estimated Propensity Score). *If the propensity score model is correctly specified, the estimator $\frac{1}{T-M+1} \sum_{t=M}^T \hat{\beta}_t^H$ based on the estimated propensity score has asymptotic variance that is no larger than the asymptotic variance of the same estimator using the known propensity score. That is, for $\mathbf{J}\tilde{\mathbf{V}}^H\mathbf{J}^\top$ in Theorem A.4, and $\mathbf{J}\mathbf{V}^H\mathbf{J}^\top$ in Theorem 1, $\mathbf{J}(\tilde{\mathbf{V}}^H - \mathbf{V}^H)\mathbf{J}^\top$ is a positive semidefinite matrix.*

The matrix \mathbf{V}^H is based on the covariance matrix of estimating equations conditional on the complete history, i.e., $\mathbf{V}^H = \text{plim}_{T \rightarrow \infty} \frac{1}{T-M+1} \sum_{t=M}^T \mathbb{V}[\mathbf{A}_t \mid \bar{H}_{t-M}^*]$ for some vector \mathbf{A}_t defined in Appendix C.1. As mentioned earlier, we cannot consistently estimate $\mathbb{V}[\mathbf{A}_t \mid \bar{H}_{t-M}^*]$ and thus \mathbf{V}^H due to the fact that we only observe a single time series. However, since $\mathbf{V}^{H^*} = \text{plim}_{T \rightarrow \infty} \frac{1}{T-M+1} \sum_{t=M}^T \mathbb{E}[\mathbf{A}_t \mathbf{A}_t^\top \mid \bar{H}_{t-M}^*]$ is an upper bound of \mathbf{V}^H , the asymptotic variance $\mathbf{J}\mathbf{V}^H\mathbf{J}^\top$ is bounded by $\mathbf{J}\mathbf{V}^{H^*}\mathbf{J}^\top$. Moreover, the following corollary shows that we can consistently estimate the upper bound of the asymptotic variance.

Corollary 1 (Consistent Estimation of Variance Bound Based on Estimated Propensity Score). *Suppose that the conditions of Theorem 1 hold. For $\mathbf{A}_t(\gamma)$ defined in Assumption A.4, let*

$$\hat{\mathbf{V}}^H = \frac{1}{T-M+1} \sum_{t=M}^T \hat{\mathbf{V}}_t^H \quad \text{with} \quad \hat{\mathbf{V}}_t^H = \mathbf{A}_t(\hat{\gamma})\mathbf{A}_t(\hat{\gamma})^\top,$$

$$\hat{\mathbf{J}} = \left[\mathbf{I} \quad -\mathbf{I} \quad -\frac{1}{T-M+1} \sum_{t=M}^T (\mathbf{Z}_t^\top \mathbf{Z}_t)^{-1} \mathbf{Z}_t^\top \tilde{\mathbf{Y}}_t^H(F_{\mathbf{h}'}; \hat{\gamma}) \quad \frac{1}{T-M+1} \sum_{t=M}^T (\mathbf{Z}_t^\top \mathbf{Z}_t)^{-1} \mathbf{Z}_t^\top \tilde{\mathbf{Y}}_t^H(F_{\mathbf{h}''}; \hat{\gamma}) \right],$$

with $\tilde{\mathbf{Y}}_t^H(F_{\mathbf{h}}; \hat{\gamma}) = \left(\tilde{Y}_{it}^H(F_{\mathbf{h}}; \hat{\gamma}), \dots, \tilde{Y}_{pt}^H(F_{\mathbf{h}}; \hat{\gamma}) \right)^\top$.

Then, if \mathbf{Q} , which depends on T , converges to the identity matrix \mathbf{I} in probability as $T \rightarrow \infty$, $\hat{\mathbf{J}}\mathbf{Q}\hat{\mathbf{V}}^H\mathbf{Q}^\top\hat{\mathbf{J}}^\top$ is a consistent estimator for $\mathbf{J}\mathbf{V}^{H^*}\mathbf{J}^\top$.

As a result, we can use the estimated variance bound to construct a conservative confidence interval for the proposed estimator when the propensity score needs to be estimated. The matrix \mathbf{Q} can be chosen as a function of the mean of IPW weights to stabilize the IPW weights that appear in $\hat{\mathbf{V}}^H$. We discuss the choice of \mathbf{Q} is in Appendix D. Our

simulation study presented in Section 4 demonstrates a good empirical coverage rate for the constructed confidence interval, even when M is relatively large. Our variance bound for the Hájek estimator provides significantly improved inference compared to a heuristic variance bound used in Papadogeorgou et al. (2022), where the coverage rate deteriorates quickly as M increases.

Appendix C presents additional theoretical results and detailed proofs on the Hájek estimator. Finally, Appendix B shows that the IPW estimators are also consistent and asymptotically normal (albeit less efficient than the Hájek estimator), and proves that their asymptotic variance bound can be consistently estimated.

3.6 Statistical test of no heterogeneous treatment effect

We develop a statistical test for treatment effect heterogeneity based on testing the null hypothesis that all coefficients of $\mathbf{z}(\mathbf{r})$ in Equation (5), other than the intercept, are equal to zero. For notational simplicity, we describe the proposed test in the setting in which $\mathbf{z}(\mathbf{r})$ does not include an intercept. The test, however, can be easily adopted in models with an intercept.

Let $\bar{\boldsymbol{\beta}} = \frac{1}{T-M+1} \sum_{t=M}^T \boldsymbol{\beta}_t^H$ and $\bar{\boldsymbol{\beta}}^* = \frac{1}{T-M+1} \sum_{t=M}^T \boldsymbol{\beta}_t^*$. We are interested in testing the null hypothesis that $H_0 : \bar{\boldsymbol{\beta}}^* = \mathbf{0}$, which holds if the treatment effect is not heterogeneous with respect to $\mathbf{z}(\mathbf{r})$, against the alternative that $H_A : \bar{\boldsymbol{\beta}}^* \neq \mathbf{0}$. We propose the test statistic

$$T_c = \frac{1}{T-M+1} \bar{\boldsymbol{\beta}}^\top (\hat{\mathbf{J}} \mathbf{Q} \hat{\mathbf{V}}^H \mathbf{Q}^\top \hat{\mathbf{J}}^\top)^{-1} \bar{\boldsymbol{\beta}},$$

and calculate a p -value as $\mathbb{P}(\chi_L^2 > T_c)$. The following theorem shows that the limiting rejecting probability under the null hypothesis is no greater than α as $T \rightarrow \infty$.

Theorem 3 (Asymptotic validity of the test). *Under the assumptions of Theorem 1 and*

the null hypothesis $\bar{\beta}^* = \mathbf{0}$, we have that

$$\limsup_{T \rightarrow \infty} \mathbb{P}(p\text{-value} < \alpha) \leq \alpha.$$

The proof is in Appendix E. By inverting this test, we obtain an $(1 - \alpha)100\%$ confidence set for $\bar{\beta}^*$ with limiting coverage that is no less than $1 - \alpha$ as $T \rightarrow \infty$ as:

$$C_\alpha = \left\{ \bar{\beta}' : \frac{1}{T - M + 1} (\bar{\beta} - \bar{\beta}')^\top (\hat{\mathbf{J}} \hat{\mathbf{Q}} \hat{\mathbf{V}}^H \hat{\mathbf{Q}}^\top \hat{\mathbf{J}}^\top)^{-1} (\bar{\beta} - \bar{\beta}') < F_{\chi_L^2}^{-1}(1 - \alpha) \right\}, \quad (6)$$

where $F_{\chi_L^2}^{-1}(q)$ is the q -quantile of the chi-square distribution with L degrees of freedom.

4 Simulation Studies

In this section, we conduct simulation studies to examine the empirical performance of our proposed methodology. To create a realistic data generating process, we base our simulations on the Iraq data introduced in Section 2. We focus on a univariate moderator but consider both spatial and spatio-temporal variables. We find that within the range of the 0.25 and 0.975 quantiles of the moderator values, the estimated CATE is essentially unbiased. Although a slight increase in bias is observed with longer intervention durations, the results remain robust, and the empirical coverage of the confidence intervals is close to the nominal level across all scenarios.

4.1 Study design

For each simulation setup, we independently generate 500 datasets. We set the length of time series to be $T = 500$, closely following the corresponding length in our Iraq data (see Section 5). We begin by generating a vector of confounders $\mathbf{X}_t = (X_1, X_2, X_{3t}, X_{4t})^\top$ by following the procedure described by Papadogeorgou et al. (2022). Specifically, X_1 and X_2 are spatial confounders; X_1 is based on the distance to the main road network and the

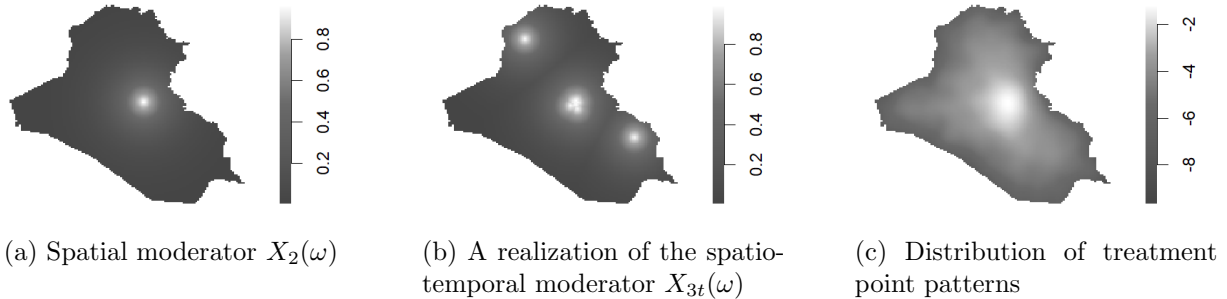


Figure 3: Panels (a) and (b) present the spatial and spatio-temporal moderator variables. Panel (c) shows the logarithm of the baseline density for the intervention distribution.

border of Iraq, while X_2 is based on the distance to Baghdad (see Figure 3a). Moreover, X_{3t} and X_{4t} are two spatio-temporal confounders based on the observed patterns of airstrikes and insurgent attacks in our Iraq data. We use the locations of all airstrikes in the entire study period to estimate a spatial density estimate of airstrike patterns, $\hat{g}(\omega)$.

At each time period t , we first generate a point pattern Z from a Poisson point process with the intensity $\exp(\rho_0 + \rho_1 \hat{g}(\omega))$ for $\rho_0 \approx -2.7$ and $\rho_1 = 8$. Then, the confounder X_{3t} is computed as a function of the distance to the closest realized point in Z , $D(\omega; Z)$, i.e., $X_{3t}(\omega) = \exp(-D(\omega; Z))$. A realization of X_{3t} at a randomly chosen time period is shown in Figure 3b. We generate X_{4t} similarly but estimate the spatial density \hat{g} based on the observed insurgent violence events with $\rho_0 \approx -3.2$ and $\rho_1 = 7$. We conduct two sets of simulation studies: one with the spatial moderator X_2 and the other with the spatio-temporal moderator X_{3t} . All variables are included as confounders in all simulations.

Given the confounders, we next generate the treatment and outcome point patterns. For each time period t , the treatment point pattern is generated from a Poisson point process with the following intensity function,

$$\lambda_t^W(\omega) = \exp \{ \alpha_0 + \boldsymbol{\alpha}_X^\top \mathbf{X}_t(\omega) + \alpha_W W_{t-1}^*(\omega) + \alpha_Y Y_{t-1}^*(\omega) \} \quad (7)$$

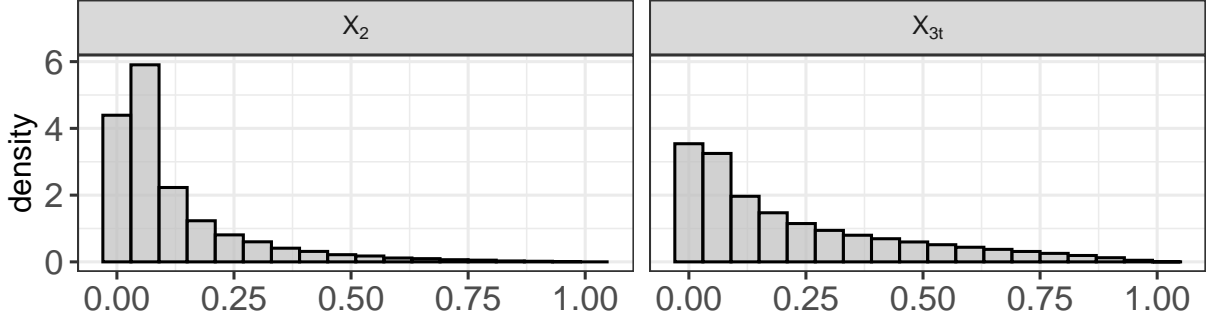


Figure 4: Histograms of spatial moderator X_2 and spatio-temporal temporal moderator X_{3t} across all pixels and all time periods.

where $Y_{t-1}^*(\omega)$ and $W_{t-1}^*(\omega)$ are the smoothed versions of the realized point patterns Y_{t-1} and W_{t-1} , respectively. Specifically, $Y_{t-1}^*(\omega) = \exp(-2D(\omega; Y_{t-1}))$, where $D(\omega; Y_{t-1})$ denotes the minimum distance of location $\omega \in \Omega$ from the observed outcome events at the previous time period, Y_{t-1} . We define $W_{t-1}^*(\omega) = \exp(-2D(\omega; W_{t-1}))$ in a similar manner.

Additionally, we generate the outcome point pattern from another Poisson process with an intensity function λ_t^Y . When the moderator is a spatial variable X_2 , we use:

$$\lambda_t^Y(\omega) = \exp \left\{ \gamma_0 + \boldsymbol{\gamma}_{\mathbf{X}}^\top \mathbf{X}_t(\omega) + \gamma_W W_{(t-3):t}^*(\omega) + \gamma_Y Y_{t-1}^*(\omega) + \gamma_1 X_2 W_{(t-3):t}^*(\omega) \right\}, \quad (8)$$

where $W_{(t-3):t}^* = \exp(-2D(\omega; \mathbf{W}_{(t-3):t}))$ with $D(\omega; \mathbf{W}_{(t-3):t})$ denoting the minimum distance of location ω to treatment locations during time period $t-3$ to t . When the moderator is a spatio-temporal variable X_{3t} , we use the following intensity function:

$$\lambda_t^Y(\omega) = \exp \left\{ \gamma_0 + \boldsymbol{\gamma}_{\mathbf{X}}^\top \mathbf{X}_t(\omega) + \gamma_W W_{(t-3):t}^*(\omega) + \gamma_Y Y_{t-1}^*(\omega) + \sum_{j=1}^4 \gamma_j X_{3,t-j}(\omega) W_{t-j+1}^*(\omega) \right\}. \quad (9)$$

These model specifications yield approximately 5 treatment events and 30 outcome events per time period on average, closely reflecting the observed data, which show an average of 4.9 airstrikes and 31.3 IED attacks per day.

We consider stochastic interventions of the form $F_{\mathbf{h}}^M = F_{h_1} \times \dots \times F_{h_M}$ where the intensity function is given by $h(\omega) = c\phi(\omega)$. We estimate ϕ from the generated treatment events, and use it as the baseline intensity (shown in Figure 3c). Here, the tuning parameter c regulates the expected number of treatment events. For $M = 1, 3, 7$, we consider the stochastic interventions with $c = 3, 5, 7$, denoted as $F_{\mathbf{h}_1}^M, F_{\mathbf{h}_2}^M$, and $F_{\mathbf{h}_3}^M$ respectively. We estimate the CATE that contrasts between any two of these interventions.

Since no closed-form expression is available, we use a Monte Carlo approximation for the true CATE values. According to Equation (7), the potential outcomes at time t depend on the realized treatments and outcomes in all previous time periods either directly or indirectly due to the fact that the model includes the lagged treatment and outcome variables. This means that the true value of the CATE is different across data sets.

As a concrete example, we outline the procedure for approximating the true CATE value $\tau_{\mathbf{h}_1, \mathbf{h}_2}(r)$ that compares two intervention distributions $F_{\mathbf{h}_1}$ and $F_{\mathbf{h}_2}$. At each time period t and a given Monte Carlo draw $k = 1, \dots, K$, we sample treatment point patterns $w_{t-M+1}^{(jk)}, \dots, w_t^{(jk)}$ from the intervention distribution $F_{\mathbf{h}_j}$ separately for $j = 1, 2$. Then, we generate outcome point patterns $y_{t-M+1}^{(jk)}, \dots, y_t^{(jk)}$ based on the treatment path $(\overline{\mathbf{W}}_{t-M}, w_{t-M+1}^{(jk)}, \dots, w_t^{(jk)})$, and compute the difference of outcomes in each pixel S_i at time t , $D_{it}^{(k)} = N_{S_i}(y_t^{2k}) - N_{S_i}(y_t^{1k})$. Let r_{it} be the value of the moderator in pixel S_i at time t . We compute $\tau_{t, \mathbf{h}_1, \mathbf{h}_2}^{(k)}(r)$ by regressing $D_{it}^{(k)}$ on $z_1(r_{it}), \dots, z_L(r_{it})$ as shown in Equation (2). Averaging $\tau_{t, \mathbf{h}_1, \mathbf{h}_2}^{(k)}(r)$ over all the iterations and time periods gives an approximation of $\tau_{t, \mathbf{h}_1, \mathbf{h}_2}^{\text{Proj.}}(r; \beta_t^*)$.

4.2 Model specifications

To examine the empirical performance of the proposed methodology, we consider the true and estimated propensity score with a correctly specified model. As described in Section 3.4,

we compute the pseudo-outcome using either the IPW weights or the stabilized Hájek weights. We also consider the truncated versions of these weights where the truncation is done at the 99th percentile. Truncation of estimated propensity scores is a common practice in applied research to avoid extreme weights.

After obtaining the pseudo-outcomes, we choose functions $z_1(r), \dots, z_L(r)$ for the working model presented in Equation (2). Figure 4 presents the histogram of spatial moderator and spatio-temporal moderator across all pixels and all time periods. Since both moderators X_2 and X_{3t} take values in $[0, 1]$, we set $z_1(r), \dots, z_L(r)$ to be the basis functions of natural cubic splines on $[0, 1]$ with equally spaced knots between 0 and 1. For all simulations, we include six basis functions in the working model, i.e., $L = 6$. At each time period, we conduct a regression of the pseudo-outcomes using the covariates formed by $z_1(r), \dots, z_L(r)$.

In total, we evaluate six estimators: IPW/Hájek estimators based on the true propensity score, IPW/Hájek estimators based on the estimated propensity score, and IPW/Hájek estimators based on the truncated estimated propensity score. We use the consistent estimators for the upper bound of the asymptotic variance discussed in Section 3.5 for constructing confidence intervals.

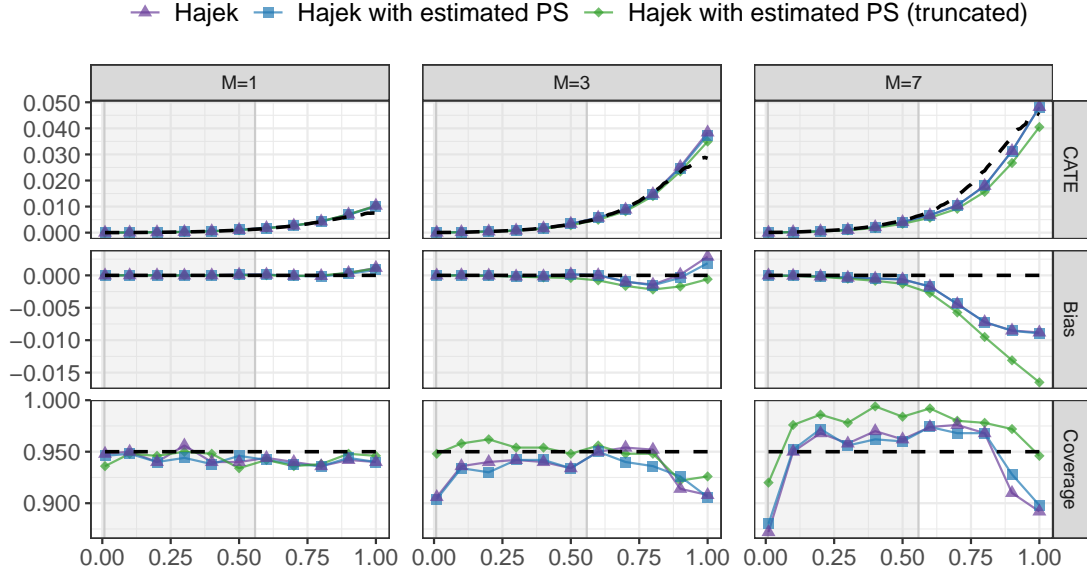
4.3 Results

We assess the empirical performance of the Hájek estimators under the most challenging scenario, which compares F_{h_1} and F_{h_3} . Figure 5 presents the true and estimated CATEs and their corresponding bias and coverage rates of 95% confidence intervals, for $M = 1, 3$, and 7, averaged over 500 Monte Carlo simulations. The shaded region in the plot highlights the range of the 0.025 and 0.975 quantiles of the moderator values, and we focus our discussion within this range. Results outside this range are mostly based on extrapolation.

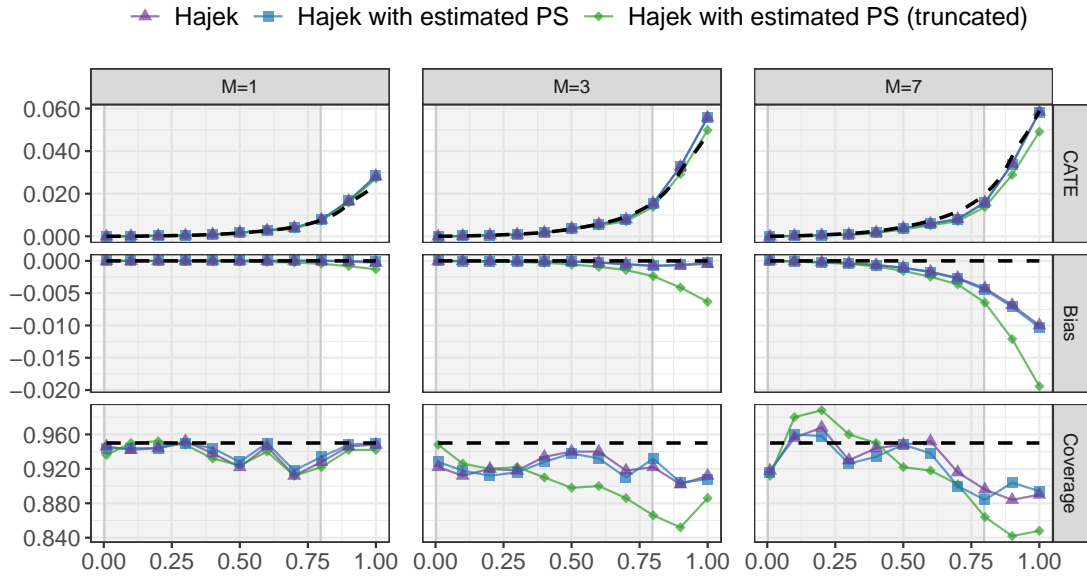
Overall, the Hájek estimators perform well within the shaded region: the estimated CATEs closely follow the true CATEs, with minimal bias, while empirical coverage rates are generally close to the nominal rate of 95%. The performance is consistently observed for both spatial and spatio-temporal moderators (Panels (a) and (b), respectively). The Hájek estimator performs equally well regardless of whether true or estimated propensity scores are used, while the use of truncated weights leads to a slightly higher bias. Even in the most challenging scenario ($M = 7$), the average bias remains below 0.002 for the spatial moderator and below 0.007 for the spatio-temporal moderator, demonstrating that the Hájek estimators are essentially unbiased for commonly observed moderator values.

As the number of intervention time periods increases, the empirical coverage decreases slightly for certain moderator values, but it remains above 0.84 throughout for both types of moderators. Notably, estimators using the estimated propensity score tend to exhibit greater coverage compared to those based on the true propensity score. In the regions with limited data that are close to the moderator value of one, the estimated CATEs exhibit small biases, especially for difficult scenarios with $M = 7$. However, the empirical coverage remains robust across all scenarios, even in these sparse regions, demonstrating that the variance estimates account well for the limited information.

Appendix F includes additional simulation results. We examine the performance of the Hájek estimator for alternative CATE contrasts. We also include the results for the IPW estimators. While the two estimators perform similarly in low-variance cases with $M = 1$, the Hájek estimators outperform the IPW estimators in scenarios with $M = 3$ and $M = 7$. We find that the Hájek estimators consistently exhibit smaller variances across all simulation scenarios than the IPW estimators. Lastly, consistent with our theoretical result, the use of estimated propensity scores generally leads to efficiency gains over that



(a) Spatial moderator



(b) Spatio-temporal moderator

Figure 5: The average of estimated CATE (first row), bias (second row) and coverage (third row) based on Hájek estimators for $F_{h_1}^M$ versus $F_{h_3}^M$ across 500 simulations. Dashed lines in the first, second, and third rows represent the true CATE, bias of zero, and the nominal coverage of 95%, respectively. Plot (a) corresponds to the spatial moderator, while plot (b) pertains to the spatio-temporal moderator, both for $M = 1, 3, 7$. The purple line with triangles denotes the estimator based on the true propensity score, while the green line with diamonds and the blue line with squares represent the estimators based on the estimated propensity scores with and without truncation, respectively. The shaded region indicates the range between the 0.025 and 0.975 quantiles of the moderator values.

of the true propensity score.

5 Empirical Analysis

In this section, we evaluate the heterogeneity of treatment effects for the effects of airstrikes on insurgent violence in Iraq during the “surge” period between February 23, 2007 and July 5, 2008. We find that increasing the intensity of airstrikes for 7 to 10 days leads to a greater number of insurgent attacks, an effect that is more pronounced in regions that have received economic aid. The moderating effect of economic aid decreases once the amount per capita exceeds about 25 US dollars.

5.1 Setup

Our analysis focuses on the two most frequent types of insurgent attacks, improvised explosive devices (IED) and small arm fire (SAF). We analyze how the effects of US airstrikes on insurgent violence change with the amount of recent aid spending. In particular, we first consider as a moderator a binary indicator for whether a district received any US aid spending in the previous month. Then, we consider the aid spending per capita in the previous month as a continuous moderator.

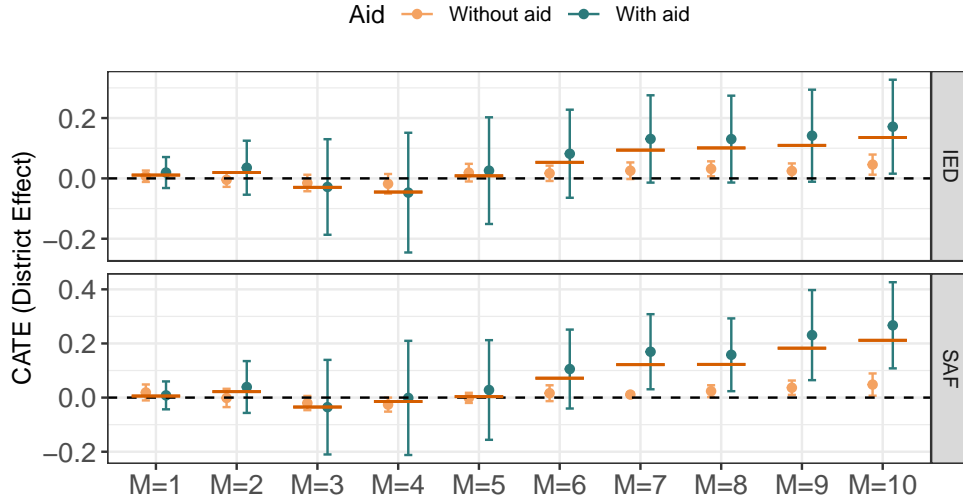
Following our simulation studies, we first estimate the baseline density of US airstrikes, denoted $\phi_0(\omega)$, using airstrikes prior to the 2007–2008 surge period. We then estimate the causal effect between the two stochastic interventions, $F_{h_1}^M$ versus $F_{h_2}^M$, where $h_1 = \phi_0(\omega)$ and $h_2 = 6\phi_0(\omega)$ for $M = 1, 2, \dots, 10$. That is, we are interested in estimating the effects of increasing the intensity of airstrikes sixfold for a period ranging from one to ten days. The scaling factor is determined based on the 25th and 75th percentiles of the observed number of airstrikes, ensuring overlap between the counterfactual and observed distributions.

5.2 Findings

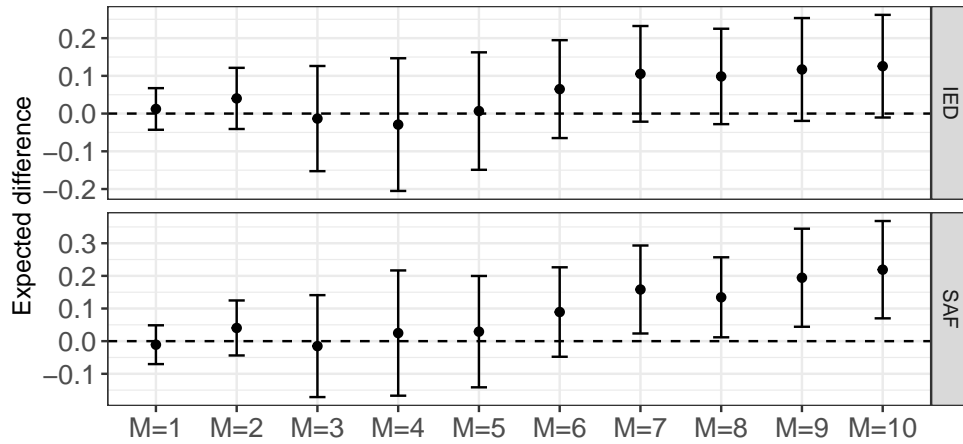
Our propensity score model is a non-homogeneous Poisson point process with intensity $\lambda(\omega) = \boldsymbol{\beta}^\top \mathbf{X}_t(\omega)$, where $\mathbf{X}_t(\omega)$ includes temporal splines, an indicator for a surge period of airstrikes, and 32 spatial or spatio-temporal surfaces. The spatio-temporal surfaces correspond to observed airstrikes, insurgent attacks, and shows of force (i.e., simulated bombing raids designed to deter insurgents) patterns from the last day, week, and month (9 surfaces), and the amount of aid spent (in US dollars) in each Iraqi district in the past month (1 surface). Time-invariant spatial covariates include distance from major cities, road networks and rivers (3 surfaces), population size (logged, measured in 2003; 1 surface), and distances from local settlements in each of the Iraqi districts (18 surfaces). In Appendix G.1, we evaluate the appropriateness of the propensity score model using out-of-sample prediction, and find that the fitted model captures the general trend of airstrikes in different governorates.

Using the estimated propensity scores, we construct the pseudo-outcomes after truncating the IPW weights at the 95th percentile and based on the stabilized weights. For our analysis, we divide Iraq into a grid of 128×128 equally sized rectangular pixels, with each pixel measuring a geographical area of approximately 9 km by 8 km. We compute pseudo-outcomes for each pixel, and the moderator value is assigned based on the Iraqi district to which the pixel’s centroid belongs. The choice of a 128×128 grid reflects a reasonable balance between computational cost and spatial resolution.

For the analysis with binary aid, we consider the model $\tau_{t, \mathbf{h}_1, \mathbf{h}_2}(r; \boldsymbol{\beta}_t) = \beta_{t,0} + \beta_{t,1}r$ for each time period, where r is the indicator variable for receiving aid in the previous month. Given that the moderator is a binary variable, we need not consider the possibility of model misspecification in this case. Under this model, the CATE, $\frac{1}{T-M+1} \sum_{t=M}^T \beta_{t,1}$,



(a) Estimated CATE



(b) Expected difference

Figure 6: Results for the binary aid moderator. Plot (a) shows the estimated CATEs of increasing airstrike intensity on the number of insurgency attacks (Improvised Explosive Device or IED in the top panel, and Small Arms Fire or SAF in the bottom panel) a district with or without aid in the previous month. The red line segments indicate the average treatment effect, scaled to be at the average district size. Plot (b) shows the estimated difference in the CATEs between a district that received aid in the previous month and those that did not. The corresponding 95% confidence intervals are also shown for all estimators.

represents the average difference, between pixels that received aid in the previous month and those that did not, in the effect of changing the stochastic intervention from $F_{h_1}^M$ to $F_{h_2}^M$. We multiply this value by the average number of pixels in a district, so that estimated quantities are interpreted as the estimated average moderation effect at the district level.

Figure 6a presents the estimated CATEs and 95% confidence intervals for $r = 0$ and $r = 1$, for interventions that span from 1 day to 10 days. It also includes the estimated average treatment effect scaled by the average number of pixels within a district. The results of IED and SAF attacks show similar patterns, suggesting that an increase in airstrikes over multiple consecutive days leads to an increase in subsequent insurgent violence. Districts with aid would experience a significant increase in SAF attacks for an increase in airstrikes spanning at least 7 days, while districts with or without aid would respond with a statistically significant increase in IED attacks for interventions spanning 10 days.

Importantly, the estimated CATE for $r = 1$ is higher than that for $r = 0$ in most cases, indicating that locations which received aid in the previous month exhibit stronger responses to intensified airstrikes. Figure 6b shows the difference in the estimated CATE for $r = 0$ and 1 with 95% confidence intervals. The confidence intervals are calculated based on Equation (6). For IED, the estimation uncertainty is too large to draw a definitive conclusion about whether regions with and without aid exhibit different reactions to the increase of airstrikes. For SAF, however, the estimated difference is positive and statistically significant for the intervention period of at least seven days. This finding suggests that when the intervention period is sufficiently long, increasing the intensity of airstrikes sixfold relative to the baseline leads to a greater number of insurgent attacks in a district that received aid in the previous month compared to a district that did not receive aid.

Since the baseline distribution of airstrikes is not uniform across space, increasing airstrike intensity relative to the baseline leads to some regions experiencing a greater increase in airstrikes than others. Figure 7a illustrates the estimated difference in the average number of airstrikes per district between the two interventions. One concern is that the significant differences observed in Figure 6b might be driven by this uneven increase

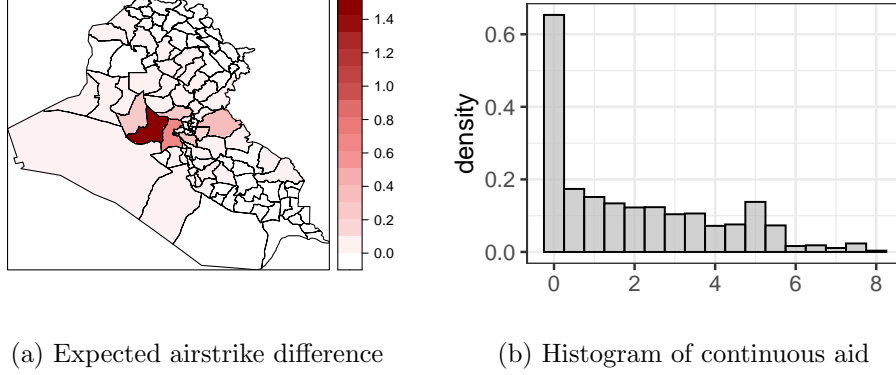


Figure 7: Panel (a) shows the expected changes in number of airstrikes under intervention $F_{h_2}^M$ over intervention $F_{h_1}^M$ for each district. Plot (b) shows the histogram of the continuous aid in the log scale

in airstrike intensity. To address this, we incorporate the expected difference in airstrikes into the regression model and perform the analysis while controlling for this expected difference. Most of the results remain consistent. The confidence interval for the CATE for $r = 0$ becomes wider, but the difference between the CATE for $r = 0$ and $r = 1$ becomes significant for IED when airstrike intensity is increased sixfold for 10 days after controlling for the expected difference in airstrikes. Detailed results are provided in Appendix G.4.

We shift our focus to the analysis of aid per capita. The histogram of continuous aid across all pixels (Figure 7b) reveals that many pixels have a value of 0 aid during some time periods. To account for this, we include an indicator for zero aid in our working model. Consistent with simulation studies, we use four natural cubic spline basis functions, $z_l(r)$, based on strictly positive aid values, using equally spaced knots. Additionally, we set $z_l(0) = 0$ for $l = 1, \dots, 4$. In summary, we consider the following working model:

$$\tau_{t, \mathbf{h}_1, \mathbf{h}_2}^{\text{Proj.}}(r; \beta_t) = \beta_{t,0} + \sum_{l=1}^4 \beta_{t,l} z_l(r) + \beta_{t,5} I\{r = 0\},$$

where r represent the aid per capita received during the previous month. We consider the

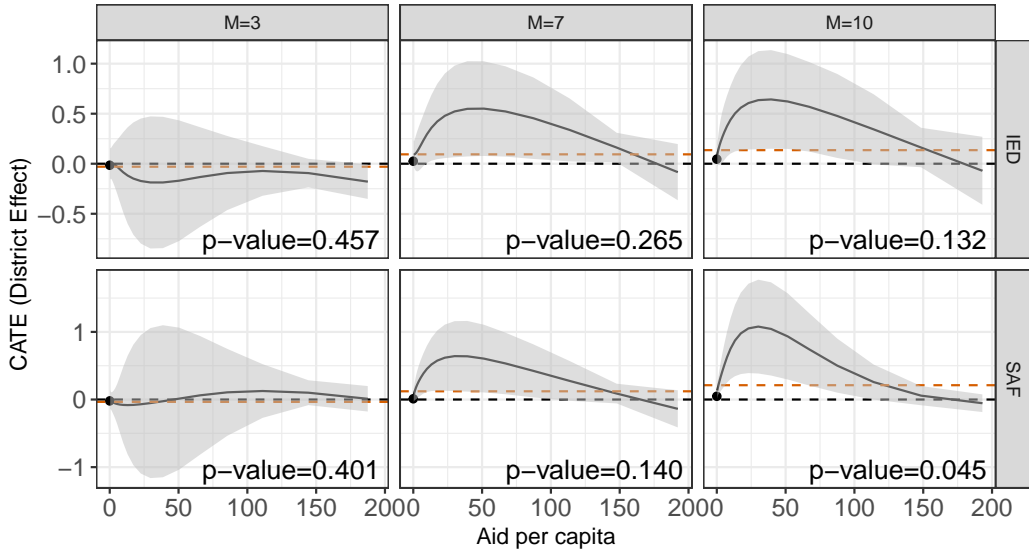


Figure 8: Estimated CATEs of increasing airstrike intensity on the number of insurgency attacks (Improvised Explosive Device or IED in the top panel, and Small Arms Fire or SAF in the bottom panel) for different values of aid per capita received in the previous month with the shaded region indicating the 95% confidence intervals. The red lines represent the estimated average treatment effects. The p-values correspond to tests for the overall heterogeneity effect.

projection CATE under this model and multiply all the estimates by the average number of pixels in a district to obtain a district-level effect.

Figure 8 displays the estimated CATEs for varying amounts of prior aid r , along with the average treatment effect when the expected number of airstrikes over the previous M days increases from one to six per day. The p-values on the plot correspond to tests for the overall heterogeneous effect, with their calculation detailed in Section 3.6. The results show similar patterns for both IED and SAF attacks. The average treatment effects are positive for $M = 7$ and $M = 10$, increasing as the intervention duration extends. For interventions lasting three days, the estimated CATE is relatively constant with the amount of economic aid per capita. However, for interventions lasting one week and 10 days, the estimated CATE increases as the amount of aid per capita rises from \$0 to \$25, followed by a gradual decline as the aid increases from \$25 to \$200. There is statistical evidence for the

heterogeneous effect of increasing airstrikes on SAF attacks (p-value < 0.05), highlighting that areas with different levels of prior aid respond differently to increased air strikes.

We evaluate the robustness of our findings to alternative specifications (Appendix G). First, we examine the heterogeneity of the treatment effect with respect to the aid covariates defined based on the previous two weeks or the previous two months. The results are overall consistent, showing the largest estimated CATE with the widest confidence interval for aid spending during the previous two weeks. For example, the estimated CATE for IED attacks when increasing airstrike intensity over 10 days is 0.20 for a district that received aid during the previous two weeks, compared to 0.15 for a district that received aid during the previous two months. Secondly, we investigate the robustness of the results to the truncation level of the inverse probability weights. We note that the results are sensitive to this choice. We observe that truncation at larger quantiles results in larger estimated CATE values and wider confidence intervals. Moreover, the heterogeneity effect becomes significant in some cases. However, the general patterns observed across all these analyses remain similar.

In sum, intensifying airstrikes for one week or more leads to a greater number of insurgent attacks. Among districts with relatively low levels of aid, those that have received a greater amount of aid in the previous month tend to exhibit a stronger response to intensified airstrikes. However, when the amount of aid is sufficiently large, increasing the intensity of airstrikes appears to have a smaller effect on the number of insurgent attacks.

6 Discussion

In this paper, we have introduced a method for analyzing treatment effect heterogeneity in spatio-temporal settings. The proposed method estimates the conditional average treatment effect without imposing structural assumptions about interference. We established the asymptotic normality of our two-stage estimator, and developed a statistical test of

no treatment effect heterogeneity. We have evaluated the performance of the proposed estimator through realistic simulation studies and demonstrated the method in the study of airstrikes and insurgent violence in Iraq.

Our empirical application shows that airstrikes increased insurgent attacks in the short term, even when aid had been disbursed in the prior month at substantial levels (up to \$25 per capita). Aid moderated these negative effects somewhat, but only after high and likely unsustainable levels of aid had been delivered. In addition, these large aid outlays were only sufficient to offset the increased attacks created by the airstrikes themselves. Taken together, our findings question whether aid and airstrikes, the two central planks in counterinsurgency, actually work to reduce short-term insurgent attacks.

There are several possible directions for future research. First, while we considered static intervention distributions across time periods, one may explore adaptive treatment assignment strategies that depend on previous outcomes. Second, the asymptotic properties derived in this paper rely on the correct specification of the propensity score model. Future work could explore estimators that are more robust to model misspecification. Finally, while we employed a parametric propensity score model, future research could incorporate semi-parametric or nonparametric models into our framework.

References

- (2007). U.s. army field manual no.3-24. University of Chicago Press, Chicago.
- Abrevaya, J., Y.-C. Hsu, and R. P. Lieli (2015). Estimating conditional average treatment effects. *Journal of Business & Economic Statistics* 33(4), 485–505.
- ACLED (2020). The armed conflict location and event data project.
- Athey, S., J. Tibshirani, and S. Wager (2019). Generalized random forests.

- Bardaka, E., M. S. Delgado, and R. J. Florax (2018). Causal identification of transit-induced gentrification and spatial spillover effects: The case of the denver light rail. *Journal of Transport Geography* 71, 15–31.
- Bargagli-Stoffi, F. J., C. Tortù, and L. Forastiere (2020). Heterogeneous treatment and spillover effects under clustered network interference. *arXiv preprint arXiv:2008.00707*.
- Barkley, B. G., M. G. Hudgens, J. D. Clemens, M. Ali, and M. E. Emch (2020). Causal inference from observational studies with clustered interference, with application to a cholera vaccine study.
- Berman, E., J. Shapiro, and J. Felter (2011). Can hearts and minds be bought? the economics of counterinsurgency in iraq. *Journal of Political Economy* 119, 766–819.
- Bind, M.-A. (2019). Causal modeling in environmental health. *Annual review of public health* 40, 23–43.
- Brunello, G., M. Fort, N. Schneeweis, and R. Winter-Ebmer (2016). The causal effect of education on health: What is the role of health behaviors? *Health economics* 25(3), 314–336.
- Christia, F., S. Zoumpoulis, M. Freedman, L. Yao, and A. Jadbabaie (2022). The effect of drone strikes on civilian communication: Evidence from yemen. *Political Science Research and Methods* 10(2), 419–427.
- Christiansen, R., M. Baumann, T. Kuemmerle, M. D. Mahecha, and J. Peters (2022). Toward causal inference for spatio-temporal data: conflict and forest loss in colombia. *Journal of the American Statistical Association* 117(538), 591–601.

- Credit, K. and M. Lehnert (2023). A structured comparison of causal machine learning methods to assess heterogeneous treatment effects in spatial data. *Journal of Geographical Systems*, 1–28.
- Crost, B., J. Felter, and P. Johnston (2014). Aid under fire: Development projects and civil conflict. *American Economic Review* 104(6), 1833–1856.
- Csörgő, M. (1968). On the strong law of large numbers and the central limit theorem for martingales. *Transactions of the American Mathematical Society* 131(1), 259–275.
- Dell, M. and P. Querubin (2018). Nation building through foreign intervention: Evidence from discontinuities in military strategies. *American Economic Review* 133(2), 701–64.
- Ding, P., A. Feller, and L. Miratrix (2019). Decomposing treatment effect variation. *Journal of the American Statistical Association* 114(525), 304–317.
- Fan, Q., Y.-C. Hsu, R. P. Lieli, and Y. Zhang (2022). Estimation of conditional average treatment effects with high-dimensional data. *Journal of Business & Economic Statistics* 40(1), 313–327.
- Giffin, A., B. Reich, S. Yang, and A. Rappold (2023). Generalized propensity score approach to causal inference with spatial interference. *Biometrics* 79(3), 2220–2231.
- Hahn, P. R., J. S. Murray, and C. M. Carvalho (2020). Bayesian regression tree models for causal inference: Regularization, confounding, and heterogeneous effects (with discussion). *Bayesian Analysis* 15(3), 965–1056.
- Hirano, K., G. W. Imbens, and G. Ridder (2003). Efficient estimation of average treatment effects using the estimated propensity score. *Econometrica* 71(4), 1161–1189.

- Imai, K. and M. Ratkovic (2013, March). Estimating treatment effect heterogeneity in randomized program evaluation. *Annals of Applied Statistics* 7(1), 443–470.
- Johnston, P. and A. Sarbahi (2016). The impact of us drone strikes on terrorism in pakistan. *International Studies Quarterly* 60(2), 203–219.
- Kennedy, E. H. (2020). Towards optimal doubly robust estimation of heterogeneous causal effects. *arXiv preprint arXiv:2004.14497*.
- Kennedy, E. H., S. Lorch, and D. S. Small (2019). Robust causal inference with continuous instruments using the local instrumental variable curve. *Journal of the Royal Statistical Society Series b: Statistical Methodology* 81(1), 121–143.
- Kocher, M., T. Pepinsky, and S. Kalyvas (2011). Aerial bombing and counterinsurgency in the vietnam war. *American Journal of Political Science* 55(2), 201–218.
- Kolak, M. and L. Anselin (2020). A spatial perspective on the econometrics of program evaluation. *International Regional Science Review* 43(1-2), 128–153.
- Lyall, J. (2019a). Bombing to lose? airpower and the dynamics of coercion in counterinsurgency wars. *Unpublished Manuscript*.
- Lyall, J. (2019b). Civilian casualties, humanitarian aid, and insurgent violence in civil wars. *International Organization* 73, 901–26.
- Meierrieks, D. and T. Gries (2013). Causality between terrorism and economic growth. *Journal of Peace Research* 50(1), 91–104.
- Papadogeorgou, G., K. Imai, J. Lyall, and F. Li (2022). Causal inference with spatio-temporal data: estimating the effects of airstrikes on insurgent violence in iraq. *Journal of the Royal Statistical Society Series B: Statistical Methodology* 84(5), 1969–1999.

- Papadogeorgou, G., F. Mealli, and C. M. Zigler (2019). Causal inference with interfering units for cluster and population level treatment allocation programs. *Biometrics* 75(3), 778–787.
- Rigterink, A. (2021). The wane of command: Evidence on drone strikes and control within terrorist organizations. *American Political Science Review* 115(1), 31–50.
- Robins, J. M., M. A. Hernan, and B. Brumback (2000). Marginal structural models and causal inference in epidemiology. *Epidemiology*, 550–560.
- Special Inspector General for Iraqi Reconstruction (2013). *Learning from Iraq: A Final Report from the Special Inspector General for Iraq Reconstruction*. Washington, D.C.: SIGIR.
- Tchetgen Tchetgen, E. J., I. R. Fulcher, and I. Shpitser (2021). Auto-g-computation of causal effects on a network. *Journal of the American Statistical Association* 116(534), 833–844.
- United States Army (2019). *The Surge, 2007-2008: The U.S. Army Campaigns in Iraq*. Washington, D.C.: U.S. Army Center of Military History.
- van der Laan, M. J., S. Rose, et al. (2011). *Targeted learning: causal inference for observational and experimental data*, Volume 4. Springer.
- van der Vaart, A. W. (2010). Time series. *VU University Amsterdam, lecture notes*.
- Wang, L., A. Adiga, J. Chen, A. Sadilek, S. Venkatramanan, and M. Marathe (2022). Causalgnn: Causal-based graph neural networks for spatio-temporal epidemic forecasting. In *Proceedings of the AAAI conference on artificial intelligence*, Volume 36, pp. 12191–12199.

- Wang, Y. (2021). Causal inference under temporal and spatial interference. *arXiv preprint arXiv:2106.15074*.
- Wang, Y., C. Samii, H. Chang, and P. Aronow (2020). Design-based inference for spatial experiments with interference. *arXiv preprint arXiv:2010.13599*.
- Wodtke, G., K. Ard, C. Bulluck, K. White, and B. Priem (2022). Concentrated poverty, ambient air pollution, and child cognitive development. *Science Advances* 8(48), 1–19.
- Yang, Y., A. K. Kuchibhotla, and E. T. Tchetgen (2023). Forster-warmuth counterfactual regression: A unified learning approach. *arXiv preprint arXiv:2307.16798*.
- Zhang, W. and K. Ning (2023). Spatiotemporal heterogeneities in the causal effects of mobility intervention policies during the covid-19 outbreak: A spatially interrupted time-series (SITS) analysis. *Annals of the American Association of Geographers* 113(5), 1112–1134.
- Zigler, C. M., K. Watts, R. W. Yeh, Y. Wang, B. A. Coull, and F. Dominici (2013). Model feedback in bayesian propensity score estimation. *Biometrics* 69(1), 263–273.
- Zürcher, C., P. Labelle, L. Borges, K. Hoare, M. A. Javid, K. Kavanagh, S. Sarna, and E. Woolner (2022, November). Impact of aid in highly fragile states: A synthesis of three systematic reviews of aid to afghanistan, mali, and south sudan, 2008-2021.

SUPPLEMENTARY APPENDIX FOR “ESTIMATING HETEROGENEOUS TREATMENT EFFECTS FOR SPATIO-TEMPORAL CAUSAL INFERENCE”

Table of Contents

A	Table of notation	3
B	Asymptotic properties of the IPW estimator	3
B.1	Regularity conditions	4
B.2	Asymptotic normality	6
B.3	Consistent estimation of variance bound for the IPW estimator	7
B.4	Proof of Theorem A.1	7
B.5	Proof of Proposition A.1	9
B.6	Proof of Theorem A.2	9
B.7	Proof of Theorem A.3	16
B.8	Proof of Corollary A.1	17
C	Asymptotic properties of the Hájek estimator	17
C.1	Regularity conditions	17
C.2	Asymptotic normality	18
C.3	Consistent estimation of variance bound for the Hájek-estimator	19
C.4	Proof of Theorem A.4	19
C.5	Proof of Proposition A.2	21

C.6	Proofs of Theorem 1 and Corollary 1	22
D	Consistent estimation of variance bound for the Hájek estimator	22
D.1	A Consistent estimator	22
D.2	Empirical performance of the proposed estimator	23
E	Statistical test of no heterogeneity	25
E.1	Proof of Lemma A.2	25
E.2	Proof of Theorem 3	25
F	Additional simulation results	27
F.1	The Hájek estimator	27
F.2	The IPW estimator	28
F.3	Efficiency due to the use of the estimated propensity score	31
F.4	Efficiency comparison of IPW and Hájek estimators	31
G	Additional results for the empirical application	36
G.1	Out-of-sample prediction for propensity scores	36
G.2	Different moderator definitions	36
G.3	Sensitivity to truncation levels of the estimated propensity scores	39
G.4	Additional analysis for the binary moderator	44

A Table of notation

Definitions for notations used in the manuscript are given in Table A.1.

Table A.1: Table of Notation

	Symbol	Description
Paths	$\overline{\mathbf{W}}_t$	Treatment over the time periods $1, \dots, t$
	$\overline{\mathbf{w}}_t$	Realized treatment assignments for time periods $1 \dots, t$
	$\overline{\mathbf{Y}}_t$	Collection of all potential outcomes for time periods $1 \dots, t$
	$\overline{\mathbf{Y}}_t$	Observed outcomes for time periods $1 \dots, t$
Covariates	$\overline{\mathcal{X}}_t$	Collection of all potential values of confounders over the time periods $1, \dots, t$
	$\overline{\mathbf{X}}_t$	Observed confounders for time periods $1 \dots, t$
	\mathbf{R}_t	Observed values of moderators for time periods $1 \dots, t$
History	\overline{H}_t	Observed history preceding the treatment at time $t + 1$
	\overline{H}_t^*	Complete history including all counterfactual values
Intervention	M	The number of time periods over which we intervene
	h	Poisson point process intensity defining the stochastic intervention
Estimands	$N_{it}(F_{\mathbf{h}})$	The expected number of outcome events in pixel S_i at time t for an intervention with intensity \mathbf{h}
	$\tau_{it}(F_{\mathbf{h}'}, F_{\mathbf{h}''})$	Expected difference in the number of outcome events for interventions $F_{\mathbf{h}'}$ over interventions $F_{\mathbf{h}''}$ at time t in pixel S_i
	$\tau_{t, \mathbf{h}', \mathbf{h}''}(\mathbf{r})$	The conditional average treatment effect of intervention with intensity \mathbf{h}' v.s. intervention with intensity \mathbf{h}'' for time period t
	$\tau_{t, \mathbf{h}', \mathbf{h}''}^{\text{Proj.}}(\mathbf{r}; \boldsymbol{\beta}_t)$	The projected conditional average treatment effect for time period t
	$\tau_{\mathbf{h}', \mathbf{h}''}^{\text{Proj.}}(\mathbf{r}; \boldsymbol{\beta}_1, \dots, \boldsymbol{\beta}_T)$	Conditional average treatment effect of intervention $F_{\mathbf{h}'}$ over $F_{\mathbf{h}''}$
Estimators	$\hat{\boldsymbol{\beta}}^I$	The IPW estimator for $\boldsymbol{\beta}_t$
	$\hat{\boldsymbol{\beta}}^H$	The Hajek estimator for $\boldsymbol{\beta}_t$

B Asymptotic properties of the IPW estimator

In this section, we present the asymptotic properties of the IPW estimator. We first formally present the regularity conditions (Appendix B.1) and then show the asymptotic normality, the variance bound, and its consistent estimation (Appendix B.2 and Ap-

pendix B.3). Those results are similar to the results for the Hájek estimator shown in Section 3.5.

B.1 Regularity conditions

We first state the regularity assumptions for establishing the asymptotic normality of the IPW estimator when the true propensity score is known.

Assumption A.1 (Regularity conditions for the IPW estimator with the true propensity score). *The following two conditions hold.*

- (a) *(Bounded outcome and covariates) There exist positive constants $\delta_Y, \delta_z < \infty$ such that $N_\Omega(Y_t) < \delta_Y$ and $|z_j(\mathbf{R}_t)| < \delta_z$ for all $j \in \{1, \dots, L\}$, $Y_t \in \bar{\mathcal{Y}}_T$ and $\mathbf{R}_t \in \bar{\mathcal{X}}_T$.*
- (b) *(Non-singularity and asymptotic variance) For all t , $\mathbf{Z}_t^\top \mathbf{Z}_t$ is non-singular and there exists a positive definite matrix $\tilde{\mathbf{V}}^I$ such that*

$$\frac{1}{T - M + 1} \sum_{t=M}^T \mathbb{V}[\mathbf{A}_t \mid \bar{H}_{t-M}^*] \xrightarrow{p} \tilde{\mathbf{V}}^I$$

as $T \rightarrow \infty$, where $\mathbf{A}_t = (\mathbf{Z}_t^\top \mathbf{Z}_t)^{-1} \mathbf{Z}_t^\top \tilde{\boldsymbol{\tau}}_t^I(\boldsymbol{\gamma}^*)$

Assumption A.1.(a) states that there exist uniform upper bounds on the number of outcome events and the absolute value of the moderator over all time period. In our empirical application, it is reasonable to assume that the number of insurgent attacks occurring in Iraq and the amount of aid does not diverge to infinity as t increases. Assumption A.1.(b) requires that the moderators for each time period are linearly independent and that the sequence of covariance matrices converges to a positive definite matrix. The assumption about the convergence of the covariance matrix is relatively mild, given that the random vector \mathbf{A}_t is bounded above and bounded away from $\mathbf{0}$.

The following two sets of assumptions are needed for the asymptotic normality of the IPW estimator with the estimated propensity score. Those assumptions are also made in Papadogeorgou et al. (2022). The first set of assumptions is about the behavior of the propensity score model.

Assumption A.2 (Regularity conditions for the propensity score model). *Assume that the parametric form of the propensity score indexed by $\boldsymbol{\gamma}$, $f(W_t = w_t \mid \bar{H}_{t-1}; \boldsymbol{\gamma})$, is correctly specified and differentiable with respect to $\boldsymbol{\gamma} \in \mathbb{R}^K$, and let*

$$\psi(W_t, \bar{H}_{t-1}; \boldsymbol{\gamma}) = \frac{\partial}{\partial \boldsymbol{\gamma}} \log f(W_t = w_t \mid \bar{H}_{t-1} = \bar{h}_{t-1}; \boldsymbol{\gamma})$$

be twice continuously differentiable score functions. Let γ^* denote the true values of the parameters, where γ^* is in an open subset of the Euclidean space. Denote $\mathcal{F}_t = \overline{H}_{t-M+1}^*$. We assume that the following conditions hold:

1. (a) $\mathbb{E}_{\gamma^*} \left[\|\psi(W_t, \overline{H}_{t-1}; \gamma^*)\|^2 \right] < \infty,$

(b) There exists a positive definite matrix \mathbf{V}_{ps} such that

$$\frac{1}{T} \sum_{t=1}^T \mathbb{E}_{\gamma^*} \left(\psi(W_t, \overline{H}_{t-1}; \gamma^*) \psi(W_t, \overline{H}_{t-1}; \gamma^*)^\top \mid \mathcal{F}_{t-1} \right) \xrightarrow{p} \mathbf{V}_{ps}$$

(c) $\frac{1}{T} \sum_{t=1}^T \mathbb{E}_{\gamma^*} \left[\|\psi(W_t, \overline{H}_{t-1}; \gamma^*)\|^2 I \left(\|\psi(W_t, \overline{H}_{t-1}; \gamma^*)\| > \epsilon \sqrt{T} \right) \mid \mathcal{F}_{t-1} \right] \xrightarrow{p} 0,$ for all $\epsilon > 0$, as $T \rightarrow \infty$.

2. For all k, j , if we denote the k^{th} element of the $\psi(w_t, \overline{H}_{t-1}; \gamma)$ vector by $\psi_k(w_t, \overline{H}_{t-1}; \gamma)$ and $P_{kjt} = \frac{\partial}{\partial \gamma_j} \psi_k(W_t, \overline{H}_{t-1}; \gamma) \mid \gamma^*$, then $\mathbb{E}_{\gamma^*} [|P_{kjt}|] < \infty$ and there exists $0 < r_{kj} \leq 2$ such that $\sum_{t=1}^T \frac{1}{t^{r_{kj}}} \mathbb{E}_{\gamma^*} (|P_{kjt} - \mathbb{E}_{\gamma^*}(P_{kjt} \mid \mathcal{F}_{t-1})|^{r_{kj}} \mid \mathcal{F}_{t-1}) \xrightarrow{p} 0$

3. There exists an integrable function $\ddot{\psi}(w_t, \overline{h}_{t-1})$ such that $\ddot{\psi}(w_t, \overline{h}_{t-1})$ dominates the second partial derivatives of $\psi(w_t, \overline{h}_{t-1}; \gamma)$ in a neighborhood of γ^* for all $(w_t, \overline{h}_{t-1})$

Assumption A.2 states that the model is correctly specified and the score function is bounded in the L^2 -norm. Moreover, the average expectation of the product of the score function with itself over all time periods stabilizes to a specific positive definite matrix. The assumption also limits the extent to which the derivative of the score function varies around its conditional expectation. Lastly, the assumption ensures that the second partial derivatives of the score function are bounded in magnitude by an integrable function, which controls their growth and guarantees stability in a neighborhood of γ^* .

Assumption A.3 (Regularity conditions on the score function of propensity score model for IPW estimators). Let $\tilde{\tau}_t^I(\gamma)$ denote the pseudo-effect depend on the parameter γ . For

$$s(\overline{H}_{t-1}, W_t, Y_t; \gamma) = (\mathbf{Z}_t^\top \mathbf{Z}_t)^{-1} \mathbf{Z}_t^\top \tilde{\tau}_t^I(\gamma) - \beta_t^*,$$

and a propensity score function $\psi(W_t, \overline{H}_{t-1}; \gamma)$ satisfying Assumption A.2, the following conditions hold.

(a) There exists $\mathbf{U} \in \mathbb{R}^{K \times L}$ such that

$$\frac{1}{T - M + 1} \sum_{t=M}^T \mathbb{E}_{\gamma^*} [\psi(W_t, \overline{H}_{t-1}; \gamma^*) s(\overline{H}_{t-1}, W_t, Y_t; \gamma^*)^\top \mid \overline{H}_{t-M}^*] \xrightarrow{p} \mathbf{U}, \text{ and}$$

$$\mathbf{V}^* = \begin{bmatrix} \tilde{\mathbf{V}}^I & \mathbf{U}^\top \\ \mathbf{U} & \mathbf{V}_{ps} \end{bmatrix} \text{ is positive definite.}$$

(b) If $P_{jt} = \frac{\partial}{\partial \gamma_j} s(\bar{H}_{t-1}, W_t, Y_t; \gamma) \Big|_{\gamma^*}$, where γ_j is the j^{th} entry of γ , then there exists $r_j \in (0, 2]$ such that

$$\frac{1}{T - M + 1} \sum_{t=M}^T \frac{1}{t^{r_j}} (|P_{jt} - \mathbb{E}_{\gamma^*}[P_{jt} | \bar{H}_{t-M}^*]|) \xrightarrow{p} 0.$$

Assumption A.3 regulates the behavior of function $s(\bar{H}_{t-1}, W_t, Y_t; \gamma)$ and the propensity score function. Specifically, it states that the average expectation of the outer product of $s(\bar{H}_{t-1}, W_t, Y_t; \gamma)$ and $s(\bar{H}_{t-1}, W_t, Y_t; \gamma)$ converges to a matrix as T grows and \mathbf{V}^* is positive definite. Furthermore, it limits how much the derivative of $s(\bar{H}_{t-1}, W_t, Y_t; \gamma)$ can vary around its conditional expectation.

B.2 Asymptotic normality

We now establish the asymptotic normality of the IPW estimator using the true and estimated propensity score.

Theorem A.1 (Asymptotic normality of the IPW estimator using the true propensity score). *Suppose that Assumptions 1, 2, and A.1. Then*

$$\frac{1}{\sqrt{T - M + 1}} \sum_{t=M}^T (\hat{\beta}_t^I - \beta_t^*) \xrightarrow{d} N(\mathbf{0}, \tilde{\mathbf{V}}^I),$$

where $\tilde{\mathbf{V}}^I$ represents the probability limit of $\frac{1}{T-M+1} \sum_{t=M}^T \mathbf{V}_t^I$ as $T \rightarrow \infty$ with $\mathbf{V}_t^I = \mathbb{V}[\hat{\beta}_t^I | \bar{H}_{t-M}^*]$ for $t \geq M$.

Theorem A.2 (Asymptotic normality of the IPW estimator using the estimated propensity score). *Suppose that Assumptions 1, 2, A.1, A.2, and A.3 hold. Let $\hat{\gamma}$ be the estimate obtained by solving the estimating equation $\sum_{t=M}^T \psi(W_t, \bar{H}_{t-1}; \gamma) = 0$, where $\psi(W_t, \bar{H}_{t-1}; \gamma)$ is defined in Assumption A.2. Then, as $T \rightarrow \infty$, we have*

$$\frac{1}{\sqrt{T - M + 1}} \sum_{t=M}^T (\hat{\beta}_t^I - \beta_t^*) \xrightarrow{d} N(\mathbf{0}, \mathbf{V}^I).$$

Theorem A.3 (Asymptotic efficiency of the IPW estimator using the estimated propensity score). *If the propensity score model is correctly specified, the estimator $\frac{1}{T-M+1} \sum_{t=M}^T \hat{\beta}_t^H$ based on the estimated propensity score has an asymptotic variance that is no greater than the asymptotic variance of the same estimator using the known propensity score. That is, for $\tilde{\mathbf{V}}^I$ defined in Theorem A.1 and \mathbf{V}^I defined in Theorem A.2, $(\tilde{\mathbf{V}}^I - \mathbf{V}^I)$ is a positive semidefinite matrix.*

B.3 Consistent estimation of variance bound for the IPW estimator

Similarly to the case of the Hájek estimator, it is not possible to consistently estimate the asymptotic variance of the IPW estimator. Thus, we consider a variance bound and propose a consistent estimator.

Proposition A.1 (Consistent estimator of the variance upper bound). *Suppose that Assumptions 1, 2, and A.1 hold. Let*

$$\hat{\mathbf{V}}^{I*} = \frac{1}{T - M + 1} \sum_{t=M}^T \hat{\boldsymbol{\beta}}_t^I \hat{\boldsymbol{\beta}}_t^{I\top}.$$

Then $\hat{\mathbf{V}}^{I*}$ is a consistent estimator of \mathbf{V}^{I*} .

Corollary A.1 (Consistent estimator of the variance upper bound using the estimated propensity score). *Suppose that Assumptions 1, 2, A.1, A.2, and A.3 hold. Moreover, let*

$$\hat{\mathbf{V}}^I = \frac{1}{T - M + 1} \sum_{t=M}^T \hat{\boldsymbol{\beta}}_t^I \hat{\boldsymbol{\beta}}_t^{I\top}$$

Then, $\hat{\mathbf{V}}^I$ is a consistent estimator of \mathbf{V}^{I*} .

B.4 Proof of Theorem A.1

We will apply Theorem A.2 of Papadogeorgou et al. (2022), which is a multivariate version of Theorem 4.16 of van der Vaart (2010). Define $\mathbf{A}_t^* = \mathbf{A}_t - \boldsymbol{\beta}_t^*$. We need to verify the existence of a filtration \mathcal{F}_t such that the following conditions hold:

1. $\mathbb{E}_{\boldsymbol{\beta}_t^*}[\mathbf{A}_t^* \mid \mathcal{F}_{t-1}] = 0$ and $\mathbb{E}_{\boldsymbol{\beta}_t^*}[\|\mathbf{A}_t^*\|] < \infty$.
2. There exists a positive definite $\tilde{\mathbf{V}}^I$ such that

$$\frac{1}{T - M + 1} \sum_{t=M}^T \mathbb{E}_{\boldsymbol{\beta}_t^*}[\mathbf{A}_t^* \mathbf{A}_t^{*\top} \mid \mathcal{F}_{t-1}] \xrightarrow{p} \tilde{\mathbf{V}}^I$$

- 3.

$$\frac{1}{T - M + 1} \sum_{t=M}^T \mathbb{E}_{\boldsymbol{\beta}_t^*} \left[\|\mathbf{A}_t^*\|^2 I \left(\|\mathbf{A}_t^*\| > \epsilon \sqrt{T} \right) \mid \mathcal{F}_{t-1} \right] \xrightarrow{p} 0$$

as $T \rightarrow \infty$ for all $\epsilon > 0$.

To check the first condition, take $\mathcal{F}_t = \overline{H}_{t-M+1}^*$. Then for a stochastic intervention $F_{\mathbf{h}}$ over M time periods,

$$\begin{aligned}
& \mathbb{E}_{\beta_t^*} \left[\tilde{Y}_{it}^I(F_{\mathbf{h}}; \hat{\gamma}) \mid \mathcal{F}_{t-1} \right] \\
&= \mathbb{E}_{\beta_t^*} \left[\prod_{j=t-M+1}^t \frac{f_{\mathbf{h}}(W_j)}{e_j(W_j)} N_{S_i}(Y_t) \mid \mathcal{F}_{t-1} \right] \\
&= \int_{\mathcal{W}^M} \prod_{j=t-M+1}^t \frac{f_{\mathbf{h}}(w_j)}{e_j(w_j)} N_{S_i}(Y_t(\overline{\mathbf{W}}_{t-M}, w_{t-M+1}, \dots, w_t)) \times \\
&\quad f(w_{t-M+1} \mid \overline{H}_{t-M}^*) f(w_{t-M+2} \mid \overline{H}_{t-M+1}^*) \dots f(w_t \mid \overline{H}_{t-1}^*) d\mathbf{w}_{(t-M+1):t} \\
&= \int_{\mathcal{W}^M} \prod_{j=t-M+1}^t \frac{f_{\mathbf{h}}(w_j)}{e_j(w_j)} N_{S_i}(Y_t(\overline{\mathbf{W}}_{t-M}, w_{t-M+1}, \dots, w_t)) \prod_{j=t-M+1}^t e_j(w_j) d\mathbf{w}_{(t-M+1):t} \\
&= \int_{\mathcal{W}^M} N_{S_i}(Y_t) \prod_{j=t-M+1}^t f_{\mathbf{h}}(w_j) d\mathbf{w}_{(t-M+1):t} \\
&= N_{it}(F_{\mathbf{h}}),
\end{aligned}$$

where the third equality follows from Assumption 1. Let $\mathbf{N}_t(F_{\mathbf{h}}) = (N_{1t}(F_{\mathbf{h}}), \dots, N_{pt}(F_{\mathbf{h}}))$, and $\tilde{\mathbf{Y}}_t^I(F_{\mathbf{h}}; \gamma) = \left(\tilde{Y}_{it}^I(F_{\mathbf{h}}; \gamma), \dots, \tilde{Y}_{pt}^I(F_{\mathbf{h}}; \gamma) \right)^\top$. Then

$$\begin{aligned}
(\mathbf{Z}_t^\top \mathbf{Z}_t)^{-1} \mathbf{Z}_t^\top \mathbb{E}_{\beta_t^*} [\tilde{\boldsymbol{\tau}}_t^I(\gamma^*) \mid \mathcal{F}_{t-1}] &= (\mathbf{Z}_t^\top \mathbf{Z}_t)^{-1} \mathbf{Z}_t^\top \mathbb{E}_{\beta_t^*} \left[\tilde{\mathbf{Y}}_t^I(F_{\mathbf{h}''}; \gamma) - \tilde{\mathbf{Y}}_t^I(F_{\mathbf{h}'}; \gamma) \mid \mathcal{F}_{t-1} \right] \\
&= (\mathbf{Z}_t^\top \mathbf{Z}_t)^{-1} \mathbf{Z}_t^\top (\mathbf{N}_t(F_{\mathbf{h}''}) - \mathbf{N}_t(F_{\mathbf{h}'})) \\
&= \beta_t^*.
\end{aligned}$$

Thus,

$$\begin{aligned}
\mathbb{E}_{\beta_t^*} [\mathbf{A}_t^* \mid \mathcal{F}_{t-1}] &= (\mathbf{Z}_t^\top \mathbf{Z}_t)^{-1} \mathbf{Z}_t^\top \mathbb{E}_{\beta_t^*} [\tilde{\boldsymbol{\tau}}_t^I(\gamma^*) - \beta_t^* \mid \mathcal{F}_{t-1}] \\
&= \beta_t^* - \beta_t^* \\
&= \mathbf{0}
\end{aligned}$$

Moreover, by Assumptions 2 and A.1(a), each term in \mathbf{A}_t^* is bounded, and so is $\mathbb{E}_{\beta_t^*} [\|\mathbf{A}_t^*\|]$.

Next, Condition 2 is satisfied by Assumption A.1(b), while Condition 3 follows from the fact that $\mathbb{E}_{\beta_t^*} [\|\mathbf{A}_t^*\|^2 \mid \mathcal{F}_{t-1}]$ is bounded. Hence, as $T \rightarrow \infty$, we have,

$$\frac{1}{\sqrt{T-M+1}} \sum_{t=M}^T \mathbf{A}_t^* \xrightarrow{d} N(\mathbf{0}, \mathbf{V})$$

and

$$\frac{1}{T-M+1} \sum_{t=M}^T \mathbb{E}_{\beta_t^*} [\mathbf{A}_t^* \mathbf{A}_t^{*\top} \mid \mathcal{F}_{t-1}] = \frac{1}{T-M+1} \sum_{t=M}^T \mathbb{V}[\mathbf{A}_t \mid \mathcal{F}_{t-1}] \xrightarrow{p} \tilde{\mathbf{V}}^I.$$

Note that

$$\frac{1}{\sqrt{T-M+1}} \sum_{t=M}^T \mathbf{A}_t^* = \frac{1}{\sqrt{T-M+1}} \sum_{t=M}^T (\hat{\beta}_t^I - \beta_t^*)$$

Thus, as $T \rightarrow \infty$, we have:

$$\frac{1}{\sqrt{T-M+1}} \sum_{t=M}^T (\hat{\beta}_t^I - \beta_t^*) \xrightarrow{d} N(\mathbf{0}, \tilde{\mathbf{V}}^I).$$

□

B.5 Proof of Proposition A.1

Let $\hat{\mathbf{V}}_t^I = \hat{\beta}_t^I \hat{\beta}_t^{I\top}$ and $\mathbf{V}_t^I = \mathbb{E}_{\beta_t^*} [\hat{\beta}_t^I \hat{\beta}_t^{I\top} \mid \bar{H}_{t-M}^*]$. Consider the sequence $\hat{\mathbf{V}}_t^I - \mathbf{V}_t^I$. Note that $\mathbb{E}[\hat{\mathbf{V}}_t^I - \mathbf{V}_t^I \mid \bar{H}_{t-M}^*] = 0$. Since $\hat{\mathbf{V}}_t^I - \mathbf{V}_t^{I*}$ is bounded, $\mathbb{E}|\hat{\mathbf{V}}_t^I - \mathbf{V}_t^{I*}| < \infty$. Also, $\sum_{t=1}^{\infty} t^{-2} \mathbb{E}[(\hat{\mathbf{V}}_t^I - \mathbf{V}_t^{I*})^2] < \infty$. Then, Theorem 1 of Csörgő (1968) implies:

$$\frac{1}{T-M+1} \sum_{t=M}^T (\hat{\mathbf{V}}_t^I - \mathbf{V}_t^{I*}) = \frac{1}{T-M+1} \sum_{t=M}^T \hat{\mathbf{V}}_t^I - \frac{1}{T-M+1} \sum_{t=M}^T \mathbf{V}_t^{I*} \xrightarrow{p} 0.$$

Since \mathbf{V}^{I*} is the probability limit of $\frac{1}{T-M+1} \sum_{t=M}^T \mathbf{V}_t^{I*}$ as $T \rightarrow \infty$, we have $\frac{1}{T-M+1} \sum_{t=M}^T \hat{\mathbf{V}}_t^I \xrightarrow{p} \mathbf{V}^{I*}$. □

B.6 Proof of Theorem A.2

We begin by introducing the following lemma. The proof of this lemma is omitted because it is similar to that of Lemma A.2 given in Papadogeorgou et al. (2022).

Lemma A.1. *Suppose that Assumption 1 holds. Let $\psi(w_t, \bar{h}_{t-1}; \gamma)$ be the score functions of a propensity score model that satisfy Assumption A.2. Recall the definition of $s(\bar{H}_{t-1}, W_t, Y_t; \gamma)$ given in Assumption A.3. Let $\mathcal{F}_t = \bar{H}_{t-M+1}^*$. Then, we have*

1. $\mathbb{E}_{\gamma^*} [s(\bar{H}_{t-1}, W_t, Y_t; \gamma^*) \psi(W_t, \bar{H}_{t-1}; \gamma^*)^\top \mid \mathcal{F}_{t-1}] = -\mathbb{E}_{\gamma^*} \left[\frac{\partial}{\partial \gamma^\top} s(\bar{H}_{t-1}, W_t, Y_t; \gamma^*) \Big|_{\gamma^*} \Big| \mathcal{F}_{t-1} \right].$
2. $\frac{\partial}{\partial \gamma_l} s(\bar{h}_{t-1}, w_t, y_t; \gamma) = -(\mathbf{Z}_t^\top \mathbf{Z}_t)^{-1} \mathbf{Z}_t^\top \tilde{\boldsymbol{\tau}}_t^I \sum_{j=t-M+1}^t \psi_l(w_t, \bar{h}_{t-1}; \gamma)$, where $\psi_l(w_t, \bar{h}_{t-1}; \gamma)$ is the l^{th} element of $\psi(w_t, \bar{h}_{t-1}; \gamma)$.

3.

$$\begin{aligned} & \frac{\partial}{\partial \gamma_m} \frac{\partial}{\partial \gamma_l} s(\bar{h}_{t-1}, w_t, y_t; \gamma) \\ &= -(\mathbf{Z}_t^\top \mathbf{Z}_t)^{-1} \mathbf{Z}_t^\top \tilde{\boldsymbol{\tau}}_t^I \left\{ \left[\sum_{j=t-M+1}^t \frac{\partial}{\partial \gamma_m} \psi_l(W_t, \bar{H}_{t-1}; \gamma) \right] \right. \\ & \quad \left. - \left[\sum_{j=t-M+1}^t \psi_m(W_t, \bar{H}_{t-1}; \gamma) \right] \left[\sum_{j=t-M+1}^t \psi_l(W_t, \bar{H}_{t-1}; \gamma) \right] \right\}. \end{aligned}$$

Proof of Theorem A.2. Let $\boldsymbol{\gamma} \in \mathbb{R}^K$ be the parameters in the propensity score model whose score function is denoted by $\psi(w_t, \bar{h}_{t-1}; \boldsymbol{\gamma})$. Consider the following estimating equations:

$$s(\bar{H}_{t-1}, W_t, Y_t; \boldsymbol{\theta}) = \begin{pmatrix} \mathbf{A}_t^* - \boldsymbol{\mu} \\ \psi(W_t, \bar{H}_{t-1}; \boldsymbol{\gamma}) \end{pmatrix}$$

where $\mathbf{A}_t^* = (\mathbf{Z}_t^\top \mathbf{Z}_t)^{-1} \mathbf{Z}_t^\top \tilde{\boldsymbol{\tau}}_t^I(\boldsymbol{\gamma}) - \boldsymbol{\beta}_t^*$ and $\boldsymbol{\theta}^\top = (\boldsymbol{\mu}^\top, \boldsymbol{\gamma}^\top)$. We apply Theorem A.3 of [Papadogeorgou et al. \(2022\)](#) to establish the asymptotic normality of the estimating equations. This requires verifying the following conditions.

1. (a) $\mathbb{E}_{\boldsymbol{\theta}^*}[s(\bar{H}_{t-1}, W_t, Y_t; \boldsymbol{\theta}^*) \mid \mathcal{F}_{t-1}] = 0$ and $\mathbb{E}_{\boldsymbol{\theta}^*}[|s(\bar{H}_{t-1}, W_t, Y_t; \boldsymbol{\theta}^*)|] < \infty$.
- (b) There exists a positive definite \mathbf{V}_a such that, as $T \rightarrow \infty$,

$$\frac{1}{T - M + 1} \sum_{t=M}^T \mathbb{E}_{\boldsymbol{\theta}^*}[s(\bar{H}_{t-1}, W_t, Y_t; \boldsymbol{\theta}^*) s(\bar{H}_{t-1}, W_t, Y_t; \boldsymbol{\theta}^*)^\top \mid \mathcal{F}_{t-1}] \xrightarrow{p} \mathbf{V}_a$$

- (c) As $T \rightarrow \infty$ for all $\epsilon > 0$, we have:

$$\frac{1}{T - M + 1} \sum_{t=M}^T \mathbb{E}_{\boldsymbol{\theta}^*} \left[\|s(\bar{H}_{t-1}, W_t, Y_t; \boldsymbol{\theta}^*)\|^2 I(\|s(\bar{H}_{t-1}, W_t, Y_t; \boldsymbol{\theta}^*)\| > \epsilon \sqrt{T}) \mid \mathcal{F}_{t-1} \right] \xrightarrow{p} 0$$

2. As $T \rightarrow \infty$, we have:

$$\frac{1}{T} \mathbb{E}_{\boldsymbol{\theta}^*} \left[\frac{\partial}{\partial \boldsymbol{\theta}^\top} s(\bar{H}_{t-1}, W_t, Y_t; \boldsymbol{\theta}) \Big|_{\boldsymbol{\theta}^*} \mid \mathcal{F}_{t-1} \right] \xrightarrow{p} \mathbf{V}_d$$

where \mathbf{V}_d is invertible.

3. For all k, j , if we denote $P_{kjt} = \frac{\partial}{\partial \theta_j} s_k(\bar{H}_{t-1}, W_t, Y_t; \boldsymbol{\theta}) \Big|_{\boldsymbol{\theta}^*}$, we have $\mathbb{E}_{\boldsymbol{\theta}^*}[|P_{kjt}|] < \infty$, and there exists $0 < r_{kj} \leq 2$ such that $\sum_{t=1}^T \frac{1}{t^{r_{kj}}} \mathbb{E}_{\boldsymbol{\theta}^*}[|P_{kjt} - \mathbb{E}_{\boldsymbol{\theta}^*}[P_{kjt} \mid \mathcal{F}_{t-1}]|^{r_{kj}} \mid \mathcal{F}_{t-1}] \xrightarrow{p} 0$ as $T \rightarrow \infty$.

4. There exists an integrable function $\ddot{\psi}(x)$ such that $\ddot{\psi}(x)$ dominates second partial derivatives of $s(\overline{H}_{t-1}, W_t, Y_t; \boldsymbol{\theta})$ in a neighborhood of $\boldsymbol{\theta}^*$ for all $\{\overline{h}_{t-1}, w_t, y_t\}$

We check each of these four conditions in turn.

Condition 1. Recall the definition of \mathbf{A}_t given in the proof of Theorem A.1 under the true value of $\boldsymbol{\gamma}$. As shown in Appendix B.4, we have $\mathbb{E}_{\boldsymbol{\theta}^*}[\mathbf{A}_t^* | \mathcal{F}_{t-1}] = 0$. Therefore, under $\boldsymbol{\theta}^{*\top} = (\boldsymbol{\mu}^{*\top}, \boldsymbol{\gamma}^{*\top}) = (\mathbf{0}^\top, \boldsymbol{\gamma}^{*\top})$, we have

$$\mathbb{E}_{\boldsymbol{\theta}^*}[s(\overline{H}_{t-1}, W_t, Y_t; \boldsymbol{\theta}^*) | \mathcal{F}_{t-1}] = 0.$$

According to Lemma A.1 of Papadogeorgou et al. (2022), we have $\mathbb{E}_{\boldsymbol{\gamma}^*}[\psi(W_t, \overline{H}_{t-1}; \boldsymbol{\gamma}^*) | \mathcal{F}_{t-1}] = 0$. Therefore, $\mathbb{E}_{\boldsymbol{\theta}^*}[s(\overline{H}_{t-1}, W_t, Y_t; \boldsymbol{\theta}^*) | \mathcal{F}_{t-1}] = 0$. Moreover, by Jensen's inequality, we have

$$\begin{aligned} \mathbb{E}_{\boldsymbol{\theta}^*}[\|s(\overline{H}_{t-1}, W_t, Y_t; \boldsymbol{\theta}^*)\|^2] &\leq \mathbb{E}_{\boldsymbol{\theta}^*}[\|s(\overline{H}_{t-1}, W_t, Y_t; \boldsymbol{\theta}^*)\|^2] \\ &\leq \mathbb{E}_{\boldsymbol{\theta}^*}[\|\mathbf{A}_t^*\|^2] + \mathbb{E}_{\boldsymbol{\theta}^*}[\|\psi(W_t, \overline{H}_{t-1}; \boldsymbol{\gamma}^*)\|^2]. \end{aligned}$$

The first term is bounded due to Assumption A.1.(a) and the second term is bounded due to Assumption A.2.1. Thus, $\mathbb{E}_{\boldsymbol{\theta}^*}[\|s(\overline{H}_{t-1}, W_t, Y_t; \boldsymbol{\theta}^*)\|] < \infty$. Note that

$$\begin{aligned} &\mathbb{E}_{\boldsymbol{\theta}^*}[s(\overline{H}_{t-1}, W_t, Y_t; \boldsymbol{\theta}^*)s(\overline{H}_{t-1}, W_t, Y_t; \boldsymbol{\theta}^*)^\top | \mathcal{F}_{t-1}] \\ &= \begin{bmatrix} \mathbb{E}_{\boldsymbol{\theta}^*}[\mathbf{A}_t^* \mathbf{A}_t^{*\top} | \mathcal{F}_{t-1}] & \mathbb{E}_{\boldsymbol{\theta}^*}[\mathbf{A}_t^* \psi(W_t, \overline{H}_{t-1}; \boldsymbol{\gamma}^*)^\top | \mathcal{F}_{t-1}] \\ \mathbb{E}_{\boldsymbol{\theta}^*}[\psi(W_t, \overline{H}_{t-1}; \boldsymbol{\gamma}^*) \mathbf{A}_t^{*\top} | \mathcal{F}_{t-1}] & \mathbb{E}_{\boldsymbol{\theta}^*}[\psi(W_t, \overline{H}_{t-1}; \boldsymbol{\gamma}^*) \psi(W_t, \overline{H}_{t-1}; \boldsymbol{\gamma}^*)^\top | \mathcal{F}_{t-1}] \end{bmatrix}. \end{aligned}$$

By Assumptions A.1.(b), A.2.1 and A.3, we have

$$\frac{1}{T - M + 1} \sum_{t=M}^T \mathbb{E}_{\boldsymbol{\theta}^*}[s(\overline{H}_{t-1}, W_t, Y_t; \boldsymbol{\theta}^*)s(\overline{H}_{t-1}, W_t, Y_t; \boldsymbol{\theta}^*)^\top | \mathcal{F}_{t-1}] \xrightarrow{p} \begin{bmatrix} \mathbf{V} & \mathbf{U}^\top \\ \mathbf{U} & \mathbf{V}_{ps} \end{bmatrix},$$

which is positive definite. For Condition (c), we observe that for $\epsilon > 0$,

$$\begin{aligned} &\frac{1}{T - M + 1} \sum_{t=M}^T \mathbb{E}_{\boldsymbol{\theta}^*}[\|s(\overline{H}_{t-1}, W_t, Y_t; \boldsymbol{\theta}^*)\|^2 I(\|s(\overline{H}_{t-1}, W_t, Y_t; \boldsymbol{\theta}^*)\| > \epsilon\sqrt{T}) | \mathcal{F}_{t-1}] \\ &= \frac{1}{T - M + 1} \sum_{t=M}^T \mathbb{E}_{\boldsymbol{\theta}^*}[\|\mathbf{A}_t^*\|^2 I(\|\mathbf{A}_t^*\|^2 + \|\psi(W_t, \overline{H}_{t-1}; \boldsymbol{\gamma}^*)\|^2 > \epsilon^2 T) | \mathcal{F}_{t-1}] \end{aligned} \quad (\text{A.1})$$

$$+ \frac{1}{T-M+1} \sum_{t=M}^T \mathbb{E}_{\theta^*} [\|\psi(W_t, \bar{H}_{t-1}; \gamma^*)\|^2 I(\|\psi(W_t, \bar{H}_{t-1}; \gamma^*)\|^2 > \epsilon^2 T - \|\mathbf{A}_t^*\|^2) \mid \mathcal{F}_{t-1}]. \quad (\text{A.2})$$

By Assumption A.2.1 and the fact that $\|\mathbf{A}_t^*\|^2$ is bounded, the term in Equation (A.1) converges in probability to 0. Since

$$I(\|\mathbf{A}_t^*\|^2 + \|\psi(W_t, \bar{H}_{t-1}; \gamma^*)\|^2 > \epsilon^2 T) \leq I(\|\mathbf{A}_t^*\|^2 > \epsilon^2 T/2) + I(\|\psi(W_t, \bar{H}_{t-1}; \gamma^*)\|^2 > \epsilon^2 T/2),$$

we have

$$\begin{aligned} & \mathbb{E}_{\theta^*} [\|\mathbf{A}_t^*\|^2 I(\|\mathbf{A}_t^*\|^2 + \|\psi(W_t, \bar{H}_{t-1}; \gamma^*)\|^2 > \epsilon^2 T) \mid \mathcal{F}_{t-1}] \\ & \leq \mathbb{E}_{\theta^*} [\|\mathbf{A}_t^*\|^2 I(\|\mathbf{A}_t^*\|^2 > \epsilon^2 T/2) \mid \mathcal{F}_{t-1}] \\ & \quad + \mathbb{E}_{\theta^*} [\|\mathbf{A}_t^*\|^2 I(\|\psi(W_t, \bar{H}_{t-1}; \gamma^*)\|^2 > \epsilon^2 T/2) \mid \mathcal{F}_{t-1}]. \end{aligned}$$

By the arguments in the Proof of Theorem A.1, we have $\frac{1}{T-M+1} \sum_{t=M}^T \mathbb{E}_{\theta^*} [\|\mathbf{A}_t^*\|^2 I(\|\mathbf{A}_t^*\|^2 > \epsilon^2 T/2) \mid \mathcal{F}_{t-1}] \xrightarrow{p} 0$. Let B be the event that $\|\mathbf{A}_t^*\|^2 \leq \|\psi(W_t, \bar{H}_{t-1}; \gamma^*)\|^2$. Then

$$\begin{aligned} & \mathbb{E}_{\theta^*} [\|\mathbf{A}_t^*\|^2 I(\|\psi(W_t, \bar{H}_{t-1}; \gamma^*)\|^2 > \epsilon^2 T/2) \mid \mathcal{F}_{t-1}] \\ & = \mathbb{E}_{\theta^*} [\|\mathbf{A}_t^*\|^2 I(\|\psi(W_t, \bar{H}_{t-1}; \gamma^*)\|^2 > \epsilon^2 T/2) \mid B, \mathcal{F}_{t-1}] \mathbb{P}(B \mid \mathcal{F}_{t-1}) \\ & \quad + \mathbb{E}_{\theta^*} [\|\mathbf{A}_t^*\|^2 I(\|\psi(W_t, \bar{H}_{t-1}; \gamma^*)\|^2 > \epsilon^2 T/2) \mid B^c, \mathcal{F}_{t-1}] \mathbb{P}(B^c \mid \mathcal{F}_{t-1}) \\ & \leq \mathbb{E}_{\theta^*} [\|\psi(W_t, \bar{H}_{t-1}; \gamma^*)\|^2 I(\|\psi(W_t, \bar{H}_{t-1}; \gamma^*)\|^2 > \epsilon^2 T/2) \mid B, \mathcal{F}_{t-1}] \mathbb{P}(B \mid \mathcal{F}_{t-1}) \\ & \quad + \mathbb{E}_{\theta^*} [\|\mathbf{A}_t^*\|^2 I(\|\mathbf{A}_t^*\|^2 > \epsilon^2 T/2) \mid B^c, \mathcal{F}_{t-1}] \mathbb{P}(B^c \mid \mathcal{F}_{t-1}) \\ & \leq \mathbb{E}_{\theta^*} [\|\psi(W_t, \bar{H}_{t-1}; \gamma^*)\|^2 I(\|\psi(W_t, \bar{H}_{t-1}; \gamma^*)\|^2 > \epsilon^2 T/2) \mid \mathcal{F}_{t-1}] \\ & \quad + \mathbb{E}_{\theta^*} [\|\mathbf{A}_t^*\|^2 I(\|\mathbf{A}_t^*\|^2 > \epsilon^2 T/2) \mid \mathcal{F}_{t-1}] \end{aligned}$$

where the last inequality follows from the law of total expectation. Since the mean of the last two terms converge in probability to 0 under Assumption A.2.1, Condition 1.(c) holds.

Condition 2. Observe that

$$\begin{aligned} \frac{\partial}{\partial \theta^\top} s(\bar{H}_{t-1}, W_t, Y_t; \theta) & = \begin{bmatrix} -\mathbf{I}_L & \frac{\partial}{\partial \gamma^\top} s_{1:L}(\bar{H}_{t-1}, W_t, Y_t; \theta) \\ \frac{\partial}{\partial \mu} \psi(W_t, \bar{H}_{t-1}; \gamma) & \frac{\partial}{\partial \gamma^\top} \psi(W_t, \bar{H}_{t-1}; \gamma) \end{bmatrix} \\ & = \begin{bmatrix} -\mathbf{I}_L & \frac{\partial}{\partial \gamma^\top} s_{1:L}(\bar{H}_{t-1}, W_t, Y_t; \theta) \\ \mathbf{0} & \frac{\partial}{\partial \gamma^\top} \psi(W_t, \bar{H}_{t-1}; \gamma) \end{bmatrix} \end{aligned} \quad (\text{A.3})$$

By Lemma A.1, we have

$$\begin{aligned} & -\frac{1}{T-M+1} \sum_{t=M}^T \mathbb{E}_{\boldsymbol{\theta}^*} \left[\frac{\partial}{\partial \boldsymbol{\gamma}^\top} s_{1:L}(\bar{H}_{t-1}, W_t, Y_t; \boldsymbol{\theta}^*) \mid \mathcal{F}_{t-1} \right] \\ &= \frac{1}{T-M+1} \sum_{t=M}^T \mathbb{E}_{\boldsymbol{\theta}^*} \left[s_{1:L}(\bar{H}_{t-1}, W_t, Y_t; \boldsymbol{\theta}^*) \psi(W_t, \bar{H}_{t-1}; \boldsymbol{\gamma}^*)^\top \mid \mathcal{F}_{t-1} \right] \xrightarrow{p} \mathbf{U}^\top. \end{aligned}$$

Moreover, by Lemma A.1 of Papadogeorgou et al. (2022), we have

$$-\frac{1}{T-M+1} \sum_{t=M}^T \mathbb{E}_{\boldsymbol{\gamma}^*} \left[\frac{\partial}{\partial \boldsymbol{\gamma}^\top} \psi(W_t, \bar{H}_{t-1}; \boldsymbol{\gamma}) \Big|_{\boldsymbol{\gamma}^*} \mid \mathcal{F}_{t-1} \right] \xrightarrow{p} \mathbf{V}_{ps}.$$

Since \mathbf{V}_{ps} is positive definite, it is also invertible. Hence

$$-\frac{1}{T-M+1} \sum_{t=M}^T \mathbb{E}_{\boldsymbol{\theta}^*} \left[\frac{\partial}{\partial \boldsymbol{\theta}^\top} s(\bar{H}_{t-1}, W_t, Y_t; \boldsymbol{\theta}) \Big|_{\boldsymbol{\theta}^*} \right] \xrightarrow{p} \begin{bmatrix} \mathbf{I}_L & \mathbf{U}^\top \\ \mathbf{0} & \mathbf{V}_{ps} \end{bmatrix},$$

and this limit matrix is invertible.

Condition 3. Let $s_k(\bar{H}_{t-1}, W_t, Y_t; \boldsymbol{\theta})$ be the k^{th} element of $s(\bar{H}_{t-1}, W_t, Y_t; \boldsymbol{\theta})$. We need to show that for $j, k = 1, \dots, L+K$, if we denote

$$P_{kjt} = \frac{\partial}{\partial \theta_j} s_k(\bar{H}_{t-1}, W_t, Y_t; \boldsymbol{\theta}) \Big|_{\boldsymbol{\theta}^*},$$

then $\mathbb{E}_{\boldsymbol{\theta}^*}[|P_{kjt}|] < \infty$, and there exists $0 < r_{kj} \leq 2$ such that

$$\sum_{t=1}^T \frac{1}{t^{r_{kj}}} \mathbb{E}_{\boldsymbol{\theta}^*} \left[|P_{kjt} - \mathbb{E}_{\boldsymbol{\theta}^*}[P_{kjt} | \mathcal{F}_{t-1}]|^{r_{kj}} \mid \mathcal{F}_{t-1} \right] \xrightarrow{p} 0$$

as $T \rightarrow \infty$. We will consider four cases.

Case1: For $L < k, j \leq K+L$, the desired condition holds by Assumption A.2.1.

Case2: Let $1 \leq k, j \leq L$. By Equation (A.3), we have $P_{jkt} = -1$ or 0 . Thus, $P_{kjt} = \mathbb{E}_{\boldsymbol{\theta}^*}[P_{kjt} | \mathcal{F}_{t-1}]$ and $\mathbb{E}_{\boldsymbol{\theta}^*}[|P_{kjt}|] < \infty$.

Case3: Let $1 \leq j \leq L$ and $L < k \leq K+L$. Then

$$\frac{\partial}{\partial \theta_j} s_k(\bar{H}_{t-1}, W_t, Y_t; \boldsymbol{\theta}) = 0.$$

Therefore, the condition is satisfied.

Case4: For $1 \leq k \leq L$ and $L < j \leq K + L$, there exists $0 < r_{kj} \leq 2$ such that

$$\sum_{t=1}^T \frac{1}{t^{r_{kj}}} \mathbb{E}_{\boldsymbol{\theta}^*} [|P_{kjt} - \mathbb{E}_{\boldsymbol{\theta}^*}[P_{kjt} | \mathcal{F}_{t-1}]|^{r_{kj}} | \mathcal{F}_{t-1}] \xrightarrow{p} 0$$

by Assumption A.3.(b). Moreover, Lemma A.1 implies that

$$\begin{aligned} \mathbb{E}_{\boldsymbol{\theta}^*} [|P_{kjt}|] &= \mathbb{E}_{\boldsymbol{\theta}^*} \left[\left| \frac{\partial}{\partial \gamma_{j-L}} s_k(\bar{H}_{t-1}, W_t, Y_t; \boldsymbol{\theta}) \Big|_{\boldsymbol{\theta}^*} \right| \right] \\ &= \mathbb{E}_{\boldsymbol{\theta}^*} \left[\left| -(\mathbf{Z}_t^\top \mathbf{Z}_t)^{-1} \mathbf{Z}_t^\top \tilde{\boldsymbol{\tau}}_t^I(\boldsymbol{\gamma}^*) \sum_{t'=t-M+1}^t \psi_{j-L}(W_{t'}, \bar{H}_{t'-1}; \boldsymbol{\gamma}^*) \right| \right] \end{aligned}$$

By Assumption A.1, \mathbf{Z}_t and $\tilde{\boldsymbol{\tau}}_t^I(\boldsymbol{\gamma}^*)$ are bounded. Since

$$\begin{aligned} \mathbb{E}_{\boldsymbol{\gamma}^*} [|\psi_{j-L}(W_{t'}, \bar{H}_{t'-1}; \boldsymbol{\gamma}^*)|^2] &\leq \mathbb{E}_{\boldsymbol{\gamma}^*} [\psi_{j-L}(W_{t'}, \bar{H}_{t'-1}; \boldsymbol{\gamma}^*)^2] \\ &\leq \mathbb{E}_{\boldsymbol{\gamma}^*} [|\psi(W_{t'}, \bar{H}_{t'-1}; \boldsymbol{\gamma}^*)|^2] < \infty, \end{aligned}$$

where the first inequality follows from Jensen's inequality and the second inequality follows from Assumption A.2. Therefore, it follows that $\mathbb{E}_{\boldsymbol{\theta}}[|P_{kjt}|] < \infty$.

Condition 4. We need to show that there exists an integrable function $\ddot{\psi}(x)$ such that $\ddot{\psi}(x)$ dominates the second partial derivatives of $s(\bar{H}_{t-1}, W_t, Y_t; \boldsymbol{\theta})$ in a neighborhood of $\boldsymbol{\theta}^*$ for all $\{\bar{h}_{t-1}, w_t, y_t\}$. Let $k, l, m = 1, \dots, K + L$. We consider the following three cases.

Case1: If $l \leq L$ or $m \leq L$, then $\frac{\partial}{\partial \theta_m} \frac{\partial}{\partial \theta_j} \psi(W_t, \bar{H}_{t-1}; \boldsymbol{\gamma}_k) = 0$, implying that the condition is satisfied.

Case2: If $k, l, m > L$, the condition holds by Assumption A.2.3.

Case3: Suppose $k \leq L$ and $m, l > L$. Lemma A.1 implies:

$$\begin{aligned} \frac{\partial}{\partial \gamma_m} \frac{\partial}{\partial \gamma_l} s_k(\bar{h}_{t-1}, w_t, y_t; \boldsymbol{\theta}) &= -(\mathbf{Z}_t^\top \mathbf{Z}_t)^{-1} \mathbf{Z}_{t,k}^\top \tilde{\boldsymbol{\tau}}_t^I(\boldsymbol{\gamma}) \left\{ \sum_{j=t-M+1}^t \frac{\partial}{\partial \gamma_{m-L}} \psi_{l-L}(w_j, \bar{h}_{j-1}; \boldsymbol{\gamma}) \right. \\ &\quad \left. - \sum_{j=t-M+1}^t \psi_{m-L}(w_j, \bar{h}_{j-1}; \boldsymbol{\gamma}) \sum_{j=t-M+1}^t \psi_{l-L}(w_j, \bar{h}_{j-1}; \boldsymbol{\gamma}) \right\}. \end{aligned}$$

Note that $|(\mathbf{Z}_t^\top \mathbf{Z}_t)^{-1} \mathbf{Z}_{t,k}^\top \tilde{\boldsymbol{\tau}}_t^I(\boldsymbol{\gamma})| \leq \delta$ for some $\delta \in \mathbb{R}$, so

$$\left| \frac{\partial}{\partial \gamma_m} \frac{\partial}{\partial \gamma_l} s_k(\bar{h}_{t-1}, w_t, y_t; \boldsymbol{\theta}) \right|$$

$$\begin{aligned}
&\leq \delta \left| \sum_{j=t-M+1}^t \frac{\partial}{\partial \gamma_{m-L}} \psi_{l-L}(w_j, \bar{h}_{j-1}; \gamma) \right| \\
&\quad + \delta \left| \sum_{j=t-M+1}^t \sum_{j'=t-M+1}^t \psi_{m-L}(w_j, \bar{h}_{j-1}; \gamma) \psi_{l-L}(w_{j'}, \bar{h}_{j'-1}; \gamma) \right| \\
&\leq \sum_{j=t-M+1}^t \delta \left| \frac{\partial}{\partial \gamma_{m-L}} \psi_{l-L}(w_j, \bar{h}_{j-1}; \gamma) \right| \\
&\quad + \sum_{j=t-M+1}^t \sum_{j'=t-M+1}^t \delta \left| \psi_{m-L}(w_j, \bar{h}_{j-1}; \gamma) \psi_{l-L}(w_{j'}, \bar{h}_{j'-1}; \gamma) \right|
\end{aligned}$$

Consider the first term. Assumption A.2 implies that the second derivatives of $\psi(w_t, \bar{h}_{t-1}; \gamma)$ is dominated by $\ddot{\psi}(w_t, \bar{h}_{t-1})$ in a neighborhood of γ^* . Let $B_\epsilon(\gamma^*)$ be an open ball contained in the neighborhood. By Taylor's expansion, we have

$$\left| \frac{\partial}{\partial \gamma_{m-L}} \psi_{l-L}(w_t, \bar{h}_{t-1}; \gamma) \right| \leq \left| \frac{\partial}{\partial \gamma_{m-L}} \psi_{l-L}(w_t, \bar{h}_{t-1}; \gamma^*) \right| + \epsilon K \ddot{\psi}(w_t, \bar{h}_{t-1}),$$

on the ball $B_\epsilon(\gamma^*)$. By Assumption A.2.2, the quantity on the right hand side is an integrable function fixed in γ , where we denote the maximum of these functions over m, l by $\ddot{\psi}_1(w_t, \bar{h}_{t-1})$.

Next, consider the second term. On the open ball $B_\epsilon(\gamma^*)$, we have

$$|\psi_{m-1}(w_t, \bar{h}_{t-1}; \gamma)| \leq |\psi_{m-1}(w_t, \bar{h}_{t-1}; \gamma^*)| + \epsilon K \ddot{\psi}_1(w_t, \bar{h}_{t-1}),$$

and $\mathbb{E}_{\gamma^*}[|\psi_{m-1}(w_t, \bar{h}_{t-1}; \gamma^*)|] < \infty$ by Assumption A.2. Then, the right hand side is an integrable function fixed in γ where we denote the maximum of these functions over m by $\ddot{\psi}_2(w_t, \bar{h}_{t-1})$. Putting these together, we have

$$\left| \frac{\partial}{\partial \gamma_m} \frac{\partial}{\partial \gamma_l} s_k(\bar{h}_{t-1}, w_t, y_t; \boldsymbol{\theta}) \right| \leq M \delta \ddot{\psi}_1(w_t, \bar{h}_{t-1}) + M^2 \delta [\ddot{\psi}_2(w_t, \bar{h}_{t-1})]^2,$$

where the right hand side is an integrable function that satisfy the condition.

Finally, we need to show that the solution of the following equation is consistent for $\boldsymbol{\theta}^*$,

$$\frac{1}{T-M+1} \sum_{t=M}^T s(\bar{H}_{t-1}, W_t, Y_t; \boldsymbol{\theta}) = 0.$$

Let $s_{1:L}(\bar{H}_{t-1}, W_t, Y_t; \boldsymbol{\theta})$ denote the first L entries of $s(\bar{H}_{t-1}, W_t, Y_t; \boldsymbol{\theta})$. Theorem A.1 shows that the IPW estimator based on the true propensity score is consistent, while the pa-

parameter estimates of the propensity score model $\hat{\gamma}$ are also consistent for γ . Furthermore, $s_{1:L}(\bar{H}_{t-1}, W_t, Y_t; \boldsymbol{\theta})$ is a continuous function of the propensity score, which is itself continuous in γ . Thus, Slutsky's theorem implies that solving the following equation with the estimated propensity score parameters is also consistent,

$$\frac{1}{T - M + 1} \sum_{t=M}^T s_{1:L}(\bar{H}_{t-1}, W_t, Y_t; \boldsymbol{\theta}) = 0.$$

Hence, all the conditions of Theorem A.3 in Papadogeorgou et al. (2022) are satisfied, and as $T \rightarrow \infty$, we have

$$\sqrt{T}(\hat{\boldsymbol{\theta}}_T - \boldsymbol{\theta}^*) \xrightarrow{d} N(0, \mathbf{V}_{\boldsymbol{\theta}}),$$

where $\hat{\boldsymbol{\theta}}_T$ is the solution to

$$\frac{1}{T - M + 1} \sum_{t=M}^T s(\bar{H}_{t-1}, W_t, Y_t; \boldsymbol{\theta}) = 0$$

and $\mathbf{V}_{\boldsymbol{\theta}} = \mathbf{A}^{-1} \mathbf{B} (\mathbf{A}^{-\top})$ for

$$\mathbf{A} = \begin{bmatrix} \mathbf{I}_L & \mathbf{U}^\top \\ \mathbf{0} & \mathbf{V}_{ps} \end{bmatrix} \quad \text{and} \quad \mathbf{B} = \begin{bmatrix} \tilde{\mathbf{V}}^I & \mathbf{U}^\top \\ \mathbf{U} & \mathbf{V}_{ps} \end{bmatrix}. \quad (\text{A.4})$$

Note that $\frac{1}{T-M+1} \sum_{t=M}^T \hat{\boldsymbol{\beta}}_t^I - \boldsymbol{\beta}_t^*$ is the first L entries of $\hat{\boldsymbol{\theta}}_T$. As a result, we have

$$\frac{1}{\sqrt{T - M + 1}} \sum_{t=M}^T (\hat{\boldsymbol{\beta}}_t^I - \boldsymbol{\beta}_t^*) \xrightarrow{d} N(0, \mathbf{V}^I).$$

□

B.7 Proof of Theorem A.3

The asymptotic variance \mathbf{V}^I corresponds to the $L \times L$ submatrix located in the upper-left corner of matrix $\mathbf{A}^{-1} \mathbf{B} \mathbf{A}^{-\top}$ where \mathbf{A}, \mathbf{B} are defined in Equation (A.4). We have

$$\begin{aligned} \mathbf{A}^{-1} \mathbf{B} \mathbf{A}^{-\top} &= \begin{bmatrix} \mathbf{I}_L & \mathbf{U}^\top \\ \mathbf{0} & \mathbf{V}_{ps} \end{bmatrix}^{-1} \begin{bmatrix} \tilde{\mathbf{V}}^I & \mathbf{U}^\top \\ \mathbf{U} & \mathbf{V}_{ps} \end{bmatrix} \begin{bmatrix} \mathbf{I}_L & \mathbf{U}^\top \\ \mathbf{0} & \mathbf{V}_{ps} \end{bmatrix}^{-\top} \\ &= \begin{bmatrix} \mathbf{I}_L^{-1} & -\mathbf{I}_L^{-1} \mathbf{U}^\top \mathbf{V}_{ps}^{-1} \\ \mathbf{0} & \mathbf{V}_{ps}^{-1} \end{bmatrix} \begin{bmatrix} \tilde{\mathbf{V}}^I & \mathbf{U}^\top \\ \mathbf{U} & \mathbf{V}_{ps} \end{bmatrix} \begin{bmatrix} \mathbf{I}_L^{-\top} & \mathbf{0} \\ -\mathbf{V}_{ps}^{-1\top} \mathbf{U}^\top \mathbf{I}_L^{-1\top} & \mathbf{V}_{ps}^{-\top} \end{bmatrix} \end{aligned}$$

$$= \begin{bmatrix} \tilde{\mathbf{V}}^I - \mathbf{U}^\top \mathbf{V}_{ps}^{-1} \mathbf{U}^\top & \dots \\ \dots & \dots \end{bmatrix}.$$

Note that \mathbf{V}^I is the asymptotic variance of the estimator based on the true propensity score. Let \mathbf{x} be a nonzero vector in \mathbb{R}^L . Then $\mathbf{x}^* = \mathbf{U}^\top \mathbf{x} \in \mathbb{R}^K$. Since \mathbf{V}_{ps} is positive definite, so is \mathbf{V}_{ps}^{-1} , implying $\mathbf{x}^\top \mathbf{U}^\top \mathbf{V}_{ps}^{-1} \mathbf{U}^\top \mathbf{x} = \mathbf{x}^{*\top} \mathbf{V}_{ps}^{-1} \mathbf{x}^* \geq 0$. Thus, $\mathbf{U}^\top \mathbf{V}_{ps}^{-1} \mathbf{U}^\top$ is a positive semidefinite matrix, completing the proof. \square

B.8 Proof of Corollary A.1

The proof follows directly from the proof of Proposition A.1 and the fact that $\hat{\gamma}$ is consistent for γ . \square

C Asymptotic properties of the Hájek estimator

In this section, we present the asymptotic properties of Hájek estimator based on either the true or estimated propensity score. We begin by stating the required regularity conditions and then establish that the Hájek estimator is asymptotically normal. Although the asymptotic variance is not identifiable, we derive its upper bound and propose a consistent estimator of the bound.

C.1 Regularity conditions

We represent an additional assumption that is required to achieve the asymptotic normality of the Hájek estimator. For $M \leq t \leq T$, define

$$\beta'_t = (\mathbf{Z}_t^\top \mathbf{Z}_t)^{-1} \mathbf{Z}_t^\top \mathbf{N}_t(F_{h'}) \text{ and } \beta''_t = (\mathbf{Z}_t^\top \mathbf{Z}_t)^{-1} \mathbf{Z}_t^\top \mathbf{N}_t(F_{h''}).$$

Assumption A.4. *Define*

$$\mathbf{A}_t = \begin{pmatrix} (\mathbf{Z}_t^\top \mathbf{Z}_t)^{-1} \mathbf{Z}_t^\top \tilde{\mathbf{Y}}_t^H(F_{h'}; \gamma^*) \\ (\mathbf{Z}_t^\top \mathbf{Z}_t)^{-1} \mathbf{Z}_t^\top \tilde{\mathbf{Y}}_t^H(F_{h''}; \gamma^*) \\ \rho_{th'}(\gamma^*) \\ \rho_{th''}(\gamma^*) \end{pmatrix}.$$

Then, there exists a positive definite matrix \mathbf{V}^H such that as $T \rightarrow \infty$,

$$\frac{1}{T - M + 1} \sum_{t=M}^T \mathbb{V}[\mathbf{A}_t \mid \bar{H}_{t-M}^*] \xrightarrow{p} \tilde{\mathbf{V}}^H.$$

Assumption A.4 is slightly stronger than Assumption A.1.(b), since $\tilde{\tau}_t^H(\gamma) = \tilde{\mathbf{Y}}_t^H(F_{h''}; \gamma) - \tilde{\mathbf{Y}}_t^H(F_{h'}; \gamma)$.

The next assumption is similar to Assumption A.3 with a different form of $s(\bar{H}_{t-1}, W_t, Y_t; \gamma)$.

Assumption A.5 (Regularity conditions on score function of propensity score model for Hájek estimators). *For a stochastic intervention F_h , let $\rho_{th}(\gamma) = \prod_{j=t-M+1}^t \frac{f_h(W_t)}{e_t(W_t; \gamma)}$ and $\tilde{\mathbf{Y}}_t^H(F_h; \gamma) = \rho_{th}(\gamma) (N_{S_1}(Y_t), \dots, N_{S_p}(Y_t))^\top$, and $\tilde{\tau}_t^H(\gamma) = \tilde{\mathbf{Y}}_t^H(F_{h''}; \gamma) - \tilde{\mathbf{Y}}_t^H(F_{h'}; \gamma)$. Define*

$$s(\bar{H}_{t-1}, W_t, Y_t; \gamma) = \begin{pmatrix} (\mathbf{Z}_t^\top \mathbf{Z}_t)^{-1} \mathbf{Z}_t^\top \tilde{\mathbf{Y}}_t^H(F_{h'}; \gamma) - \beta'_t \\ (\mathbf{Z}_t^\top \mathbf{Z}_t)^{-1} \mathbf{Z}_t^\top \tilde{\mathbf{Y}}_t^H(F_{h''}; \gamma) - \beta''_t \\ \rho_{th'}(\gamma) - 1 \\ \rho_{th''}(\gamma) - 1 \end{pmatrix},$$

and a propensity score function $\psi(W_t, \bar{H}_{t-1}; \gamma)$ satisfying Assumption A.2, the following conditions hold.

(a) There exists $\mathbf{U} \in \mathbb{R}^{K \times 2L}$ such that

$$\frac{1}{T-M+1} \sum_{t=M}^T \mathbb{E}_{\gamma^*} [\psi(W_t, \bar{H}_{t-1}; \gamma^*) s(\bar{H}_{t-1}, W_t, Y_t; \gamma^*)^\top \mid \bar{H}_{t-M}^*] \xrightarrow{p} \mathbf{U}, \text{ and}$$

$$\mathbf{V}^* = \begin{bmatrix} \tilde{\mathbf{V}}^H & \mathbf{U}^\top \\ \mathbf{U} & \mathbf{V}_{ps} \end{bmatrix} \text{ is positive definite.}$$

(b) If $P_{jt} = \frac{\partial}{\partial \gamma_j} s(\bar{H}_{t-1}, W_t, Y_t; \gamma) \Big|_{\gamma^*}$, where γ_j is the j^{th} entry of γ , then there exists $r_j \in (0, 2]$ such that

$$\frac{1}{T-M+1} \sum_{t=M}^T \frac{1}{t^{r_j}} \left(|P_{jt} - \mathbb{E}_{\theta^*}[P_{jt} \mid \bar{H}_{t-M}^*]| \right) \xrightarrow{p} 0.$$

C.2 Asymptotic normality

The asymptotic normality of the Hájek estimator based on the estimated propensity score is presented as Theorem 1. Here, we state the analogous result for the Hájek estimator with the true propensity score.

Theorem A.4 (Asymptotic normality of the Hájek estimator using the true propensity score). *Suppose that Assumptions 1, 2, A.1, and A.4 hold. Then,*

$$\frac{1}{\sqrt{T-M+1}} \sum_{t=M}^T (\hat{\beta}_t^H - \beta_t^*) \xrightarrow{d} N(0, J\mathbf{V}^H J^\top),$$

where $\tilde{\mathbf{V}}^H$ represents the probability limit of $\frac{1}{T-M+1} \sum_{t=M}^T \tilde{\mathbf{V}}_t^H$ as $T \rightarrow \infty$ with $\tilde{\mathbf{V}}_t^H = \mathbb{V}[\mathbf{A}_t \mid \bar{H}_{t-M}^*]$ for $t \geq M$, where \mathbf{A}_t and \mathbf{J} are defined as,

$$\mathbf{A}_t = \begin{pmatrix} (\mathbf{Z}_t^\top \mathbf{Z}_t)^{-1} \mathbf{Z}_t^\top \tilde{\mathbf{Y}}_t^H(F_{\mathbf{h}'}; \gamma^*) \\ (\mathbf{Z}_t^\top \mathbf{Z}_t)^{-1} \mathbf{Z}_t^\top \tilde{\mathbf{Y}}_t^H(F_{\mathbf{h}''}; \gamma^*) \\ \rho_{t\mathbf{h}'}(\gamma^*) \\ \rho_{t\mathbf{h}''}(\gamma^*) \end{pmatrix},$$

$$\text{and } \mathbf{J} = \begin{bmatrix} \mathbf{I} & -\mathbf{I} & -\frac{1}{T-M+1} \sum_{t=M}^T \boldsymbol{\beta}'_t & \frac{1}{T-M+1} \sum_{t=M}^T \boldsymbol{\beta}''_t \end{bmatrix}.$$

C.3 Consistent estimation of variance bound for the Hájek-estimator

For the case of the estimated propensity score, the result is stated as Corollary 1. We state the result for the Hájek estimator with the true propensity score.

Proposition A.2 (Consistent estimation of variance bound for the Hájek estimator with the true propensity score). *Suppose that Assumptions 1, 2, A.1, and A.4 hold. Let*

$$\hat{\mathbf{V}}^H = \frac{1}{T-M+1} \sum_{t=M}^T \hat{\mathbf{V}}_t^H \text{ with } \hat{\mathbf{V}}_t^H = \mathbf{A}_t \mathbf{A}_t^\top \text{ and}$$

$$\hat{\mathbf{J}} = \begin{bmatrix} \mathbf{I} & -\mathbf{I} & -\frac{1}{T-M+1} \sum_{t=M}^T (\mathbf{Z}_t^\top \mathbf{Z}_t)^{-1} \mathbf{Z}_t^\top \tilde{\mathbf{Y}}_t^H(F_{\mathbf{h}'}; \gamma^*) & \frac{1}{T-M+1} \sum_{t=M}^T (\mathbf{Z}_t^\top \mathbf{Z}_t)^{-1} \mathbf{Z}_t^\top \tilde{\mathbf{Y}}_t^H(F_{\mathbf{h}''}; \gamma^*) \end{bmatrix}$$

Then $\hat{\mathbf{J}} \hat{\mathbf{V}}^H \hat{\mathbf{J}}^\top$ is a consistent estimator for $\mathbf{J} \mathbf{V}^{H*} \mathbf{J}^\top$.

C.4 Proof of Theorem A.4

The proof is similar to that of Theorem A.1. The key difference is the definition of \mathbf{A}_t^* . We apply Theorem A.2 of Papadogeorgou et al. (2022). Set $\mathcal{F}_t = \bar{H}_{t-M+1}^*$, and define $\mathbf{A}_t^* = \mathbf{A}_t - (\boldsymbol{\beta}'_t, \boldsymbol{\beta}''_t, \rho_{\mathbf{h}'}, \rho_{\mathbf{h}''})^\top$ where $\rho_{\mathbf{h}'} = \rho_{\mathbf{h}''} = 1$.

We first show that \mathbf{A}_t^* is a martingale difference sequence, i.e., $\mathbb{E}[\mathbf{A}_t^*] = 0$ and $\mathbb{E}[|\mathbf{A}_t^*|] < \infty$. By similar arguments used in the proof of Theorem A.1 (see Appendix B.4), for any $F_{\mathbf{h}}$, we have $\mathbb{E}[\tilde{\mathbf{Y}}_t^H(F_{\mathbf{h}}) \mid \mathcal{F}_{t-1}] = N_t(F_{\mathbf{h}})$, and thus,

$$\mathbb{E}[(\mathbf{Z}_t^\top \mathbf{Z}_t)^{-1} \mathbf{Z}_t^\top \tilde{\mathbf{Y}}_t^H(F_{\mathbf{h}'}; \gamma^*) \mid \mathcal{F}_{t-1}] = (\mathbf{Z}_t^\top \mathbf{Z}_t)^{-1} \mathbf{Z}_t^\top N_t(F_{\mathbf{h}}) = \boldsymbol{\beta}'_t.$$

We have

$$\mathbb{E}[\rho_{t\mathbf{h}'} \mid \mathcal{F}_{t-1}] = \int_{\mathcal{W}^M} \prod_{j=t-M+1}^t \frac{f_{\mathbf{h}'}(w_j)}{e_j(w_j)} f(w_j \mid \bar{H}_{j-1}^*) d\mathbf{w}_{(t-M+1):t}$$

$$\begin{aligned}
&= \int_{\mathcal{W}^M} \prod_{j=t-M+1}^t \frac{f_{\mathbf{h}'}(w_j)}{e_j(w_j)} e_j(w_j) d\mathbf{w}_{(t-M+1):t} \\
&= \int_{\mathcal{W}^M} \prod_{j=t-M+1}^t f_{\mathbf{h}'}(w_j) d\mathbf{w}_{(t-M+1):t} \\
&= 1.
\end{aligned}$$

where the second equality follows from Assumption 1.

Similarly, $\mathbb{E}[(\mathbf{Z}_t^\top \mathbf{Z}_t)^{-1} \mathbf{Z}_t^\top \tilde{\mathbf{Y}}_t^H (F_{\mathbf{h}''}) \mid \mathcal{F}_{t-1}] = \boldsymbol{\beta}_t''$ and $\mathbb{E}[\rho_{t\mathbf{h}''} \mid \mathcal{F}_{t-1}] = 1$. Thus, $\mathbb{E}[\mathbf{A}_t^* \mid \mathcal{F}_{t-1}] = \mathbf{0}$. Furthermore, since every element in \mathbf{A}_t^* is bounded by Assumptions 2 and A.1.(a), $\|\mathbf{A}_t^*\|$ is bounded and hence $\mathbb{E}[\|\mathbf{A}_t^*\|] < \infty$. For an arbitrary $\epsilon > 0$, $I(\|\mathbf{A}_t^*\| > \epsilon\sqrt{T}) = 0$ for large t , since $\|\mathbf{A}_t^*\|$ is bounded. Therefore, as $T \rightarrow \infty$ for all $\epsilon > 0$, we have

$$\frac{1}{T-M+1} \sum_{t=M}^T E \left[\|\mathbf{A}_t^*\|^2 I(\|\mathbf{A}_t^*\| > \epsilon\sqrt{T}) \mid \mathcal{F}_{t-1} \right] \xrightarrow{p} 0.$$

The remaining condition of the multivariate Martingale central limit theorem is satisfied by Assumption A.4. Hence,

$$\frac{1}{\sqrt{T-M+1}} \sum_{t=M}^T \mathbf{A}_t^* \xrightarrow{d} N(\mathbf{0}, \tilde{\mathbf{V}}^H)$$

where, as $T \rightarrow \infty$,

$$\frac{1}{T-M+1} \sum_{t=M}^T \mathbb{E}[\mathbf{A}_t^* \mathbf{A}_t^{*\top} \mid \mathcal{F}_{t-1}] \xrightarrow{p} \tilde{\mathbf{V}}^H.$$

Then, as $T \rightarrow \infty$, we have

$$\sqrt{T-M+1}(\hat{\boldsymbol{\theta}} - \boldsymbol{\theta}^*) \xrightarrow{d} N(\mathbf{0}, \tilde{\mathbf{V}}^H),$$

where

$$\begin{aligned}
\boldsymbol{\theta} &= \frac{1}{T-M+1} \left(\sum_{t=M}^T \boldsymbol{\beta}_t', \sum_{t=M}^T \boldsymbol{\beta}_t'', \rho_{\mathbf{h}'}, \rho_{\mathbf{h}''} \right)^\top, \\
\hat{\boldsymbol{\theta}} &= \frac{1}{T-M+1} \sum_{t=M}^T \left((\mathbf{Z}_t^\top \mathbf{Z}_t)^{-1} \mathbf{Z}_t^\top \tilde{\mathbf{Y}}_t^H (F_{\mathbf{h}'}), (\mathbf{Z}_t^\top \mathbf{Z}_t)^{-1} \mathbf{Z}_t^\top \tilde{\mathbf{Y}}_t^H (F_{\mathbf{h}''}), \rho_{t\mathbf{h}'}, \rho_{t\mathbf{h}''} \right)^\top.
\end{aligned}$$

Finally, we apply the Delta method. Define

$$h(\boldsymbol{\theta}) = \frac{\frac{1}{T-M+1} \sum_{t=M}^T \boldsymbol{\beta}'_t}{\rho_{\mathbf{h}'}} - \frac{\frac{1}{T-M+1} \sum_{t=M}^T \boldsymbol{\beta}''_t}{\rho_{\mathbf{h}''}}.$$

The Jacobian matrix is

$$\mathbf{J}(\boldsymbol{\theta}) = \begin{bmatrix} \frac{1}{\rho_{\mathbf{h}'}} \mathbf{I} & -\frac{1}{\rho_{\mathbf{h}''}} \mathbf{I} & -\frac{\frac{1}{T-M+1} \sum_{t=M}^T \boldsymbol{\beta}'_t}{\rho_{\mathbf{h}'}^2} & \frac{\frac{1}{T-M+1} \sum_{t=M}^T \boldsymbol{\beta}''_t}{\rho_{\mathbf{h}''}^2} \end{bmatrix}$$

where \mathbf{I} is the identity matrix. Denote

$$\mathbf{J} = \mathbf{J}(\boldsymbol{\theta}^*) = \begin{bmatrix} \mathbf{I} & -\mathbf{I} & -\frac{1}{T-M+1} \sum_{t=M}^T \boldsymbol{\beta}'_t & \frac{1}{T-M+1} \sum_{t=M}^T \boldsymbol{\beta}''_t \end{bmatrix}$$

Then, we obtain,

$$\sqrt{T-M+1}(h(\hat{\boldsymbol{\theta}}) - h(\boldsymbol{\theta}^*)) \xrightarrow{d} N(\mathbf{0}, \mathbf{J} \tilde{\mathbf{V}}^H \mathbf{J}^\top)$$

as $T \rightarrow \infty$. Thus, as $T \rightarrow \infty$, we have

$$\frac{1}{\sqrt{T-M+1}} \sum_{t=M}^T (\hat{\boldsymbol{\beta}}_t^H - \boldsymbol{\beta}_t^*) \xrightarrow{d} N(\mathbf{0}, \mathbf{J} \tilde{\mathbf{V}}^H \mathbf{J}^\top).$$

□

C.5 Proof of Proposition A.2

Assuming the same notations in the previous proof. Note that

$$\hat{\boldsymbol{\theta}} = \begin{bmatrix} 1, 1, -\frac{1}{T-M+1} \sum_{t=M}^T ((\mathbf{Z}_t^\top \mathbf{Z}_t)^{-1} \mathbf{Z}_t^\top \tilde{\mathbf{Y}}_t^H(F_{\mathbf{h}'}; \boldsymbol{\gamma}^*))^\top, \\ \frac{1}{T-M+1} \sum_{t=M}^T ((\mathbf{Z}_t^\top \mathbf{Z}_t)^{-1} \mathbf{Z}_t^\top \tilde{\mathbf{Y}}_t^H(F_{\mathbf{h}''}; \boldsymbol{\gamma}^*))^\top \end{bmatrix}^\top$$

is a consistent estimator of $\boldsymbol{\theta}$. So $\hat{\mathbf{J}} = \mathbf{J}(\hat{\boldsymbol{\theta}})$ is a consistent estimator of $\mathbf{J}(\boldsymbol{\theta})$. By similar arguments used in Appendix B.5, we have $\hat{\mathbf{V}}^H \xrightarrow{p} \mathbf{V}^{H^*}$. Hence, $\hat{\mathbf{J}} \hat{\mathbf{V}}^H \hat{\mathbf{J}}^\top \xrightarrow{p} \mathbf{J} \mathbf{V}^{H^*} \mathbf{J}^\top$. □

Remark A.1. By Slutsky's theorem, if \mathbf{Q} is a matrix such that $\mathbf{Q} \xrightarrow{p} \mathbf{I}$ as $T \rightarrow \infty$, then $\hat{\mathbf{J}} \mathbf{Q} \hat{\mathbf{V}}^H \hat{\mathbf{Q}}^\top \hat{\mathbf{J}}^\top$ is also a consistent estimator for $\mathbf{J} \mathbf{V}^{H^*} \mathbf{J}^\top$.

C.6 Proofs of Theorem 1 and Corollary 1

The proof of Theorem 1 follows directly from that of Theorem A.2 with the following alternative definition,

$$s(\bar{H}_{t-1}, W_t, Y_t; \boldsymbol{\theta}) = \begin{pmatrix} (\mathbf{Z}_t^\top \mathbf{Z}_t)^{-1} \mathbf{Z}_t^\top \tilde{\mathbf{Y}}_t^H(F_{h'}; \gamma) - \beta'_t - \boldsymbol{\mu}_1 \\ (\mathbf{Z}_t^\top \mathbf{Z}_t)^{-1} \mathbf{Z}_t^\top \tilde{\mathbf{Y}}_t^H(F_{h''}; \gamma) - \beta''_t - \boldsymbol{\mu}_2 \\ \rho_{th'}(\gamma) - 1 - \mu_3 \\ \rho_{th''}(\gamma) - 1 - \mu_4 \\ \psi(W_t, \bar{H}_{t-1}; \gamma) \end{pmatrix}.$$

Thus, we omit the details. In addition, the proof of Corollary 1 follows directly from Proposition A.2 and the fact that $\hat{\gamma}$ is a consistent estimator of γ^* .

D Consistent estimation of variance bound for the Hájek estimator

In this section, we discuss the consistent estimation of the variance bound for the Hájek estimator, and evaluate the empirical performance of several proposed estimators through a simulation study.

D.1 A Consistent estimator

According to Remark A.1 above, the estimator $\hat{\mathbf{J}}\hat{\mathbf{Q}}\hat{\mathbf{V}}^H\mathbf{Q}^\top\hat{\mathbf{J}}^\top$ is a consistent estimator of the true variance bound whenever \mathbf{Q} is a consistent estimator of the identity matrix I . Recall $\rho_{h'} = \frac{1}{T-M+1} \sum_{t=M}^T \rho_{th'}$ and $\rho_{h''} = \frac{1}{T-M+1} \sum_{t=M}^T \rho_{th''}$. Moreover, Let $\xi_{h'}$ and $\xi_{h''}$ denote the mean IPW weights for interventions $F_{h'}$ and $F_{h''}$, respectively when $M = 1$, i.e.,

$$\xi_{h'} = \frac{1}{T} \sum_{t=1}^M \frac{f_{h'}(W_t)}{e_t(W_t; \hat{\gamma})} \quad \text{and} \quad \xi_{h''} = \frac{1}{T} \sum_{t=1}^M \frac{f_{h''}(W_t)}{e_t(W_t; \hat{\gamma})}.$$

Note that all the $\rho_{h'}$, $\rho_{h''}$, $\xi_{h'}$ and $\xi_{h''}$ converge to 1 in probability as $T \rightarrow \infty$. Thus, we can construct following consistent estimators: $\hat{\mathbf{J}}\hat{\mathbf{Q}}\hat{\mathbf{V}}^H\mathbf{Q}^\top\hat{\mathbf{J}}^\top$ where

$$\mathbf{Q} = \begin{pmatrix} \rho_{h'}^{-1} \mathbf{I}_L & \mathbf{0} & \mathbf{0} & \mathbf{0} \\ \mathbf{0} & \rho_{h''}^{-1} \mathbf{I}_L & \mathbf{0} & \mathbf{0} \\ 0 & 0 & \xi_{h'}^{-M} & 0 \\ 0 & 0 & 0 & \xi_{h''}^{-M} \end{pmatrix}$$

While $\rho_{h'}^{-1}\mathbf{I}_L$ and $\rho_{h''}^{-1}\mathbf{I}_L$ are used to stabilize the pseudo-outcomes, $\xi_{h'}^{-M}$ and $\xi_{h''}^{-M}$ stabilize the IPW weights at each time period by the mean of all single time period IPW weights. Our simulation study demonstrates that this estimator performs well across all considered scenarios, producing confidence intervals with empirical coverage close to the nominal level.

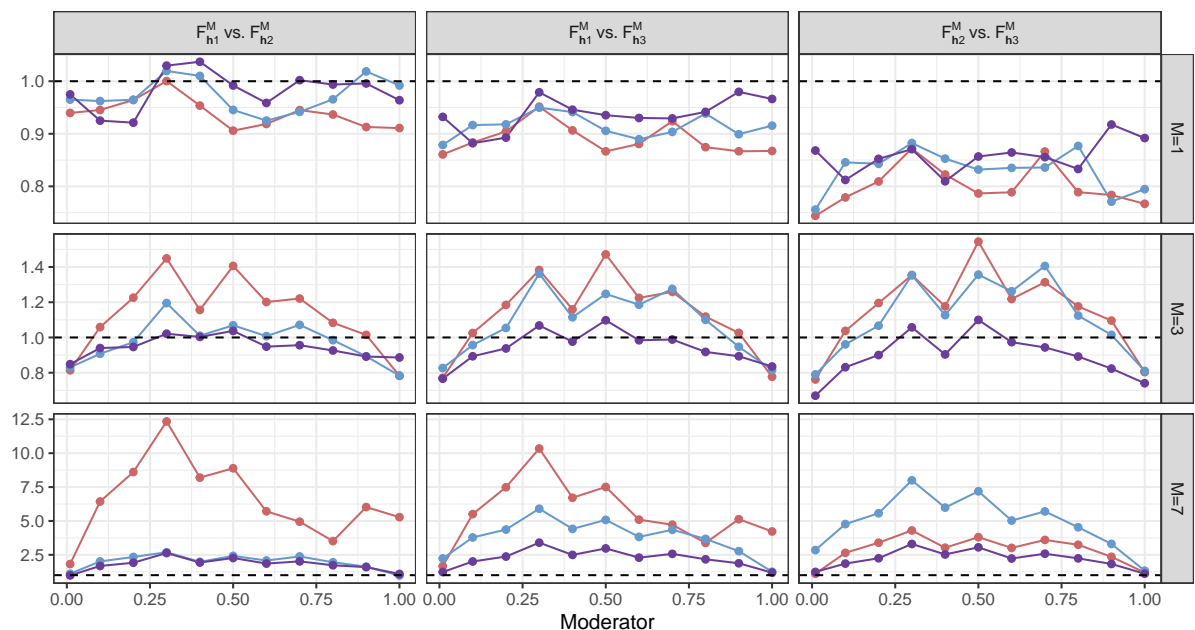
D.2 Empirical performance of the proposed estimator

In this section, we examine the empirical performance of the proposed variance bound estimator through a simulation study. We generate data of different lengths T (200, 500, 1000), consider interventions over different time periods M (1, 3, 7), and analyze two types of moderators: spatial and spatio-temporal. For each scenario, we conducted 500 simulations, where the data-generating process follows the same design as described in Section 4.1.

For each simulation, we compute the square root of the estimated variance bound for the Hájek estimator, averaged over all simulations. We also calculate the Monte Carlo standard deviation of the Hájek estimator. We report the ratio of these two values in Figure A.1. Theoretically, this ratio should be greater than 1.

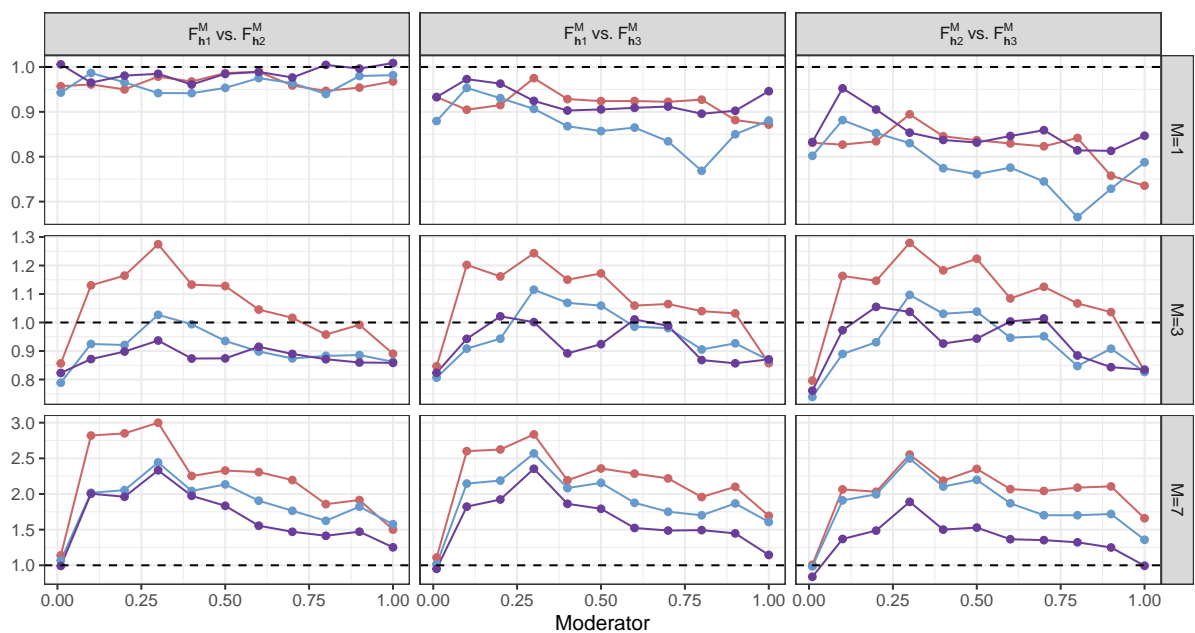
Figure A.1a examines the empirical performance of the variance bound estimator when the moderator is spatial. Each row corresponds to a different intervention time period M (1, 3, 7), and each column compares the results under different interventions. The results show that the ratio of the square root of the variance bound to the Monte Carlo standard deviation generally exceeds 1, aligning with theoretical expectations. However, for $M = 1$, the ratio occasionally falls below 1, particularly when T is small. As T increases from 200 to 1000, the ratio becomes more stable and approaches 1 across all moderator values, reflecting the improved accuracy of the estimator with longer time periods. Furthermore, for larger M (3 and 7), the trends are smoother, suggesting that longer intervention periods reduce variability in the performance of the variance bound estimator.

Figure A.1b presents the results for the spatio-temporal moderator. Similarly to the results for the spatial moderator, the rows correspond to different intervention time periods M , while the columns compare the results under different interventions. The ratio of square root of the variance bound to the Monte Carlo standard deviation remains close to or above 1, particularly for larger values of M and T . As T increases, the ratio stabilizes and approaches 1, especially when $M = 3$ or $M = 7$. Compared to the spatial moderator case, the spatio-temporal results exhibit less fluctuation, even for small T , indicating that the variance bound estimator performs more reliably under the spatio-temporal setting.



(a) Spatial moderator

— T=200 — T=500 — T=1000



(b) Spatio-temporal moderator

Figure A.1: Ratio of the square root of the estimated variance bound, averaged across 500 simulations, to the mean standard deviation of the Hájek estimator based on the estimated propensity score with a spatio-temporal moderator. The standard deviation is computed by the Monte Carlo approximation. Interventions are considered over different time periods ($M = 1, 3, 7$) and for time series of varying lengths ($T = 200, 500, 1000$).

E Statistical test of no heterogeneity

In this section, we prove Theorem 3. To do this, we first prove the following lemma, which shows the limiting reference distribution of the test statistic under the null hypothesis.

Lemma A.2. *Suppose that the assumptions of Theorem 1 hold and $\bar{\beta}^* = \mathbf{0}$. Then, as $T \rightarrow \infty$, we have:*

$$\frac{1}{T - M + 1} (\bar{\beta} - \bar{\beta}^*)^\top (\mathbf{J}\mathbf{V}^H \mathbf{J}^\top)^{-1} (\bar{\beta} - \bar{\beta}^*) \xrightarrow{d} \chi_L^2.$$

E.1 Proof of Lemma A.2

According to Theorem 1, we have, as $T \rightarrow \infty$,

$$\frac{1}{\sqrt{T - M + 1}} (\bar{\beta} - \bar{\beta}^*) \xrightarrow{d} N(\mathbf{0}, \mathbf{J}\mathbf{V}^H \mathbf{J}^\top),$$

Since $\mathbf{J}\mathbf{V}^H \mathbf{J}^\top$ is positive definite, by Cholesky decomposition, we have $(\mathbf{J}\mathbf{V}^H \mathbf{J}^\top)^{-1} = \mathbf{L}\mathbf{L}^\top$ for some lower triangular matrix \mathbf{L} . Then, as $T \rightarrow \infty$,

$$\frac{\mathbf{L}^\top}{\sqrt{T - M + 1}} (\bar{\beta} - \bar{\beta}^*) \xrightarrow{d} N(0, I),$$

By continuous mapping theorem, we have, as $T \rightarrow \infty$,

$$\begin{aligned} \frac{1}{T - M + 1} (\bar{\beta} - \bar{\beta}^*)^\top (\mathbf{L}\mathbf{L}^\top)^{-1} (\bar{\beta} - \bar{\beta}^*) &= \frac{1}{T - M + 1} (\bar{\beta} - \bar{\beta}^*)^\top (\mathbf{J}\mathbf{V}^H \mathbf{J}^\top)^{-1} (\bar{\beta} - \bar{\beta}^*) \\ &\xrightarrow{d} \chi_L^2. \end{aligned}$$

□

E.2 Proof of Theorem 3

By Lemma A.2, we have

$$\lim_{T \rightarrow \infty} \mathbb{P} \left(\frac{1}{T - M + 1} (\bar{\beta} - \mathbf{0})^\top (\mathbf{J}\mathbf{V}^H \mathbf{J}^\top)^{-1} (\bar{\beta} - \mathbf{0}) > \chi_{1-\alpha, L}^2 \right) = \alpha$$

Since $\mathbf{V}^{H*} - \mathbf{V}^H$ is positive semidefinite matrix,

$$\frac{1}{T - M + 1} \bar{\beta}^\top (\mathbf{J}\mathbf{V}^{H*} \mathbf{J}^\top)^{-1} \bar{\beta} \geq \frac{1}{T - M + 1} \bar{\beta}^\top (\mathbf{J}\mathbf{V}^H \mathbf{J}^\top)^{-1} \bar{\beta}.$$

Therefore,

$$\mathbb{P}\left(\frac{1}{T-M+1}\bar{\boldsymbol{\beta}}^\top(\mathbf{J}\mathbf{V}^{H*}\mathbf{J}^\top)^{-1}\bar{\boldsymbol{\beta}} > \chi_{1-\alpha,L}^2\right) \geq \mathbb{P}\left(\frac{1}{T-M+1}\bar{\boldsymbol{\beta}}^\top(\mathbf{J}\mathbf{V}^H\mathbf{J}^\top)^{-1}\bar{\boldsymbol{\beta}} > \chi_{1-\alpha,L}^2\right).$$

This implies,

$$\limsup_{T \rightarrow \infty} \mathbb{P}\left(\frac{1}{T-M+1}\bar{\boldsymbol{\beta}}^\top(\mathbf{J}\mathbf{V}^{H*}\mathbf{J}^\top)^{-1}\bar{\boldsymbol{\beta}} > \chi_{1-\alpha,L}^2\right) \leq \alpha.$$

Let $n \in \mathbb{N}$ be given. Define $\mathbf{D} = (\hat{\mathbf{J}}\hat{\mathbf{Q}}\hat{\mathbf{V}}^H\hat{\mathbf{Q}}^\top\hat{\mathbf{J}}^\top)^{-1} - (\mathbf{J}\mathbf{V}^{H*}\mathbf{J}^\top)^{-1}$. Since $\hat{\mathbf{J}}\hat{\mathbf{Q}}\hat{\mathbf{V}}^H\hat{\mathbf{Q}}^\top\hat{\mathbf{J}}^\top$ is a consistent estimator of $\mathbf{J}\mathbf{V}^{H*}\mathbf{J}^\top$, $(\hat{\mathbf{J}}\hat{\mathbf{Q}}\hat{\mathbf{V}}^H\hat{\mathbf{Q}}^\top\hat{\mathbf{J}}^\top)^{-1}$ is a consistent estimator of $(\mathbf{J}\mathbf{V}^{H*}\mathbf{J}^\top)^{-1}$. Therefore, we have $\lim_{T \rightarrow \infty} \mathbb{P}(\|\mathbf{D}\| > \frac{1}{n}) = 0$. Since $\bar{\boldsymbol{\beta}}$ is bounded, we have

$$\lim_{T \rightarrow \infty} \mathbb{P}\left(\left|\bar{\boldsymbol{\beta}}^\top \mathbf{D} \bar{\boldsymbol{\beta}}\right| > \frac{1}{n}\right) \leq \lim_{T \rightarrow \infty} \mathbb{P}\left(\|\bar{\boldsymbol{\beta}}\|^2 \|\mathbf{D}\| > \frac{1}{n}\right) = 0.$$

Note that

$$\begin{aligned} & \mathbb{P}\left(\frac{1}{T-M+1}\bar{\boldsymbol{\beta}}^\top(\hat{\mathbf{J}}\hat{\mathbf{V}}^H\hat{\mathbf{J}}^\top)^{-1}\bar{\boldsymbol{\beta}} > \chi_{1-\alpha,L}^2 + \frac{1}{n}\right) \\ &= \mathbb{P}\left(\frac{1}{T-M+1}\bar{\boldsymbol{\beta}}^\top(\mathbf{J}\mathbf{V}^{H*}\mathbf{J}^\top)^{-1}\bar{\boldsymbol{\beta}} + \bar{\boldsymbol{\beta}}^\top \mathbf{D} \bar{\boldsymbol{\beta}} > \chi_{1-\alpha,L}^2 + \frac{1}{n}\right) \\ &\leq \mathbb{P}\left(\frac{1}{T-M+1}\bar{\boldsymbol{\beta}}^\top(\mathbf{J}\mathbf{V}^{H*}\mathbf{J}^\top)^{-1}\bar{\boldsymbol{\beta}} > \chi_{1-\alpha,L}^2\right) + \mathbb{P}\left(\left|\bar{\boldsymbol{\beta}}^\top \mathbf{D} \bar{\boldsymbol{\beta}}\right| > \frac{1}{n}\right) \\ &\leq \alpha + \mathbb{P}\left(\left|\bar{\boldsymbol{\beta}}^\top \mathbf{D} \bar{\boldsymbol{\beta}}\right| > \frac{1}{n}\right). \end{aligned}$$

Taking the lim sup of both sides, we obtain

$$\limsup_{T \rightarrow \infty} \mathbb{P}\left(\frac{1}{T-M+1}\bar{\boldsymbol{\beta}}^\top(\hat{\mathbf{J}}\hat{\mathbf{V}}^H\hat{\mathbf{J}}^\top)^{-1}\bar{\boldsymbol{\beta}} > \chi_{1-\alpha,L}^2 + \frac{1}{n}\right) \leq \alpha + 0 = \alpha.$$

Let E_n denote the event that

$$\frac{1}{T-M+1}\bar{\boldsymbol{\beta}}^\top(\hat{\mathbf{J}}\hat{\mathbf{V}}^H\hat{\mathbf{J}}^\top)^{-1}\bar{\boldsymbol{\beta}} > \chi_{1-\alpha,L}^2 + \frac{1}{n}.$$

Since $\{E_n\}_{n \geq 1}$ is an increasing sequence of events, taking the limit of $n \rightarrow \infty$, we have

$$\limsup_{T \rightarrow \infty} \mathbb{P}\left(\frac{1}{T-M+1}\bar{\boldsymbol{\beta}}^\top(\hat{\mathbf{J}}\hat{\mathbf{V}}^H\hat{\mathbf{J}}^\top)^{-1}\bar{\boldsymbol{\beta}} > \chi_{1-\alpha,L}^2\right) \leq \alpha.$$

Note that

$$\mathbb{P}(\text{p-value} < \alpha) = \mathbb{P}(T_c > \chi_{1-\alpha, L}^2) = \mathbb{P}\left(\frac{1}{T - M + 1} \bar{\boldsymbol{\beta}}^\top (\hat{\mathbf{J}} \hat{\mathbf{V}}^H \hat{\mathbf{J}}^\top)^{-1} \bar{\boldsymbol{\beta}} > \chi_{1-\alpha, L}^2\right).$$

We obtain the desired result,

$$\limsup_{T \rightarrow \infty} \mathbb{P}(\text{p-value} < \alpha) \leq \alpha.$$

□

F Additional simulation results

In this section, we present additional simulation results for the Hájek and IPW estimators. We also compare those two estimators and examine the efficiency gain resulting from the use of the estimated propensity score rather than the true propensity score.

F.1 The Hájek estimator

We present additional simulation results for the Hájek estimator. Figure A.2 shows the results for the comparison between the two interventions, $F_{\mathbf{h}_1}^M$ and $F_{\mathbf{h}_2}^M$, while Figure A.3 compares $F_{\mathbf{h}_2}^M$ with $F_{\mathbf{h}_3}^M$.

In Figure A.2, we present results for the comparison between $F_{\mathbf{h}_1}^M$ and $F_{\mathbf{h}_2}^M$. For the spatial moderator (Figure A.2a), we observe that the Hájek estimator performs well for $M = 1$, with estimated CATEs closely tracking the true CATEs and minimal bias. The empirical coverage of the 95% confidence intervals remains close to the nominal level within the shaded region, highlighting the 0.025 and 0.975 quantiles of the moderator values. However, as M increases to 3 and 7, the bias begins to increase slightly near the upper end of the moderator range (values close to 1), particularly for the estimator using truncated weights. This indicates that longer time series may be required in these regions to achieve better performance. For the spatio-temporal moderator (Figure A.2b), similar trends emerge. The Hájek estimator performs well for small M , with coverage rates remaining stable and close to 0.95. However, for $M = 7$, the bias increases for larger moderator values, although it remains small overall. Notably, estimators using the truncated weights tend to exhibit higher coverage rates, especially in scenarios where the data are sparse.

In Figure A.3, we present results for the comparison between $F_{\mathbf{h}_2}^M$ and $F_{\mathbf{h}_3}^M$. For the spatial moderator (Figure A.3a), the Hájek estimator again performs well when $M = 1$, with minimal bias and empirical coverage rates close to the nominal 0.95 level. As M increases, deviations from the true CATE become more apparent near the upper range of

the moderator values, particularly for truncated weights. In the spatio-temporal moderator case (Figure A.3b), the performance of the Hájek estimator remains robust for $M = 1$, with small bias and stable coverage rates. For larger M , the estimated CATEs continue to closely follow the true CATEs within the shaded region, although small biases appear near the large values of the moderator. Similarly to the spatial case, the truncated-weight estimators tend to have slightly larger bias, but higher empirical coverage rates compared to the estimators using true or estimated propensity scores.

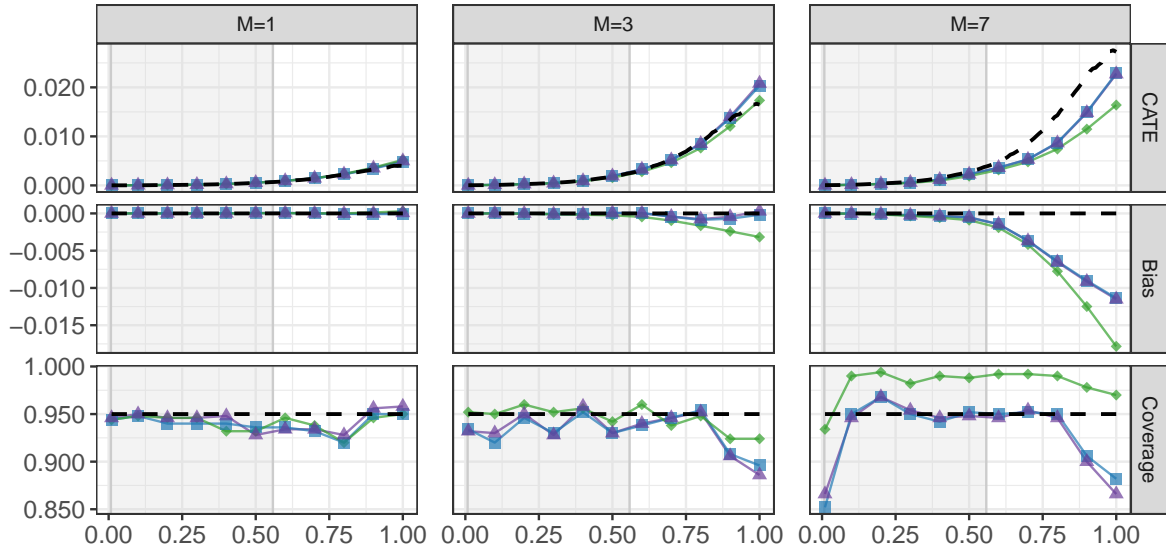
Overall, these additional results demonstrate that the Hájek estimator performs consistently well in the different scenarios. For both spatial and spatio-temporal moderators, the empirical coverage rates remain close to the nominal 95% level, especially for small M . However, as M increases, deviations from the true CATEs become noticeable at higher moderator values, suggesting that longer time series are needed to maintain performance in sparse regions. The use of truncated weights leads to slightly higher bias but generally improves coverage, particularly for the spatial moderator.

F.2 The IPW estimator

We present the performance of IPW estimators in the simulation studies described in Section 4. Figures A.4, A.5, and A.6 show the results of the comparison of $F_{h_1}^M$ v.s $F_{h_2}^M$, $F_{h_1}^M$ v.s $F_{h_3}^M$ and $F_{h_2}^M$ v.s $F_{h_3}^M$ respectively.

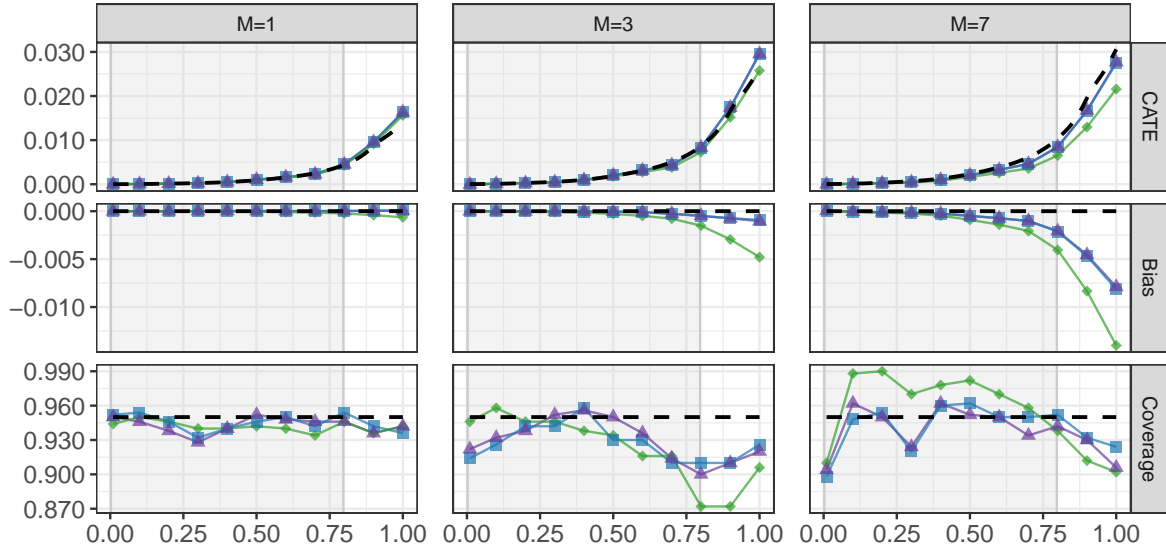
In Figure A.4, which compares $F_{h_1}^M$ and $F_{h_2}^M$, the IPW estimators perform well in the spatial moderator case when $M = 1$, where the estimated CATEs align closely with the true CATEs and exhibit minimal bias. The empirical coverage remains near the nominal 95% level. As M increases to 3 and 7, unstabilized weights result in larger biases, particularly near the upper range of the moderator values, and the empirical coverage deteriorate as M increases. For $M = 7$ the coverage is about 60% for spatial moderator and 70% for spatio-temporal when using untruncated and unstabilized IPW weights. In contrast, stabilized weights produce smaller biases and maintain more reliable coverage. For the spatio-temporal moderator, a similar pattern holds: stabilized weights consistently outperform their unstabilized counterparts, delivering more accurate estimates and better coverage properties. Additionally, estimators using the estimated propensity scores generally achieve comparable or even superior performance relative to those based on the true propensity scores.

Figure A.5 displays the results for $F_{h_1}^M$ versus $F_{h_3}^M$. In the spatial moderator case, the IPW estimators perform well when $M = 1$, but as M increases, bias becomes more pronounced for unstabilized weights, particularly near higher moderator values. Empirical coverage remains mostly stable across the range but drops for larger M . Similar trends



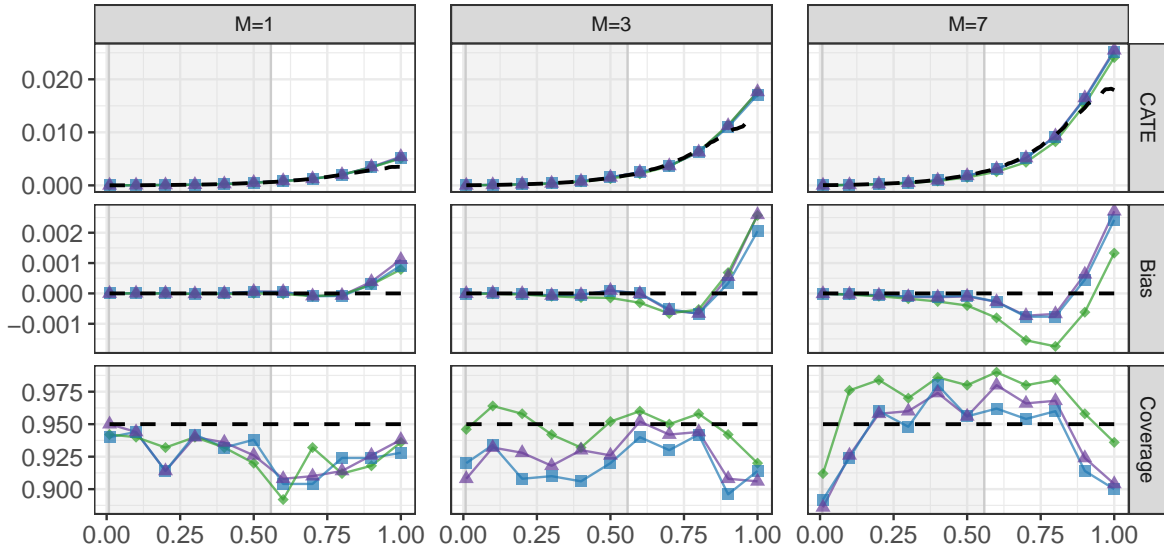
(a) Spatial moderator

▲ Hajek
 ■ Hajek with estimated PS
 ◆ Hajek with estimated PS (truncated)



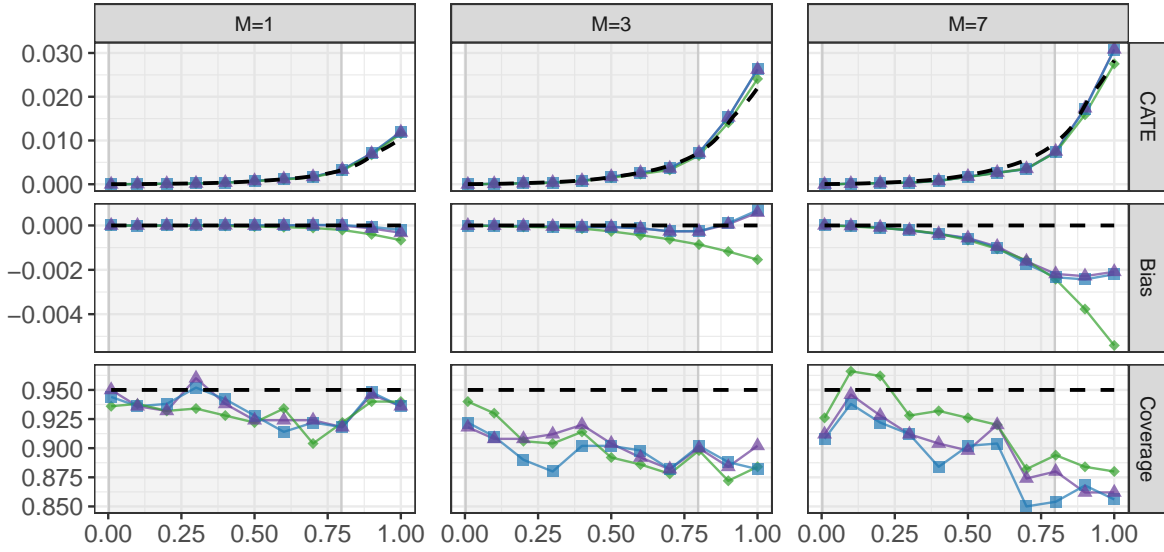
(b) Spatio-temporal moderator

Figure A.2: The average of estimated CATE (first row), bias (second row) and coverage (third row) based on the Hájek estimator for $F_{h_1}^M$ versus $F_{h_2}^M$ across 500 simulations. Dashed lines in the first, second, and third rows represent the true CATE, zero bias, and the theoretical minimum coverage, respectively. Plot (a) corresponds to the spatial moderator, while plot (b) pertains to the spatio-temporal moderator, both for various values of $M = 1, 3, 7$. The purple line with triangles denotes the estimator based on the true propensity score, while the green line with diamonds and the blue line with squares represent the estimators based on the estimated propensity scores with and without truncation, respectively. The shaded region indicates the range between the 0.025 and 0.975 quantiles of the moderator values.



(a) Spatial moderator

—▲ Hajek —■ Hajek with estimated PS —◆ Hajek with estimated PS (truncated)



(b) Spatio-temporal moderator

Figure A.3: The average of estimated CATE (first row), bias (second row) and coverage (third row) based on the Hájek estimator for $F_{h_2}^M$ versus $F_{h_3}^M$ across 500 simulations. Dashed lines in the first, second, and third rows represent the true CATE, zero bias, and the theoretical minimum coverage, respectively. Plot (a) corresponds to the spatial moderator, while plot (b) pertains to the spatio-temporal moderator, both for various values of $M = 1, 3, 7$. The purple line with triangles denotes the estimator based on the true propensity score, while the green line with diamonds and the blue line with squares represent the estimators based on the estimated propensity scores with and without truncation, respectively. The shaded region indicates the range between the 0.025 and 0.975 quantiles of the moderator values.

are observed for the spatio-temporal moderator. Notably, the use of estimated propensity scores continues to produce results similar to, or occasionally better than, those based on true propensity scores.

For $F_{h_2}^M$ versus $F_{h_3}^M$, the results are shown in Figure A.6. In the spatial moderator case, the IPW estimators again perform well for $M = 1$, with estimated CATEs exhibiting minimal bias and empirical coverage close to 0.95. As M increases, unstabilized weights result in noticeable bias at higher moderator values and the coverage drops. In particular, for $M = 7$, the empirical coverage falls below 50% for all IPW-type estimators. The spatio-temporal results are consistent with earlier findings.

Overall, the IPW estimators perform well in low-variance settings, such as $M = 1$. However, for larger values of M , stabilized weights substantially enhance performance, reducing bias and improving empirical coverage. Across all comparisons and moderator types, estimators based on the estimated propensity scores often outperform those using the true propensity scores. These findings align with broader results in causal inference, where stabilized weights are known to improve finite-sample properties, especially in higher-variance settings.

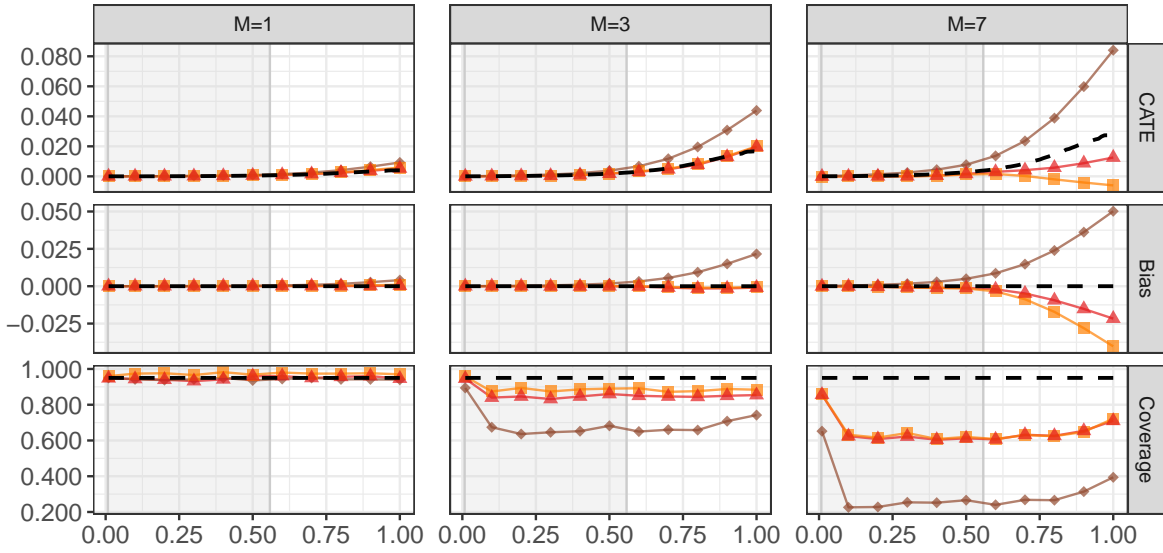
F.3 Efficiency due to the use of the estimated propensity score

We examine the relative efficiency of the IPW and Hájek estimators when using the estimated propensity score rather than the true propensity score. In particular, we computed the Monte Carlo standard deviation of the estimators across 500 simulations and present the ratio of standard deviation for the proposed estimator based on the true propensity score over that based on the estimated propensity score. If the ratio is greater than 1, the estimated propensity score makes the Hájek and IPW estimators more efficient than the true propensity score. According to Theorem 2 and Theorem A.3, these ratios should be no less than 1 asymptotically.

The results are shown in Figure A.7. We find that the estimated propensity score yields a significant efficiency gain for the IPW estimator for $M = 1$ and $M = 3$, while the variance ratio for the Hájek estimator remains close to 1 in all scenarios. Occasionally, the variance ratio falls below 1, especially in high-variability scenarios with $M = 7$. This may be because the Monte Carlo variance does not sufficiently approximate the true asymptotic variances for the sample sizes considered.

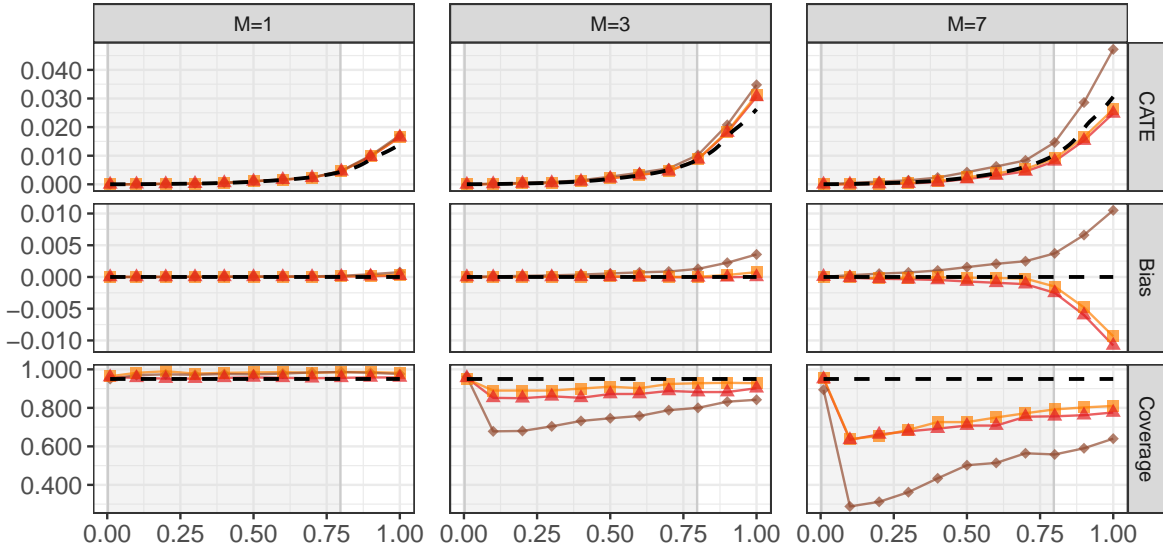
F.4 Efficiency comparison of IPW and Hájek estimators

Finally, we compare the variance of the IPW estimator with that of the Hájek estimator. We compute the Monte Carlo standard deviation of the IPW and Hájek estimators based on



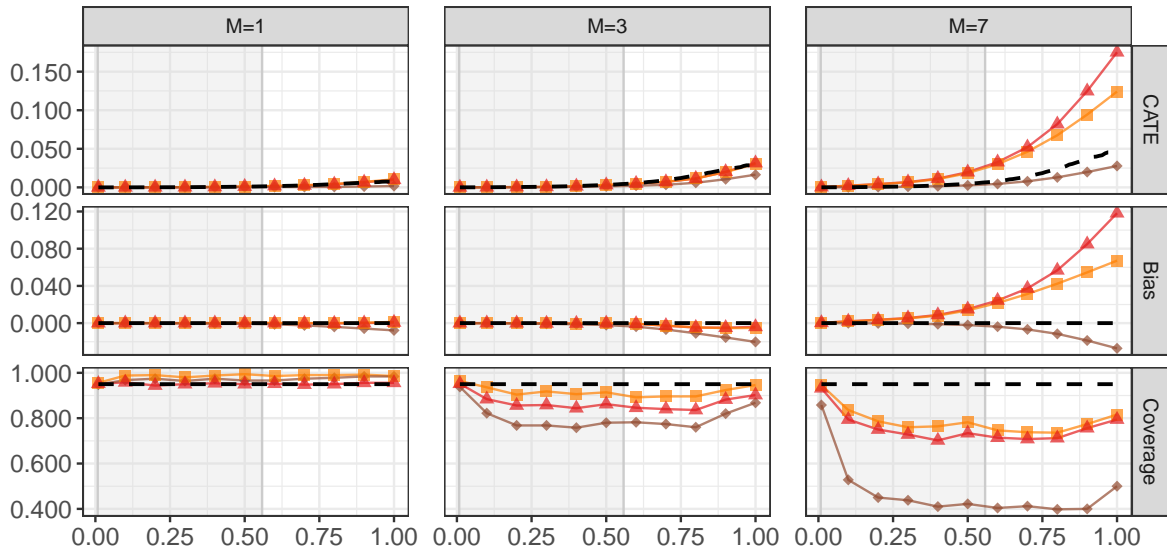
(a) Spatial moderator

—▲ IPW —■ IPW with estimated PS —◆ IPW with estimated PS (truncated)



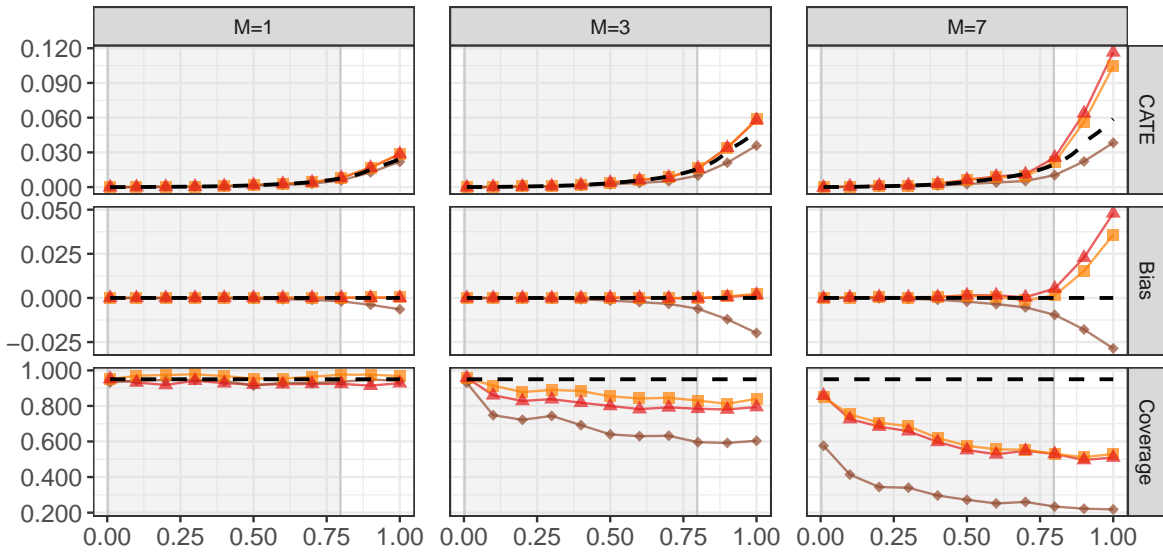
(b) Spatio-temporal moderator

Figure A.4: The average of estimated CATE (first row), bias (second row) and coverage (third row) based on IPW estimators for $F_{h_1}^M$ versus $F_{h_2}^M$ across 500 simulations. Dashed lines in the first, second, and third rows represent the true CATE, zero bias, and the theoretical minimum coverage, respectively. Plot (a) corresponds to the spatial moderator, while plot (b) pertains to the spatio-temporal moderator, both for various values of $M = 1, 3, 7$. The purple line with triangles denotes the estimator based on the true propensity score, while the green line with diamonds and the blue line with squares represent the estimators based on the estimated propensity scores with and without truncation, respectively. The shaded region indicates the range between the 0.025 and 0.975 quantiles of the moderator values.



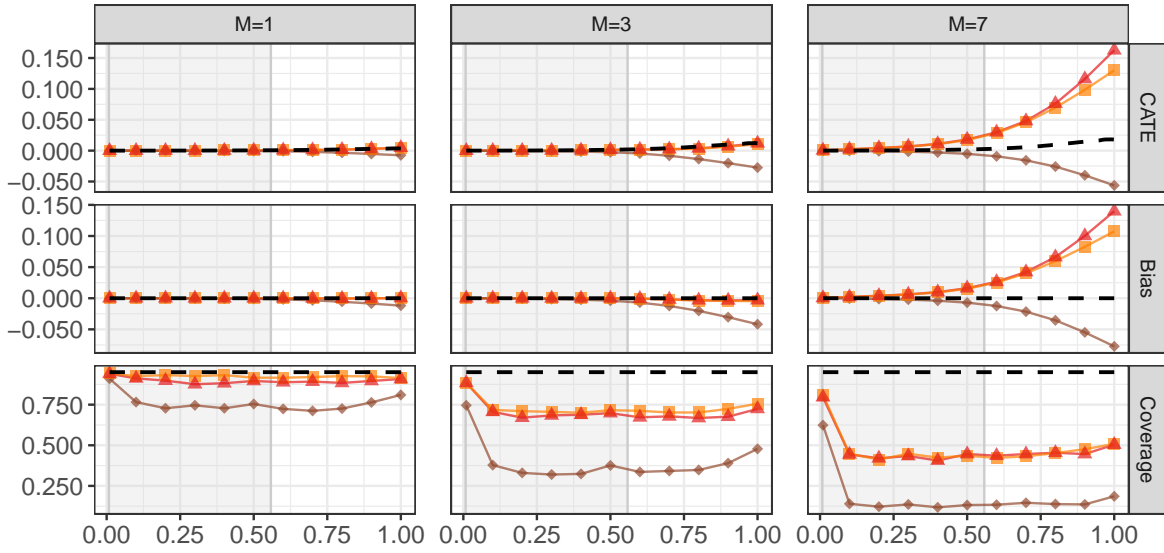
(a) Spatial moderator

—▲ IPW —■ IPW with estimated PS —◆ IPW with estimated PS (truncated)



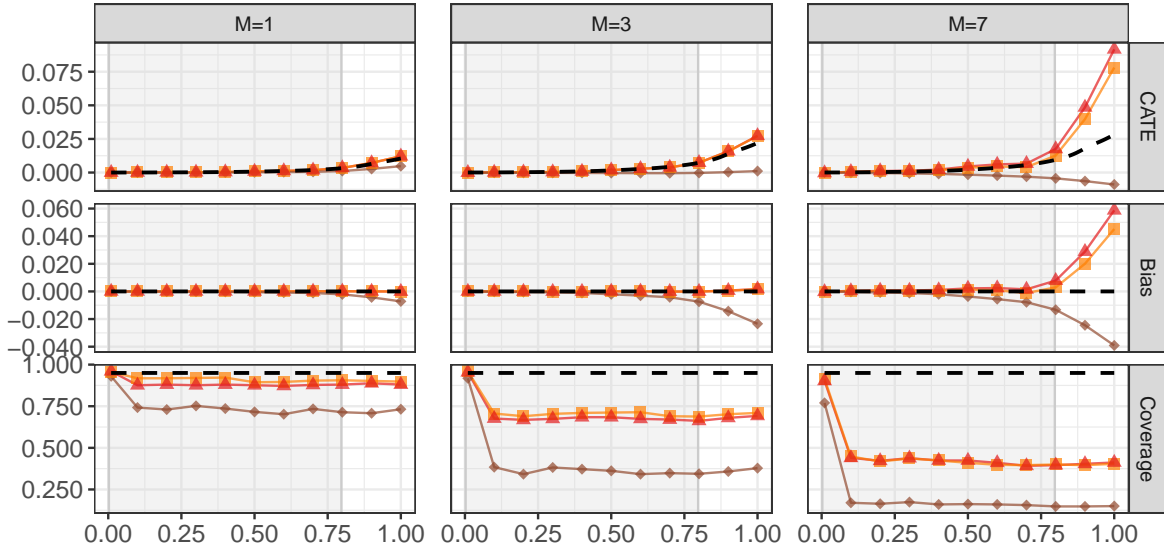
(b) Spatio-temporal moderator

Figure A.5: The average of estimated CATE (first row), bias (second row) and coverage (third row) based on IPW estimators for $F_{\mathbf{h}_1}^M$ versus $F_{\mathbf{h}_3}^M$ across 500 simulations. Dashed lines in the first, second, and third rows represent the true CATE, zero bias, and the theoretical minimum coverage, respectively. Plot (a) corresponds to the spatial moderator, while plot (b) pertains to the spatio-temporal moderator, both for various values of $M = 1, 3, 7$. The purple line with triangles denotes the estimator based on the true propensity score, while the green line with diamonds and the blue line with squares represent the estimators based on the estimated propensity scores with and without truncation, respectively. The shaded region indicates the range between the 0.025 and 0.975 quantiles of the moderator values.



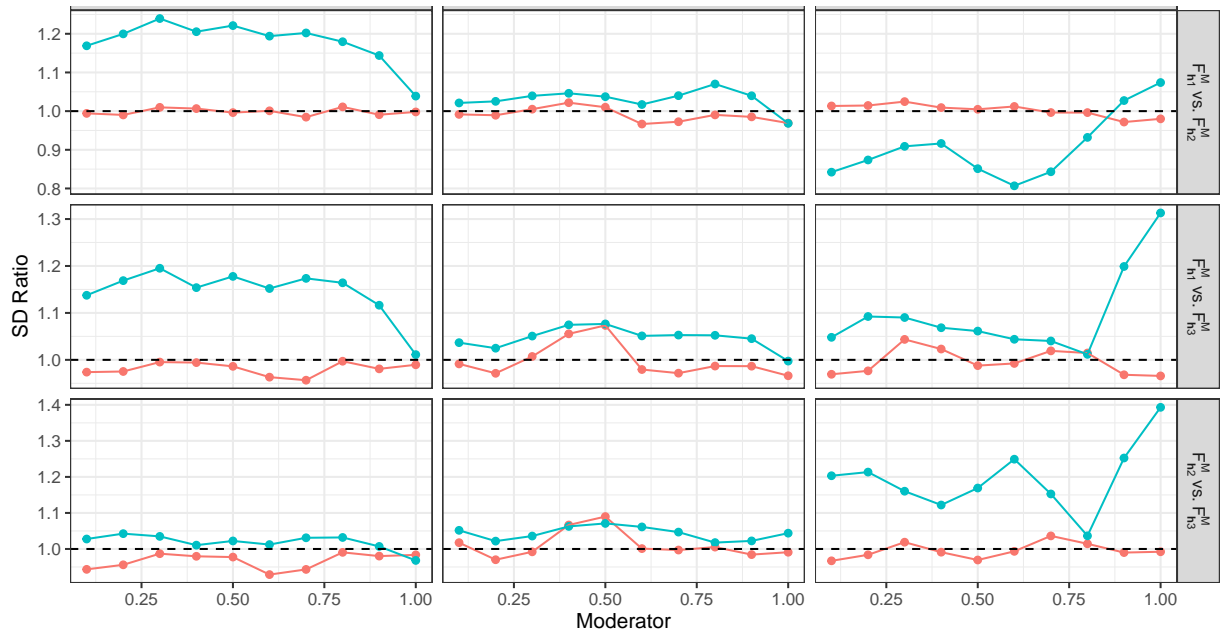
(a) Spatial moderator

—▲ IPW —■ IPW with estimated PS —◆ IPW with estimated PS (truncated)

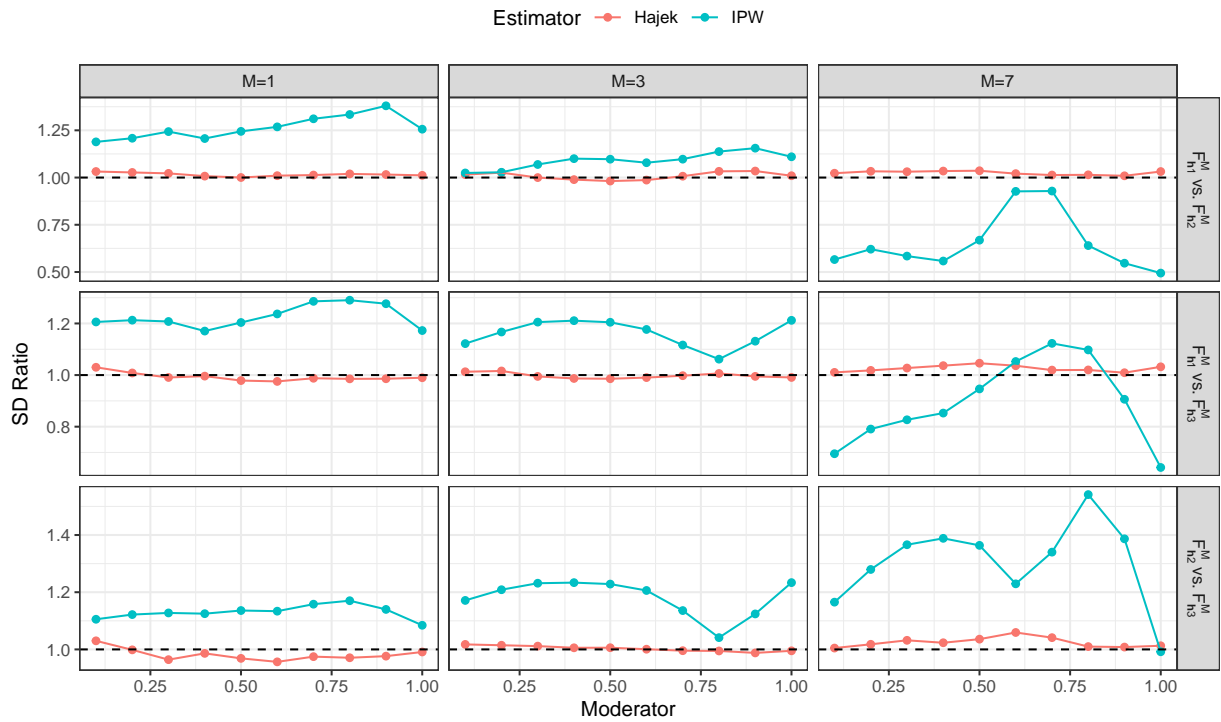


(b) Spatio-temporal moderator

Figure A.6: The average of estimated CATE (first row), bias (second row) and coverage (third row) based on IPW estimators for $F_{h_2}^M$ versus $F_{h_3}^M$ across 500 simulations. Dashed lines in the first, second, and third rows represent the true CATE, zero bias, and the theoretical minimum coverage, respectively. Plot (a) corresponds to the spatial moderator, while plot (b) pertains to the spatio-temporal moderator, both for various values of $M = 1, 3, 7$. The purple line with triangles denotes the estimator based on the true propensity score, while the green line with diamonds and the blue line with squares represent the estimators based on the estimated propensity scores with and without truncation, respectively. The shaded region indicates the range between the 0.025 and 0.975 quantiles of the moderator values.



(a) Spatial moderator



(b) Spatio-temporal moderator

Figure A.7: Standard deviation ratio of the proposed estimator based on the true propensity score over the proposed estimator based on the estimated propensity score. The results are based on Monte Carlo approximation with $T = 1000$ and 500 simulations. The estimated propensity score is obtained from the correctly specified model. We compare interventions that are over different time periods: $M = 1, 3, 7$. In one time period, the expected number of outcome events yielded by $F_{h_1}^M$, $F_{h_2}^M$ and $F_{h_3}^M$ are 3, 5, 7 respectively.

the estimated propensity score across 500 simulations with $T = 500$ under several scenarios. Figure A.8 presents the ratio of these estimated variances. We find that the Hájek estimator is consistently more efficient than the IPW estimator in all scenarios considered here.

G Additional results for the empirical application

In this section, we present the results of an additional empirical analysis. We first evaluate the quality of the propensity score model using out-of-sample prediction. We then conduct two additional analyses — one with different moderator definitions and the other with different ways of truncating the estimated propensity score. Finally, we use an additional model specification with the binary aid moderator.

G.1 Out-of-sample prediction for propensity scores

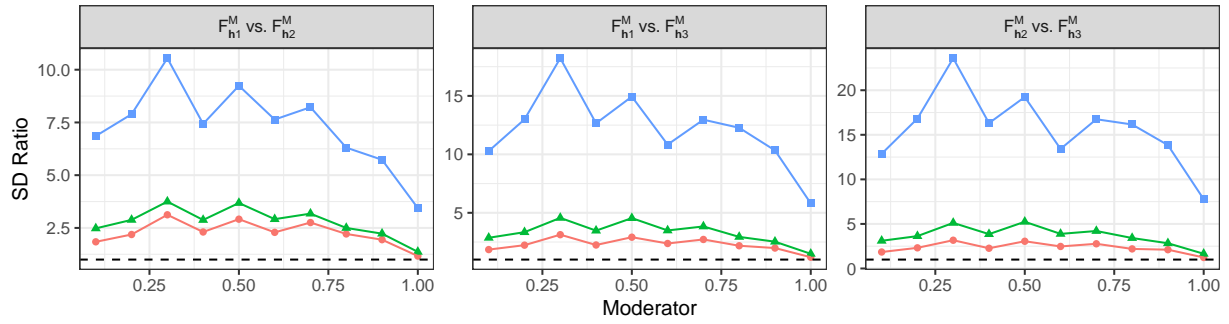
To evaluate the appropriateness of the propensity score model, we compare the predicted number of airstrikes with the observed number of airstrikes in the following four governorates in Iraq: Baghdad, Diyala, Salah al-Din, and Anbar. We assess both out-of-sample predictions, where the model is trained on the first 80% of the observations, and in-sample predictions, where the model is trained using the entire dataset.

Figure A.9 presents the results. The estimated propensity score model captures the general trend of airstrikes in these governorates, although it misses some spikes. The discrepancies are likely due to the large variance in the outcome that is inherent in any point process. Furthermore, the model trained on the first 80% of the data performs similarly to the estimated model using all observations, suggesting that the propensity score model is not overfit.

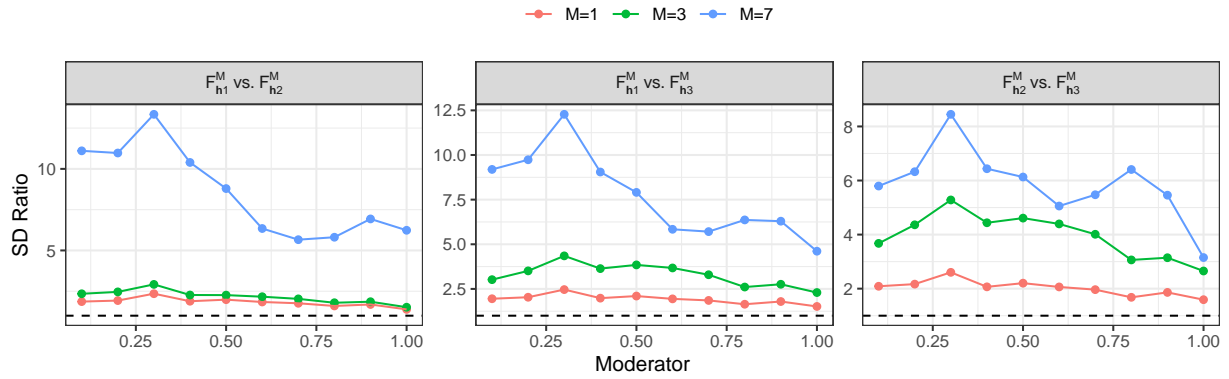
G.2 Different moderator definitions

We conduct an analysis similar to the one presented in Section 5 but define the aid moderator using different lag lengths. Specifically, for the binary moderator, we consider the indicators of aid provision during the previous two weeks and two months. For the continuous moderator, we use the aid per capita received in the previous two weeks and two months. The results for the binary aid moderator are presented in Figures A.10 and A.11, while Figures A.12 and A.13 show the corresponding results for the continuous aid moderator.

For the binary moderator, the results are largely consistent across the two lag lengths. As seen in Figures A.10 and A.11, the estimated CATEs remain stable across all intervention lengths $M = 1, \dots, 10$, with confidence intervals overlapping between the two-week and two-month definitions of aid. For SAF, the CATEs become statistically significant



(a) Spatial moderator



(b) Spatio-temporal moderator

Figure A.8: Standard deviation ratio of the Hájek estimator based on the true propensity score over the IPW estimator based on the true propensity score. The results are based on Monte Carlo approximation with $T = 500$ and 500 simulations. We compare interventions that are over different time periods: $M = 1, 3, 7$. In one time period, the expected number of outcome events yielded by $F_{h_1}^M$, $F_{h_2}^M$ and $F_{h_3}^M$ are 3, 5, 7 respectively.

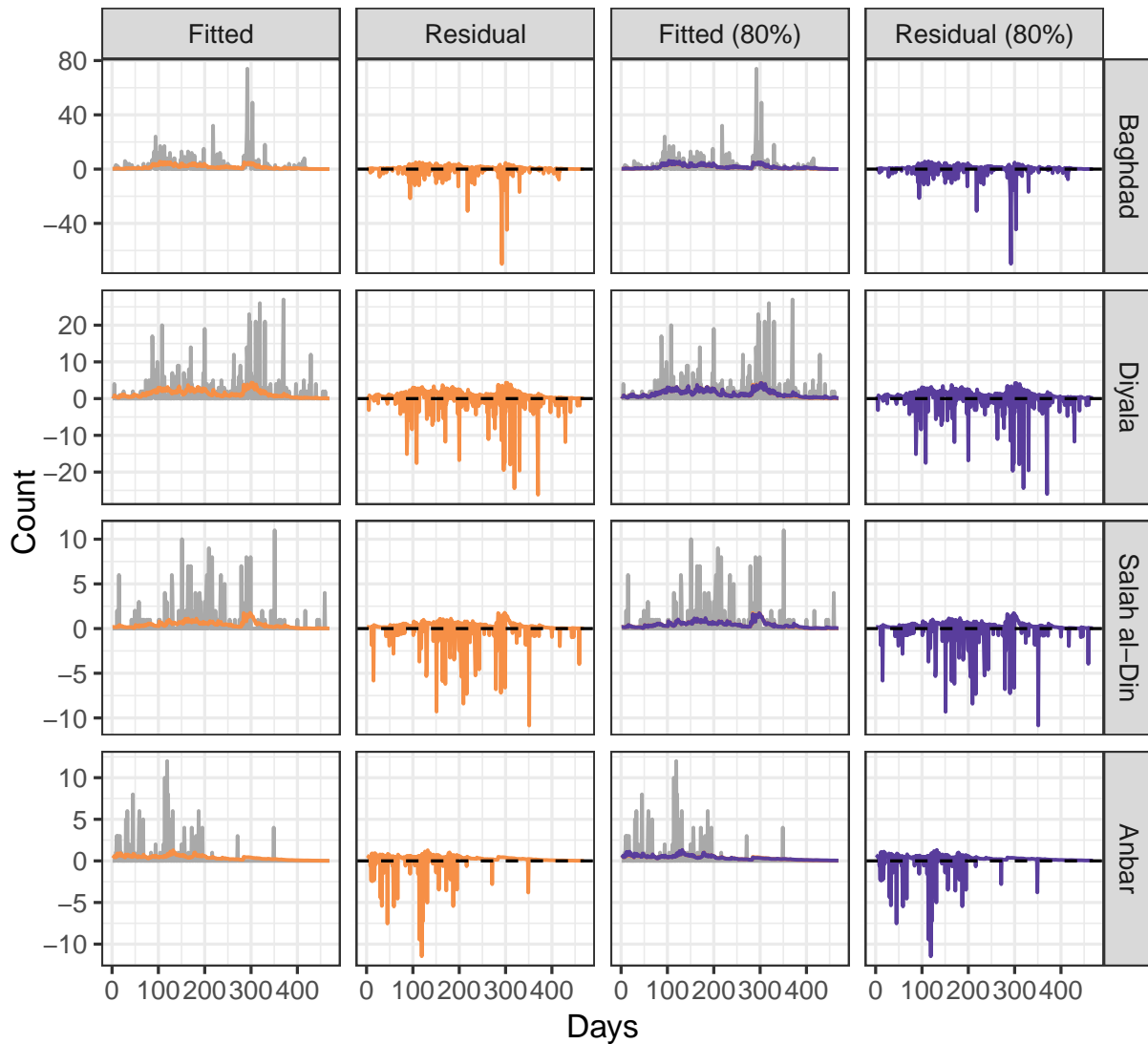


Figure A.9: Actual and predicted counts of airstrikes for four governorate in Iraq (rows). In the first column, the orange and gray lines indicate the fitted and actual counts, respectively. The second column shows the residual plot. In the third and fourth columns, the blue line indicates the results of out-of-sample prediction employing the first 80% of observations.

when the intervention lasts at least seven days, regardless of the lag length. Similarly, for IED, the results remain inconclusive, consistent with the findings in the main analysis.

For the continuous moderator, shown in Figures A.12 and A.13, the results show some sensitivity to the lag length, particularly for longer intervention periods. Although the overall patterns remain similar across the lag lengths, the magnitude of the estimated CATEs tends to be larger when the moderator is the provision of aid over the previous two weeks compared to the previous two months. For example, for IED attacks with $M = 10$, the estimated CATE is 0.20 for districts that received aid during the previous two weeks, compared to 0.15 for those who received aid during the previous two months. This

difference reflects the more immediate effect of the recent aid provision.

Across all durations of the intervention M , confidence intervals tend to be wider when using aid in the previous two weeks, particularly for SAF. This increased uncertainty is likely due to greater variability in the short-term aid measure, which may capture more noise relative to the more stable two-month lag. For shorter intervention lengths ($M = 3$ and $M = 7$), the differences in the estimated CATEs between the two lag lengths are minor, and overall trends remain consistent. Specifically, CATEs exhibit a flat pattern for small M , increase for moderate M , and decrease as M becomes large, regardless of the lag length.

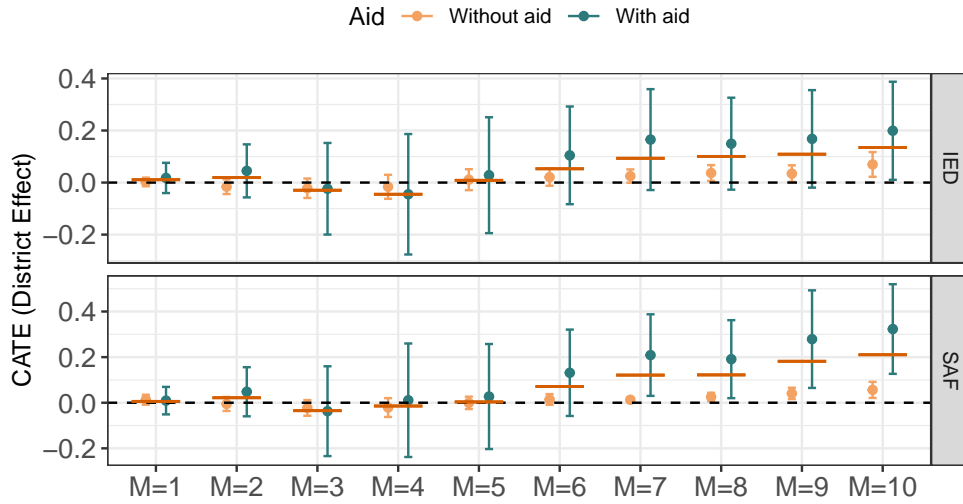
In summary, while the choice of lag length affects the magnitude and precision of the estimated CATEs, the overall patterns observed in the main analysis are preserved. Aid provision during the previous two weeks tends to produce slightly larger estimated effects and wider confidence intervals compared to aid measured over the previous two months, particularly for longer intervention.

G.3 Sensitivity to truncation levels of the estimated propensity scores

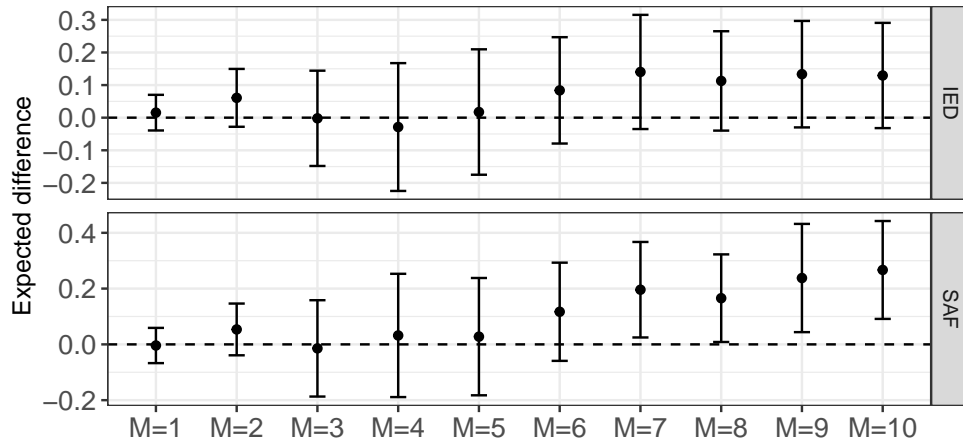
To evaluate the sensitivity of our results to the level of truncation of the estimated propensity scores, we compare the results using truncation at the 90% and 98% quantiles. Figures A.14 and A.15 show the results for the binary aid moderator, while Figures A.16 and A.17 present the corresponding results for the continuous aid moderator.

For the binary aid moderator, truncating the propensity scores at higher quantiles, such as 98%, tends to produce larger estimates of the CATEs with wider confidence intervals compared to truncation at the 90% quantile. As shown in Figure A.14 and Figure A.15, general patterns remain consistent across truncation levels. For SAF, the estimated difference in CATEs between districts with and without aid becomes positive and statistically significant for intervention periods of at least 7 days. However, for IED, the estimation uncertainty is substantial, and the results remain inconclusive regardless of the truncation level.

For the continuous aid moderator, results are shown in Figure A.16 and Figure A.17. Here, we observe greater sensitivity to the choice of truncation level. Higher truncation levels, such as the 98% quantile, lead to larger estimated CATEs and wider confidence intervals, reflecting the increased variability of the estimates. For instance, in Figure A.16, the estimated CATE for SAF at $M = 10$ decreases substantially when moving from the 90% to the 98% truncation level. Although the magnitude of the estimates changes, the



(a) Estimated CATE

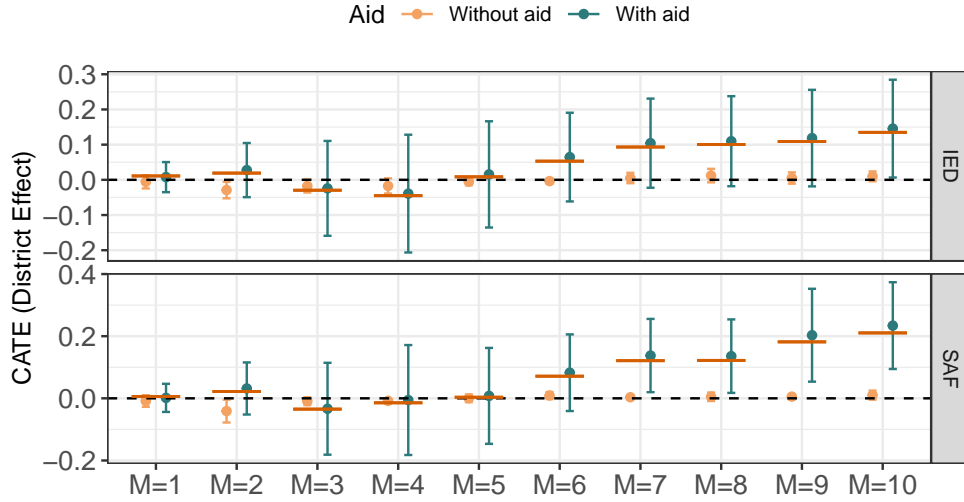


(b) Expected difference

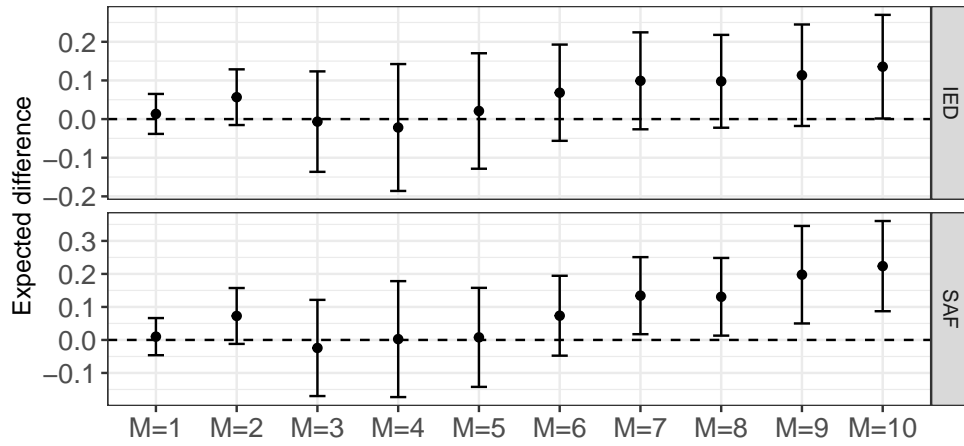
Figure A.10: Results for the binary aid moderator. Plot (a) shows the estimated CATEs of increasing airstrike intensity on the number of insurgency attacks (Improvised Explosive Device or IED in the top panel, and Small Arms Fire or SAF in the bottom panel) a district with or without aid in the previous *two weeks*. The red line segments indicate the average treatment. Plot (b) shows the estimated difference in the CATEs between a district that received aid in the previous *two weeks* and those that did not. The corresponding 95% confidence intervals are also shown for all estimators.

overall patterns are preserved at all truncation levels, with CATE estimates exhibiting little change for small values of M , increasing for moderate values, and decreasing as M becomes large.

The p-values corresponding to tests of no heterogeneity effect are also reported in the figures. For the continuous aid moderator, the p-values tend to decrease as M increases, suggesting stronger evidence of heterogeneity for longer intervention periods. However,



(a) Estimated CATE



(b) Expected difference

Figure A.11: Results for the binary aid moderator. Plot (a) shows the estimated CATEs of increasing airstrike intensity on the number of insurgency attacks (Improvised Explosive Device or IED in the top panel, and Small Arms Fire or SAF in the bottom panel) a district with or without aid in the previous *two months*. The red line segments indicate the average treatment. Plot (b) shows the estimated difference in the CATEs between a district that received aid in the previous *two months* and those that did not. The corresponding 95% confidence intervals are also shown for all estimators.

there are cases where the significance depends on the truncation level. For example, in Figure A.16, the p-values for SAF at $M = 10$ are significant when truncated at the level 90%, while the same results are not significant under the 98% truncation level (Figure A.17).

Overall, while the choice of truncation level affects the magnitude and precision of the estimated effects, it does not alter the general trends observed in the main analysis. For the binary aid moderator, the estimated CATEs for SAF remain positive and significant for

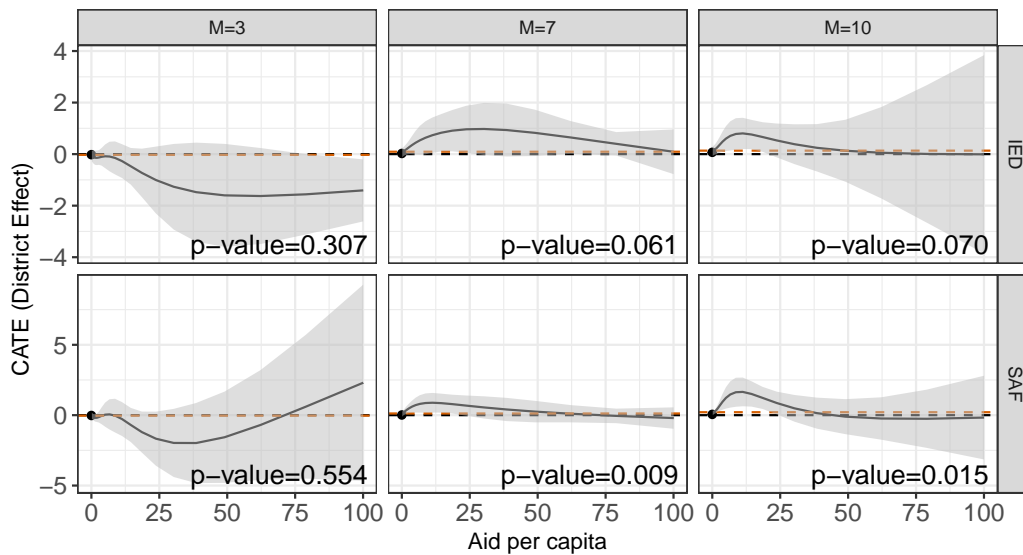


Figure A.12: Estimated CATEs of increasing airstrike intensity on the number of insurgency attacks (Improvised Explosive Device or IED in the top panel, and Small Arms Fire or SAF in the bottom panel) for different values of aid per capita received in the previous *two weeks* with the shaded region indicating the 95% confidence intervals. The red lines represent the estimated average treatment effects. The p-values correspond to tests for the overall heterogeneity effect.

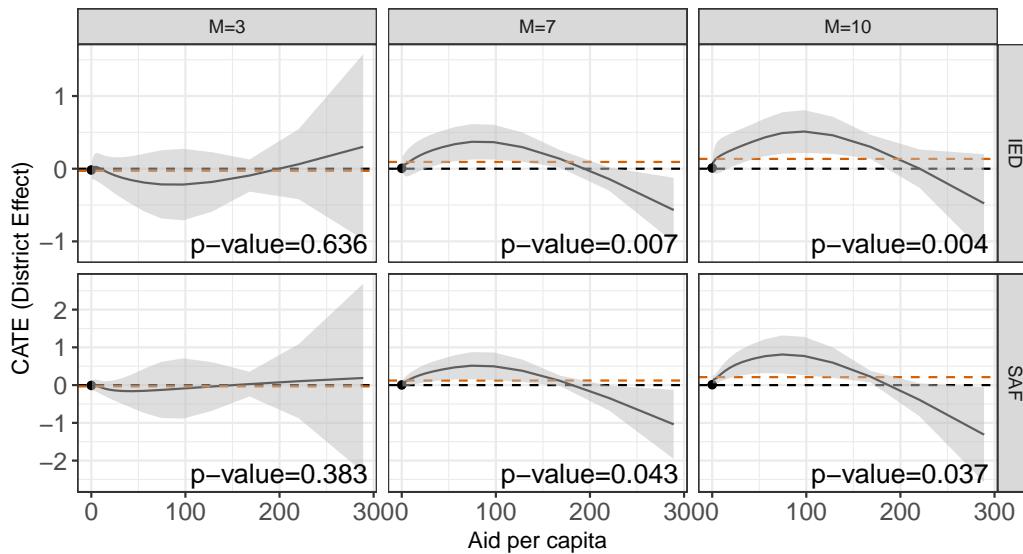
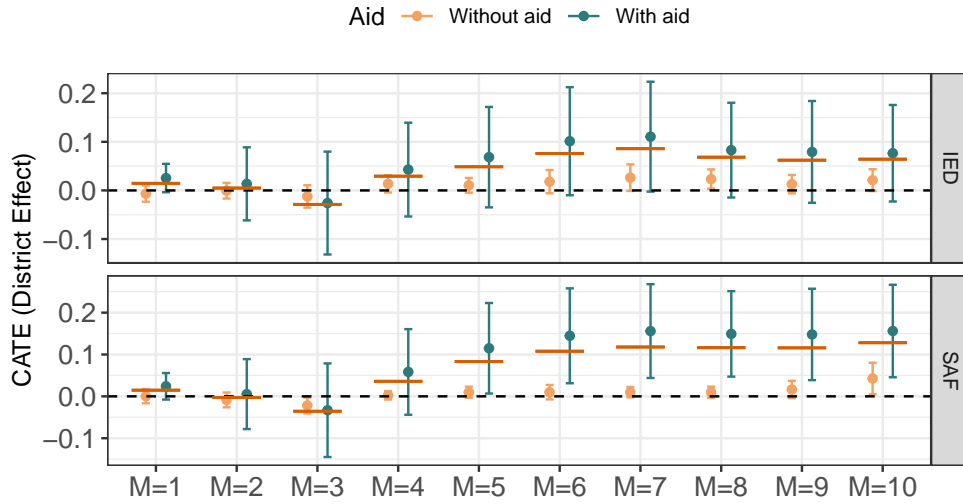
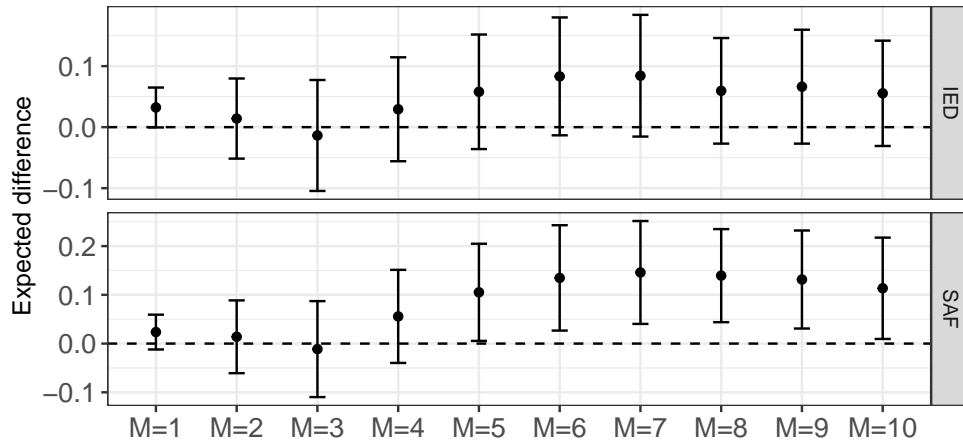


Figure A.13: Estimated CATEs of increasing airstrike intensity on the number of insurgency attacks (Improvised Explosive Device or IED in the top panel, and Small Arms Fire or SAF in the bottom panel) for different values of aid per capita received in the previous *two months* with the shaded region indicating the 95% confidence intervals. The red lines represent the estimated average treatment effects. The p-values correspond to tests for the overall heterogeneity effect.



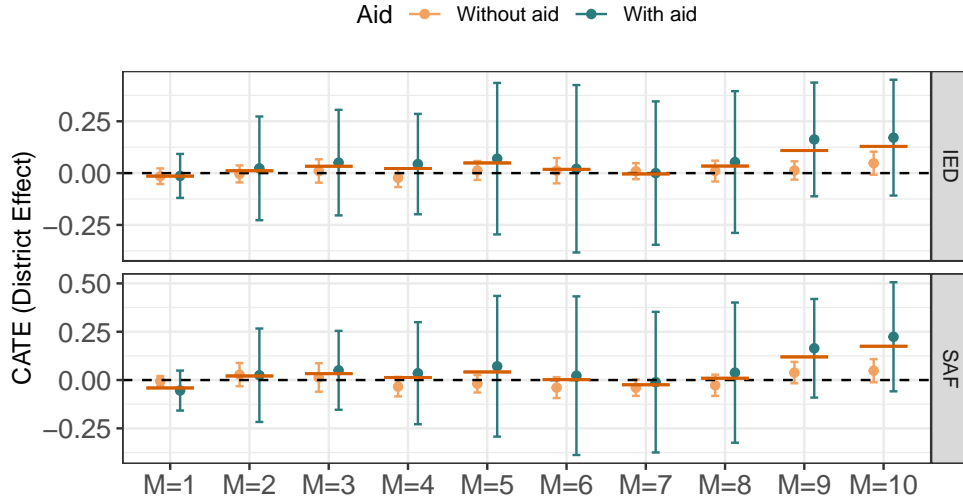
(a) Estimated CATE



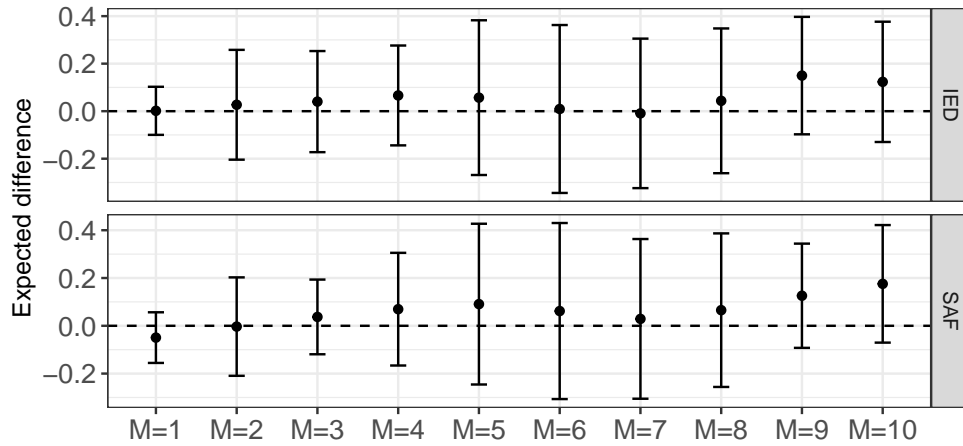
(b) Expected difference

Figure A.14: Results for the binary aid moderator based on propensity scores truncated at the 90th percentile. Plot (a) shows the estimated CATEs of increasing airstrike intensity on the number of insurgency attacks (Improved Explosive Device or IED in the top panel, and Small Arms Fire or SAF in the bottom panel) a district with or without aid in the previous one months. The red line segments indicate the average treatment. Plot (b) shows the estimated difference in the CATEs between a district that received aid in the previous one months and those that did not. The corresponding 95% confidence intervals are also shown for all estimators.

intervention periods of at least seven days, while the results for IED remain inconclusive. For the continuous aid moderator, the results are more sensitive to truncation, but the observed patterns are robust, with evidence of heterogeneity increasing as the intervention period grows longer.



(a) Estimated CATE



(b) Expected difference

Figure A.15: Results for the binary aid moderator based on propensity scores truncated at the 98th percentile. Plot (a) shows the estimated CATEs of increasing airstrike intensity on the number of insurgency attacks (Improved Explosive Device or IED in the top panel, and Small Arms Fire or SAF in the bottom panel) a district with or without aid in the previous one months. The red line segments indicate the average treatment. Plot (b) shows the estimated difference in the CATEs between a district that received aid in the previous one months and those that did not. The corresponding 95% confidence intervals are also shown for all estimators.

G.4 Additional analysis for the binary moderator

As discussed in Section 5, the baseline distribution of airstrikes is not uniform across space, which means that increasing airstrike intensity relative to baseline causes some regions to experience a greater increase in airstrikes than others. To account for this variation, we study how the treatment effect varies with the binary moderator, defined as the indicator

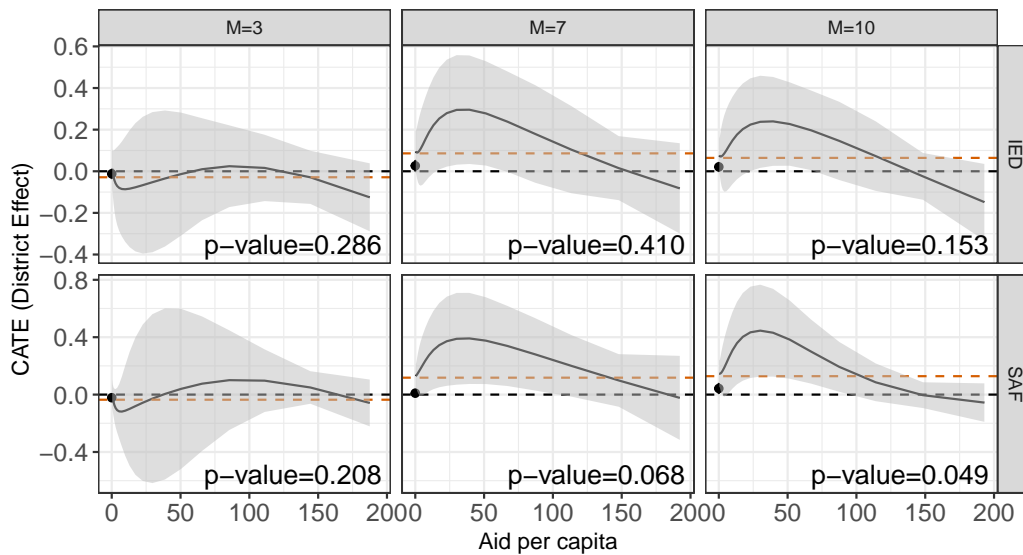


Figure A.16: Estimated CATEs of increasing airstrike intensity on the number of insurgency attacks (Improved Explosive Device or IED in the top panel, and Small Arms Fire or SAF in the bottom panel) for different values of aid per capita received in the previous two weeks with the shaded region indicating the 95% confidence intervals. The red lines represent the estimated average treatment effects. The results are using propensity scores truncated at the 90th percentile.

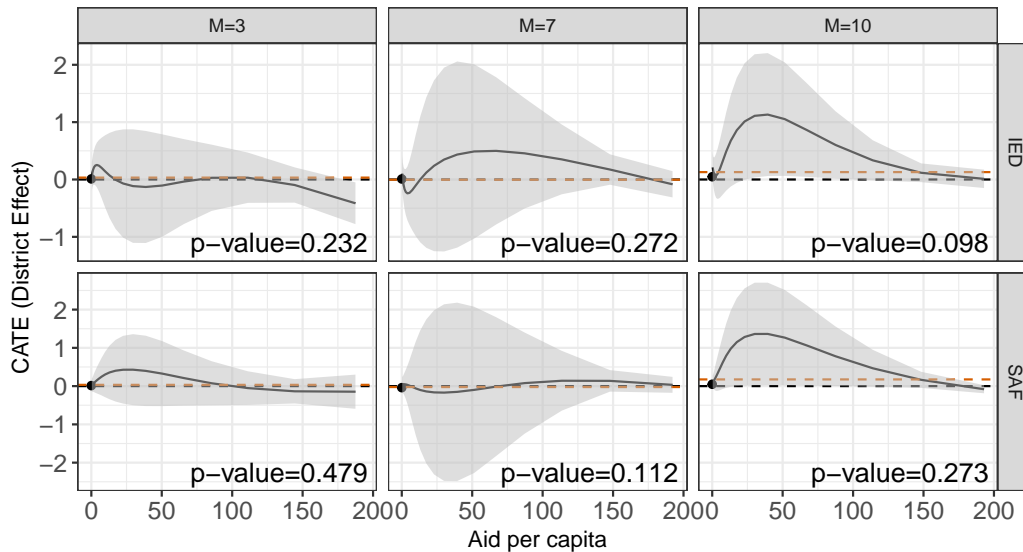


Figure A.17: Estimated CATEs of increasing airstrike intensity on the number of insurgency attacks (Improved Explosive Device or IED in the top panel, and Small Arms Fire or SAF in the bottom panel) for different values of aid per capita received in the previous two months with the shaded region indicating the 95% confidence intervals. The red lines represent the estimated average treatment effects. The results are using propensity scores truncated at the 98th percentile. The p-values correspond to tests for the overall heterogeneity effect.

of receiving aid during the previous month, while controlling for expected changes in the number of airstrikes.

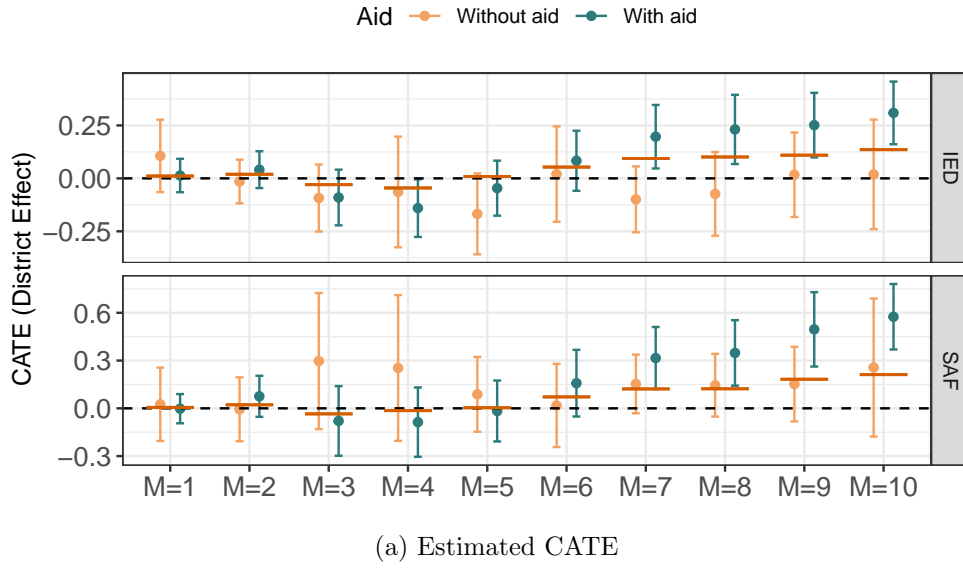
Specifically, we include the expected change in airstrike numbers and its interaction with the aid indicator in the regression model. The model is given by:

$$\tau_{t,h_1,h_2}^{\text{Proj.}}(r; \boldsymbol{\beta}_t) = \beta_{t,0} + \beta_{t,1}r + \beta_{t,2}q + \beta_{t,3}r \times q,$$

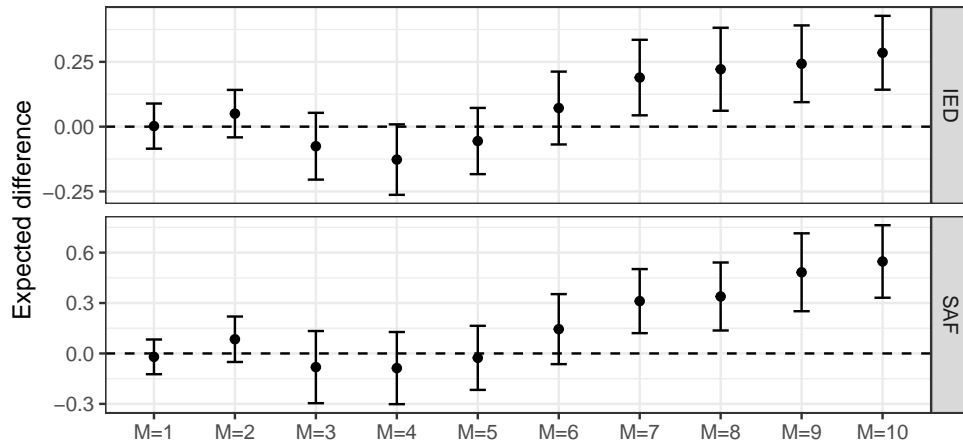
where r is the binary aid moderator, and q is the expected change in the number of airstrikes in a district. After estimating the coefficients, we plug in the median value of q to represent the expected airstrike intensity and compare the CATEs for areas with and without aid.

Figure A.18 presents the results for both IED and SAF attacks. Plot (a) shows the estimated CATEs for intervention windows ranging from $M = 1$ to $M = 10$, while Plot (b) displays the estimated difference in the CATEs between districts with and without aid. The findings generally align with the results in Section 5, where the expected intensity of airstrikes was not included in the model. For SAF attacks, districts that received aid in the previous month continue to show a stronger reaction to airstrikes, particularly when the intervention spans at least seven days. Importantly, for IED attacks, the estimated differences in CATEs now become statistically significant, suggesting a stronger effect in regions with prior aid.

Overall, controlling for expected airstrike intensity does not alter the main conclusion that regions receiving aid in the previous month exhibit a stronger response to increased airstrike intensity. These results indicate that the observed heterogeneity in treatment effects is not driven by differences in the intensity of airstrikes across regions with and without aid.



(a) Estimated CATE



(b) Expected difference

Figure A.18: Results for the binary aid moderator for regions with *median level* of increased airstrike intensity. Plot (a) shows the estimated CATEs of increasing airstrike intensity on the number of insurgency attacks (Improved Explosive Device or IED in the top panel, and Small Arms Fire or SAF in the bottom panel) a district with or without aid in the previous one months controlling the expected changes in the airstrike intensity. The red line segments indicate the average treatment. Plot (b) shows the estimated difference in the CATEs between a district that received aid in the previous one months and those that did not. The corresponding 95% confidence intervals are also shown for all estimators.